Review of Element Analysis of Industrial Materials by In-Line Laser—Induced Breakdown Spectroscopy (LIBS)

Johannes D. Pedarnig [1,*], **Stefan Trautner** [1], **Stefan Grünberger** [1], **Nikolaos Giannakaris** [1], **Simon Eschlböck-Fuchs** [2] and **Josef Hofstadler** [2]

1   Institute of Applied Physics, Johannes Kepler University Linz, A-4040 Linz, Austria; stefan.trautner@tgw-group.com (S.T.); stefan.gruenberger@jku.at (S.G.); nikolaos.giannakaris@jku.at (N.G.)
2   Voestalpine Stahl GmbH, A-4020 Linz, Austria; simon.eschlboeck-fuchs@voestalpine.com (S.E.-F.); Josef.Hofstadler@voestalpine.com (J.H.)
*   Correspondence: johannes.pedarnig@jku.at

Abstract: Laser-induced breakdown spectroscopy (LIBS) is a rapidly developing technique for chemical materials analysis. LIBS is applied for fundamental investigations, e.g., the laser plasma matter interaction, for element, molecule, and isotope analysis, and for various technical applications, e.g., minimal destructive materials inspection, the monitoring of production processes, and remote analysis of materials in hostile environment. In this review, we focus on the element analysis of industrial materials and the in-line chemical sensing in industrial production. After a brief introduction we discuss the optical emission of chemical elements in laser-induced plasma and the capability of LIBS for multi-element detection. An overview of the various classes of industrial materials analyzed by LIBS is given. This includes so-called Technology materials that are essential for the functionality of modern high-tech devices (smartphones, computers, cars, etc.). The LIBS technique enables unique applications for rapid element analysis under harsh conditions where other techniques are not available. We present several examples of LIBS-based sensors that are applied in-line and at-line of industrial production processes.

1. Introduction

Laser-induced breakdown spectroscopy (LIBS) is a versatile technique for the analysis of the chemical composition of many classes of materials. Solids, liquids, gases, powders, biological, and organic material, aerosols, and micro and nanoparticles are investigated and the type and abundance of chemical elements in such materials is determined by LIBS [1–8]. This laser-based analytical method is fast and robust, enables multi-element detection, does not require laborious sample preparation, and can be employed for field measurements under harsh conditions. For these reasons, LIBS is becoming one of the key techniques for element analysis of complex materials besides X-ray fluorescence spectrometry (XRF), spark optical emission spectrometry (spark OES), prompt gamma neutron activation analysis (PGNAA), and others [9]. LIBS has enormous potential for various applications and LIBS-based sensors are employed in many areas: industry (e.g., for materials analysis on-site or in-line with production processes), security (e.g., for remote detection of hazardous materials such as CBRNE threats [10]), mineralogy and geological materials [11,12], cultural heritage [13,14], biomedicine (e.g., identification of bacteria [15–18]), deep-sea inspection [19,20], space exploration (e.g., for analysis of Martian rocks using the LIBS sensors in ChemCam and SuperCam on board of the NASA Mars rovers Curiosity and Perseverance [21–24]), environmental measurements [25–28], and many others. The number of scientific papers on LIBS that are published per year is increasing rapidly (Figures A1 and A2 in Appendix A).

In LIBS, material is pulsed-laser ablated from the surface of a sample and the optical radiation of the laser-induced plasma (LIP) is analyzed by optical emission spectroscopy [29,30]. Short nanosecond laser pulses are employed for the sampling of material, typically, as stable and robust nanosecond laser sources operating at various wavelengths, pulse energies and repetition rates are available. However, ultrashort femtosecond lasers offer several advantages for LIBS compared to conventional nanosecond lasers and femtosecond-LIBS experiences a growing number of applications (e.g., [31–38]). In most studies, the optical emission of atomic and molecular species in the plasma is analyzed spectroscopically. Furthermore, recent studies have successfully demonstrated the remote isotope analysis by LIBS-based molecular isotope spectroscopy [39,40].

For the quantitative analysis of the chemical composition of plasma and sample calibration-based methods are frequently employed. Certified reference materials (CRM) are measured with the LIBS system and calibration curves for the analyte species are derived by univariate or multivariate regression procedures. With chemometric methods and machine learning techniques, large spectral data sets can be evaluated and the extraction of information from multidimensional data cubes can be automated [41,42]. The calibration-based approach enables quantifying trace concentrations (ppm range). However, matrix-matched reference materials have to be measured under the same conditions as the sample materials. With laboratory-based analytical methods such as laser-ablation inductively coupled plasma mass spectrometry/optical emission spectroscopy (LA-ICP-MS/OES) much smaller element concentrations (ppb range) can be resolved [43–47]. Calibration-free (CF) LIBS is complementary to calibration-based LIBS and can be employed to quantify the major elements in a sample material without measuring CRMs. In CF-LIBS, the concentration of major components is derived directly from measured LIBS spectra by modeling the laser-induced plasma and the optical plasma emission [48,49]. This approach is of interest as matrix-matched calibration samples are not required and constraints regarding the control of experimental parameters are less stringent.

2. Plasma Emission and Multi-Element Detection

For a laser-induced plasma that is optically thin and in local thermodynamic equilibrium (LTE), the number of photons Δn_{ki} emitted within the time interval Δt due to transitions between two atomic quantum states k and i is given by [Equation (1)]:

$$\Delta n_{ki}/\Delta t = N\ A_{ki}\ g_k\ \exp[-E_k/k_B\ T_e]/Z(T_e), \tag{1}$$

where N is the number of neutral atoms of the respective chemical element in the plasma, A_{ki} the transition probability, g_k the degeneracy factor of state k, E_k the energy of the upper level of transition, k_B the Boltzmann constant, $Z(T_e)$ the partition function, and T_e the electron temperature (= plasma temperature). The number of detected photons n_{det} depends strongly on the measurement setup and the instrumentation used [Equation (2)]:

$$n_{det} = \Delta n_{ki}/\Delta t \times (\Delta\Omega/2\ \pi)\ \tau_g\ \gamma_{det.} \tag{2}$$

The solid angle covered by the collection optics is $\Delta\Omega$, the measurement time (gate width) is τ_g, and the total detection efficiency is γ_{det} (which includes efficiencies of the light guiding system with mirrors, lenses, and fibers, of the optical imaging, and of spectrometer and electronic detector). As an example, we discuss the ablation of an iron sample containing 10 ppm of carbon impurity and the optical emission of carbon in the laser-induced plasma. With nanosecond lasers, the ablated mass per pulse is typically around 300 ng, corresponding to 3.2×10^{15} Fe atoms and $N = 3.2 \times 10^{10}$ C atoms (ignoring ions in the following). The most intense emission line of C is in the UV range at wavelength $\lambda_{ki} = 193.09$ nm and the corresponding spectroscopic parameters are $A_{ki} = 3.7\times10^8$ s^{-1}, $g_k = 3$, and $E_k = 7.7$ eV. For a typical plasma temperature of $T_e = 9000$ K the partition function of neutral C is $Z = 9.8$. The C atoms are emitting $\Delta n_{ki}/\Delta t \approx 1.8 \times 10^{14}$ photons per second. For a typical LIBS setup equipped with an Echelle spectrometer and ICCD

detector and with $\Delta\Omega/2\pi \approx 10^{-2}$, $\tau_g \approx 10$ µs, and $\gamma_{det} \approx 1.25 \times 10^{-5}$, the total detected emission signal for carbon is $n_{det} \approx 430$ photons. As a consequence of such rather low signals, the limits of detection (LOD) and of quantification (LOQ) in LIBS are typically in the ppm range (or higher, depending on the element considered). With double-pulse LIBS the emission of the laser-induced plasma can be enhanced and lower LOD values are achieved [1,6]. The measured signals depend also on the type of sample material (matrix effect) and very different limits for the same analyte may be obtained for different matrices. The measured LOD and LOQ values for many analyte elements in different matrices can be found in the literature [50]. The LOD values for solid materials are summarized in the table of elements in Figure A3 (Appendix A).

The compositional analysis of industrial materials requires multi-element detection capability. Modern electronic components used in mobile phones, computers, and cars are comprised of up to 60 chemical elements, for example. In LIBS, many different elements can be measured at the same time, making this technique especially suited for the analysis of materials with complex composition. The number of photons emitted from a laser-induced plasma per atom in the plasma and per time can be calculated considering the spectroscopic parameters of the involved atomic transition and the plasma temperature [51]. From Equation (1) this element-specific emission rate (EMRA) is calculated by [Equation (3)]:

$$\text{EMRA} = (\Delta n_{ki}/\Delta t)/N = A_{ki}\, g_k \exp[-E_k/k_B\, T_e]/Z(T_e). \tag{3}$$

Figure 1 shows the calculated emission rate of most chemical elements for a homogeneous and optically thin plasma in (local) thermodynamic equilibrium at $T_e = 10{,}000$ K.

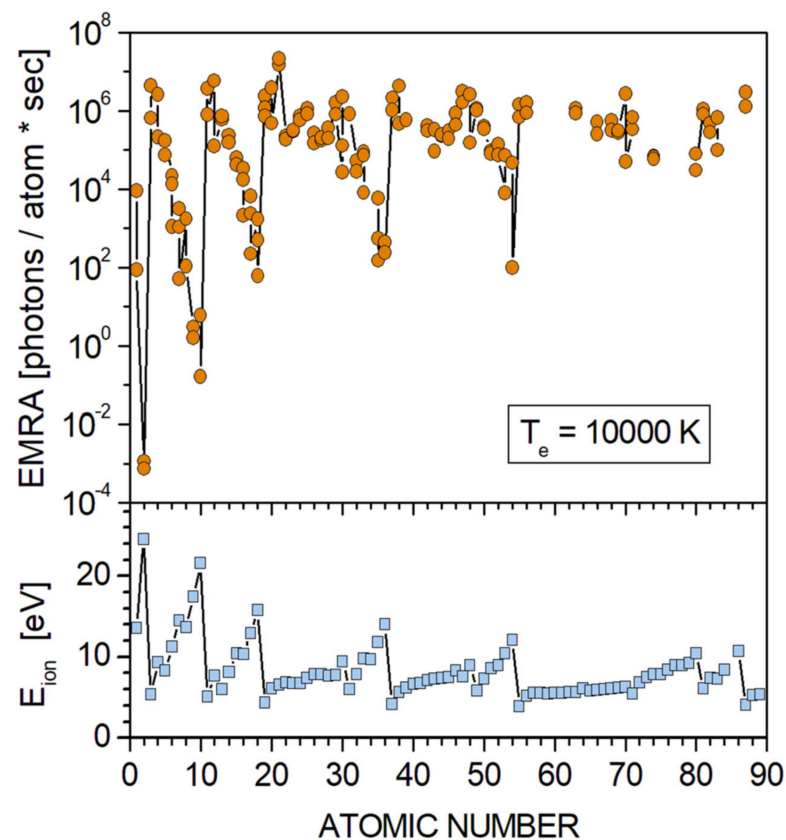**Figure 1.** Number of photons emitted per atom and second for optically thin and homogeneous LTE plasma at temperature $T_e = 10{,}000$ K. This emission rate of atoms EMRA is calculated for most chemical elements using the most intense emission lines of neutral species (upper part). The ionization energy of neutral atoms versus the atomic number of elements (lower part). The sign "*" stands for multiplication.

For each element, the most abundant isotope is selected and at least the two most intense emission lines of neutral atoms are evaluated [52,53]. Ions are not considered here as most species are neutrals in LIBS plasma measured at longer delay times with respect to the laser pulse. The emission rate varies by almost 12 orders of magnitude for the different elements. The temperature $T_e = 10,000$ K is typical in LIBS measurements employing nanosecond laser pulses with energy density (fluence) $\Phi = 1-100$ J/cm^2 for ablation. At very high nanosecond laser fluence of $\Phi \sim 10^4-10^5$ J/cm^2 the plasma species can have high ionization stages (e.g., Ti^{12+} and Sn^{11+}). The corresponding plasma temperatures are around 10^5-10^6 K and plasma emission is obtained in the extreme UV and soft X-ray spectral ranges. This regime has so far not been explored for technical applications in analytics. The lower part of Figure 1 displays the ionization energy of neutral atoms. The plasma emission and the ionization energies of elements are correlated. High energy levels are sparsely populated and atoms with high excited state and ionization energies have relatively weak emission.

In Figure 2 the emission rate of atoms in ideal plasma is presented according to the group of chemical elements in the periodic table. The numbering of groups follows the scheme of the International Union of Pure and Applied Chemistry [54].
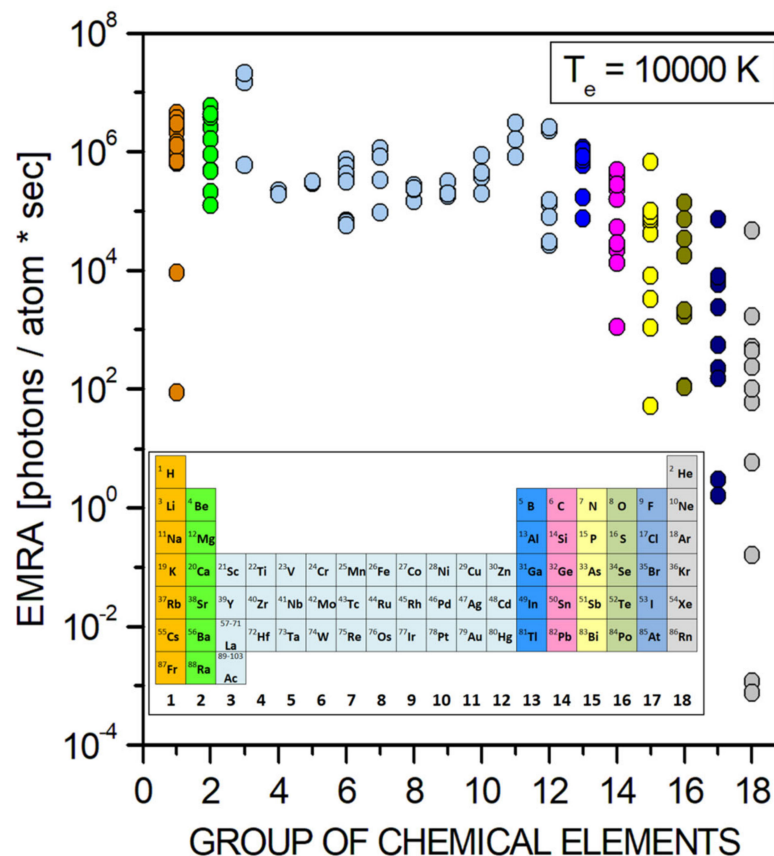

Figure 2. Emission rate EMRA of atoms in ideal plasma for most chemical elements in groups 1 to 18 of the periodic table ($T_e = 10,000$ K). Groups are numbered according to the IUPAC scheme [54]. The sign "*" stands for multiplication.

In group 1, the alkali metals (lithium to francium) show intense emission (EMRA $\approx 10^6 - 10^7$ photons/atom $\times$ sec), whereas the hydrogen emission lines are weak in comparison (EMRA $\leq 10^4$ photons/atom $\times$ sec). The alkaline earth metals (beryllium to radium, group 2), the transition metals (group 3 including lanthanoids and groups 4−12), and the elements in group 13 (boron to thallium) have rather intense emissions. From group 14 to 18 the emission rates show a trend to lower values and much larger variations for different elements within the same group. For halogens (group 17) and noble

gases (group 18) the lightest elements have the faintest emissions with EMRA ≈ 100 and 10^{-3} photons/atom $\times$ sec for fluorine and helium, respectively. Elements with high plasma emission intensities such as alkali metals, alkaline earth metals, and lanthanoids are measured with low LOD values, for example ~10 ppm for Mg and Na and ~2 ppm for Y. For halogens, on the other hand, the emission intensity is much lower and the reported LOD values are much higher, for example ~300 ppm for F, ~1000 ppm for Cl, and ~5000 ppm for Br. In real LIBS plasma, the emission intensities may be significantly lower than the calculated values. Radiation self-absorption, plasma non-homogeneity, plasma-chemical reactions, and ejection of non-luminous particles from the sample material are influencing the optical emission of the plasma. A secondary excitation of the laser-induced plasma can enhance the optical signals, homogenize the plasma [55] and improve the detection sensitivity. Techniques employed for secondary excitation in LIBS include double laser pulses [56–61], electric spark discharges [62–65], and radiofrequency [47,66,67], and microwave [68–70] radiation.

The reported LOD values of the different elements measured in solid samples and the calculated emission rates of elements are correlated. There is a clear trend to lower LOD for higher EMRA for most elements (Figure A4 in Appendix A).

3. LIBS Analysis of Industrial Materials

The rapid development of stable and robust high power laser sources, of efficient and broadband spectrometers, and of fast and sensitive detection systems has stimulated many scientific studies on LIBS in the last years. Various research groups and business enterprises are developing LIBS systems, components, and software for technical applications in the field, i.e., out-of-laboratory. Many classes of materials that are used in large scale in industrial production are investigated by LIBS. Some materials classes are listed in the following in alphabetical order. For each class of materials some references to recent scientific publications are given.

- Aluminum alloys [71–80];
- Cement and concrete [81–91];
- Coal [92–105];
- Coal ashes [106–110];
- Combustible gases such as fuel/air mixtures [111–115];
- Copper alloys [74,116–123];
- Electrolytes, battery materials, fuel cells [124–129];
- Fertilizer [130–142];
- Food [143–153];
- Food supplements [154–156];
- Gases, exhaust gases [157–167];
- Glasses [168–179];
- Glass melts [180–182];
- Magnesium alloys [183–187];
- Metal melts:
  - Aluminum [188–192],
  - Sodium [193],
  - Steel [194–203],
  - Zinc [204,205];
- Metal scrap [9,77,102,206–218];
- Minerals [219–235];
- Mineral melts, solidified [236,237];
- Mineral ores [238–244];
- Nuclear and radioactive materials [245–264];
- Oil, oil shales, and sands [265–272];
- Oil residues [273–277];
- Organic and inorganic photovoltaic materials [278–280];

- Paper and coated paper [281–283];
- Particulate matter:
  - Aerosols and air-borne particles [284–292],
  - Coarse grained powder [293–295],
  - Loose fine-grained powder [296–301],
  - Particles [297,302–307];
- Pharmaceutical substances [308–319];
- Polymers and technical polymers [59,320–336];
- Polymer waste [337–348];
- Refractory materials [349–354];
- Rubber [355–364];
- Silicon, metallurgical and solar grade silicon [365–368];
- Slag from steel production [51,55,369–377];
- Steel [194,378–401];
- Steel metal welds [402–405];
- Thin film solar cells [406–411];
- Waste electrical and electronic equipment (WEEE) [208,412–418];
- Wastewater [25,419–423];
- Wood and wood waste [424–429].

Other classes of materials that are investigated by LIBS include artefacts in cultural heritage (e.g., metallic equipment, coins, mineral materials, paintings), biological materials (e.g., bacteria, cells, tissue, bones), chemical colorants, explosives, extra-terrestrial materials, geological minerals, gemstones, ink, isotopes (e.g., hydrogen [31], uranium oxide, lithium [430]), paints, plants, seafloor (underwater inspection), soil, and thin film coatings.

4. Technology Materials

Materials and energy are among the most important resources in industrial production and are the basis for the development of new high-tech materials, novel products, and advanced devices. Technology metals are especially important to produce such materials and devices and the future need for various metals is increasing. Neodymium, for example, is used mainly to produce permanent magnets and laser crystals and the need for Nd in year 2030 is expected to be $3.8\times$ larger than the present world production of this metal [431]. Plastics are another important resource material due to their high versatility and their use in many areas. Plastics have grown enormously in importance over the last few decades and 359 million tons of plastics were produced worldwide in 2018.

4.1. Precious Metals and Minerals

The production volume of high-tech devices such as smartphones, computers, high energy density rechargeable batteries, flat panel displays, clean energy applications, and components for cars and e-cars is strongly increasing. For the industrial fabrication of such devices, large amounts of special materials are required. For example, the number of smartphones sold worldwide to end-users increased from 122 Mio devices in 2007 to more than 1520 Mio devices in 2019 [432] (for details see Figure A5 in Appendix A). Around 1300 Mio smartphones (with 1300 Mio rechargeable batteries) and 300 Mio PC's and Laptops (with 140 Mio rechargeable batteries) have been sold worldwide in 2008. The production of only these devices consumed 3, 16, and 23% of the annual global mine production of metals Ag, Pd and Co, respectively [433]. More than 50% of the global mine production of noble metals Pt and Pd and more than 80% of Rh are used only for exhaust gas catalyst systems of cars.

The global production of precious and special metals ("technology metals") by mining has drastically increased in recent years to cope with the demands. Figure 3 shows the global mine production of some technology metals in years 1990–2017 normalized to the total production since 1900 (compiled from data of the U.S. Geological Survey [434]). For many metals more, than 80% of the total material mined since 1900 has been produced

in the last few decades [433,435,436]. The available reserve of metals (in units of years) is estimated from the materials reserve (tons) known in 2019 and the amount of material (tons/year) produced in 2017 [434]. For several metals the reserve is only a few decades. The supply of more than 50 chemical elements of economic value is considered to be at risk [437]. An example of the depletion of natural resources is indium. In year 2007 the global production of In metal was 510 tons, the known global reserves 11,000 tons, and the estimated remaining time until exhaustion 19 years [431]. This risk clearly conflicts with the need of In, which is expected to increase by 3.3× (until 2030) over the present world production just for the fabrication of displays and photovoltaic devices.
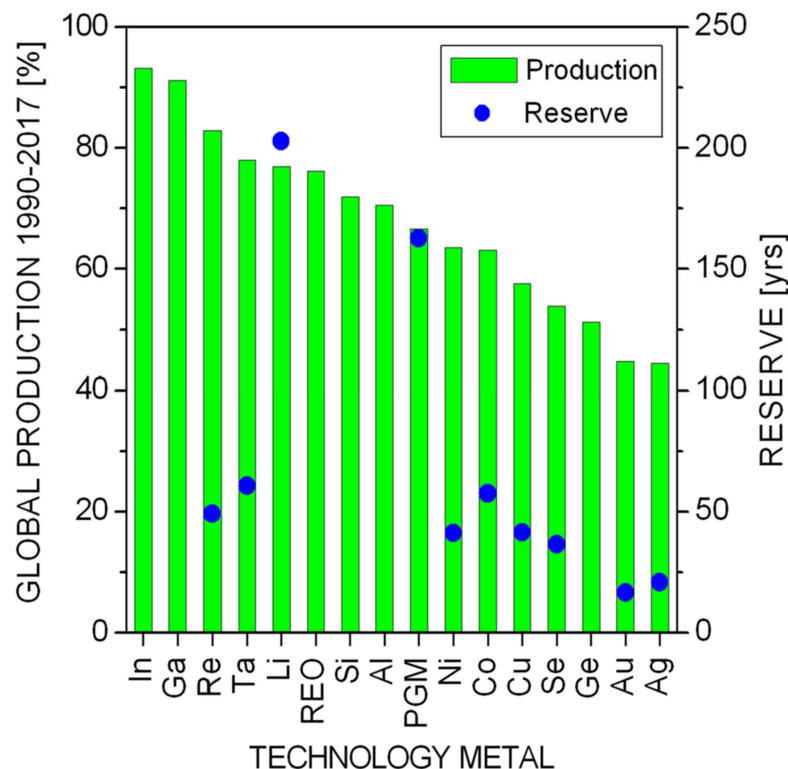

Figure 3. Global mine production of some technology metals in years 1990 to 2017 normalized to the production since 1900 (REO is rare earth oxide; PGM is platinum group metals including Pd, Pt, Ir, Os, Rh, and Ru; Si refers to silicon metal). Reserve calculated from known materials reserve and annual mine production. Data taken from [434].

Technological metals and other materials are continuously transferred from natural geogenic resources to anthropogenic resources (i.e., products, goods, buildings and other infrastructure, waste in man-made deposits) and to the environment. The global reserve for copper, for instance, is around 955 Mio tons. In 1920, 930 and 25 Mio tons were contained in geogenic and anthropogenic resources, respectively. In year 2000, the distribution has drastically changed to 495 Mio tons in geogenic resources, 360 Mio tons in anthropogenic resources, and 105 Mio tons spread in the environment [438].

4.2. Plastics Materials

The use of polymers and plastics in industry and many other areas has been strongly growing over the last decades. In 2018, the plastic production reached 359 million tons worldwide and 62 million tons in Europe [439]. China is the biggest producer of plastics worldwide (30%). Most of the plastics in Europe (EU-28 + Switzerland and Norway) are used for packaging, building/construction, automotive purposes, electronics, household, and agriculture. The share of polymers by resin type is for polyethylene (PE-LD and PE-HD) 29.7%, for polypropylene (PP) 19.3%, for polyvinyl chloride (PVC) 10%, for polyurethane

(PUR) 7.9%, for polyethylene terephthalate (PET) 7.7%, for polystyrene (PS) 6.4%, and for others (ABS, PBT, PC, PMMA, PTFE, etc.) 19%, see Figure 4. The increasing demand for plastics requires efficient treatment of the post-consumer plastic waste in order to avoid uncontrolled release of the material into the ecosphere, e.g., as marine litter [440]. The collection of post-consumer polymer and plastic waste reached 29.1 million tons in Europe in 2018 (including 17.8 Mt plastics packaging waste). This waste material was recycled (32.5%), used for energy recovery (42.6%), and disposed as landfill (24.9%), see Figure 4. The evolution of plastic post-consumer waste treatment in Europe from 2006 to 2018 shows a strong increase of materials recycling (4.7 to 9.4 Mt) and energy recovery (7.0 to 12.4 Mt) and a substantial decrease of landfill (12.9 to 7.2 Mt).
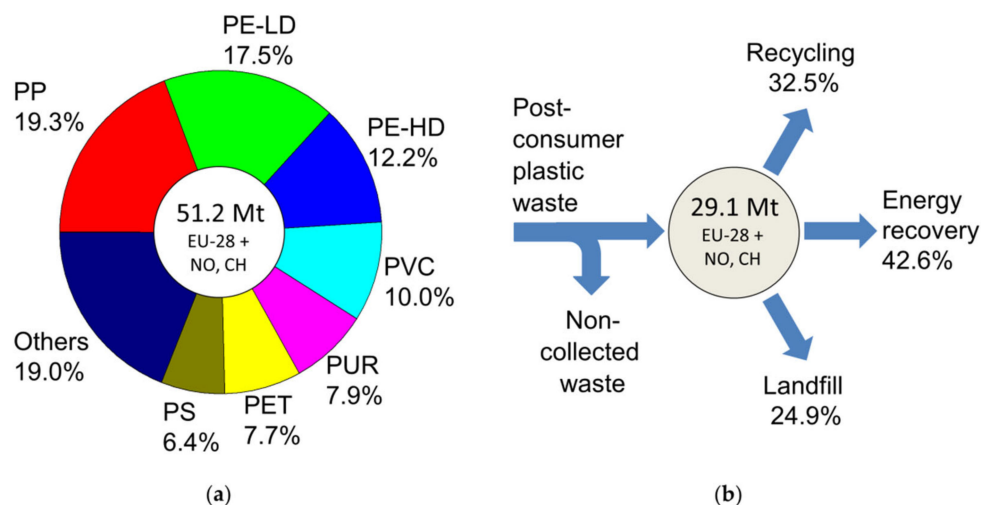

Figure 4. (**a**) European plastics demand distribution by resin type in million tons (Mt) in 2018. (**b**) Distribution of post-consumer plastic waste in Europe in 2018. Data taken from [441].

The European Strategy for Plastics in a Circular Economy [441] is aiming to transform the production and use of plastic material and products and to further increase the recycling rates for plastic waste. Different pathways of plastic recycling are assessed to reduce the emission of greenhouse gases [442]. The PVC fraction must be removed from the collected plastic waste prior to waste treatment. The removal of PVC protects machines that are processing recyclate material from damage and avoids the formation of reactive substances (e.g., HCl) and toxins in energy recovery processes.

4.3. Secondary Raw Materials

The exploitation of natural deposits and the production of primary raw materials most likely cannot be scaled up with the increasing demands. Depletion of (known) natural reserves, low abundance, and economic and environmental issues are obstacles in increasing the mine production. Secondary raw materials are produced by the recycling of end-of-life products and articles (e.g., waste), of by-products (e.g., from industrial production), and of materials after their initial use. The recovery of raw materials from anthropogenic resources is an important strategy to avoid severe shortage of commodities and to stabilize the materials supply chains. "Urban mining" of secondary raw materials has substantial economic and environmental impact as materials are used more efficiently and materials flows become manageable (circular economy [443], impact on materials flow cost accounting [444,445]). The mining of urban resources is also more energy-efficient than the production of primary raw materials. The mining of gold (average Au concentration in ore ~5 g/ton) produces approx. 17,000 tons of CO_2 per ton of Au metal [446]. The CO_2 gas emission is in large part due to the energy required to extract the ore from deep lying natural deposits and to process it. Printed circuit boards (PCB) of computers and cell phones, on the other hand, have Au concentrations of 150 and 300 g/ton, respectively, and

are easily accessible [447]. Another example is the recycling of Cu and Al, which saves more than 85% and up to 95%, respectively, of the energy required to produce the primary raw materials by mining.

The production of high-quality secondary raw materials from waste streams requires the inspection of the waste composition and the separation into different fractions and materials classes. In the recycling industry, various sensor technologies are employed in sensor-based sorting [448]. The sorting systems are using optical sensors (e.g., detecting the color or absorption/reflection/fluorescence of waste pieces) [449], X-ray transmission sensors (e.g., measuring the atomic density and element composition), magnetic and Eddy current sensors (e.g., detecting Fe and non-Fe metals), spectroscopic sensors (e.g., detecting specific absorption bands in the infrared (IR) and emission lines and bands in the ultraviolet (UV) and visible (VIS)), gamma ray-based sensors, and acoustic sensors.

5. In-Line Application of LIBS in Industrial Production

The major strengths of the LIBS technique are its robustness and versatility and its capability for rapid and stand-off multi-element detection. This enables LIBS to be used for in-line chemical sensing in industrial production under harsh conditions. Laboratory-based element analytical techniques (e.g., LA-ICP-OES/MS) are more accurate than in-line compatible techniques such as LIBS. However, in-line techniques allow for continuous sampling, the reduction of sampling errors, and the real-time detection of rapid changes in the materials composition. Hence, analytical data obtained by a less accurate but continuously performed in-line measurement may have advantages over more accurate data measured in the laboratory that are less representative. In the following we present some recent examples for in-line, at-line, and in-situ measurements of various materials (alphabetical order).

5.1. Coal and Coal Ash

Coal is still one of the major resources for the global production of electricity. Around 39% of the total electricity production worldwide was based on coal in 2015 [450]. Moreover, coal is an important raw material in various industries. The combustion efficiency of coal depends on various material properties such as chemical composition (major elements C, H, O, N, and S), heat value, moisture content, volatile matter, fixed carbon, and ash content [92,451]. In order to optimize the efficiency of power generation and to reduce the environmental pollution (e.g., by emission of SO_2) a technology for rapid in-line or at-line chemical analysis is needed.

Coal is usually analyzed by standardized ASTM laboratory methods (American Society for Testing and Materials), which requires several days for the results to be obtained. Prompt gamma neutron activation analysis (PGNAA) and X-ray fluorescence (XRF) are methods enabling in-line analysis of coal. However, radiation safety issues are of relevance for both methods. Furthermore, PGNAA requires the use of an isotope source and XRF does detect only the heavier elements ($Z \geq 11$). LIBS is a promising candidate for coal quality detection due to its advantages of real-time, in-situ, and multi-element measurement capability. A schematic of a LIBS measurement system installed in a coal-fired power plant is shown in Figure 5a [452,453]. The LIBS system was installed above a conveyor belt to analyze coal material that was transported from the crushing station to the coal bunkers (PPL Generation's Montour Power Station). For calibration, an artificial neural network (ANN) model was developed and trained with calibration samples (ASTM reference analysis). Figure 5b shows results from validation tests of the in-line LIBS system using approx. 120 coal samples that were grabbed and then analyzed by LIBS and a laboratory method. The LIBS results for the Sulphur concentration (red and black symbols, Figure 5b) were in good agreement with the lab reference analyses (black lines, Figure 5b). The measurement of S was required for optimal operation of the SO_2 reduction system of the plant. Besides S, the LIBS analyzer was detecting also Al, C, Ca, K, Mg, Na, Fe, Si, and Ti in real-time.
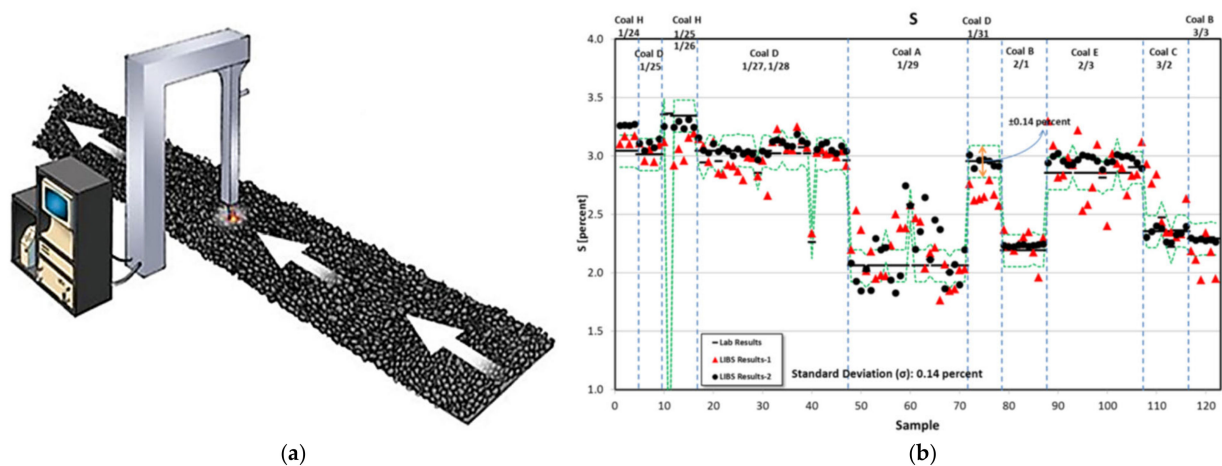
Figure 5. LIBS in-line analyzer of coal. (**a**) Schematic of measurement system for coal on conveyor belt in coal-fired power plant. (**b**) Measured concentration of Sulphur in coal for approx. 120 samples (validation tests). Adapted from [452,453].

The ash content in coal transported on a conveyor belt can be monitored online by PGNAA. However, the neutron radiation in PGNAA represents a potential health hazard requiring strict regulatory demands. LIBS does not require radioactive materials for operation and LIBS systems can be designed more compact and of less weight compared to PGNAA systems. Laser Detect Systems has developed one of the first mineral analysis systems using LIBS and has pioneered the in-line analysis of coal ash [110]. The system was installed at a conveyor belt of a coal mine in South Africa for a four-month field trial (Figure 6a).
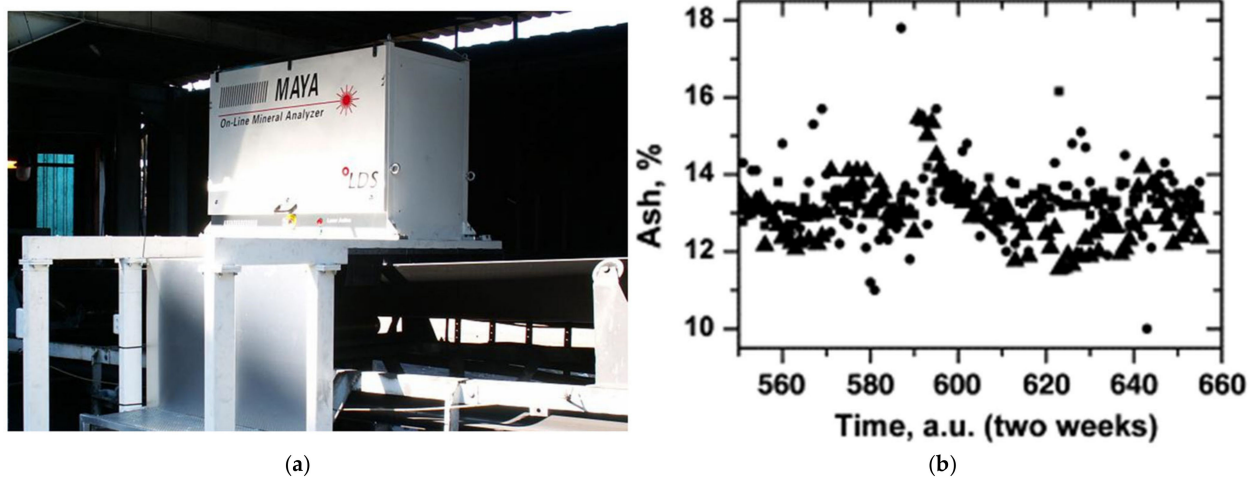

Figure 6. LIBS in-line analyzer of coal ash. (**a**) Measurement system installed at a conveyor belt (photograph: LDS Laser Detect Systems). (**b**) Real-time coal quality monitoring by LIBS (triangles) and PGNAA (squares). Reference concentrations (circles). Adapted from [110].

The analytical performance of the LIBS system was compared to a PGNAA system installed in the same line. LIBS analyzed the surface of the coal material on the belt while the PGNAA signal depended on the volume of the irradiated material. The field trial demonstrated successful online coal ash content monitoring by the LIBS analyzer. The key elements in coal and coal ash, C, Mg, Al, Si, Ca, Fe, and Ti, were measured and the in-line ash quantification by LIBS and PGNAA had the same accuracy with a mean absolute error of $\pm 0.5\%$ (Figure 6b).

The concentration of unburned carbon in fly ash is an important criterion for evaluating the combustion efficiency of coal-fired power plants and the commercial value of fly ash

as a secondary raw material. A high concentration of unburned carbon can have adverse impact on the combustion efficiency and on the value of the ash. The carbon concentration is presently measured off-line by manually obtaining fly ash samples from the precipitator ash hoppers or flue gas streams and sending the samples to a laboratory. Depending on the laboratory test procedure employed, the results may not be available for up to 24 h. This procedure takes several hours and delays the combustion optimization process. For online measurements a LIBS system and a two-stage cyclone measurement system were developed to quantify the carbon content in fly ash in real-time [106]. The cyclone system in combination with a 1 ns pulse-width laser enabled to eliminate the effect of CO_2 on the unburned carbon content. A schematic diagram of a boiler control system using LIBS in a coal-fired power plant for fly ash measurement is shown in Figure 7a.
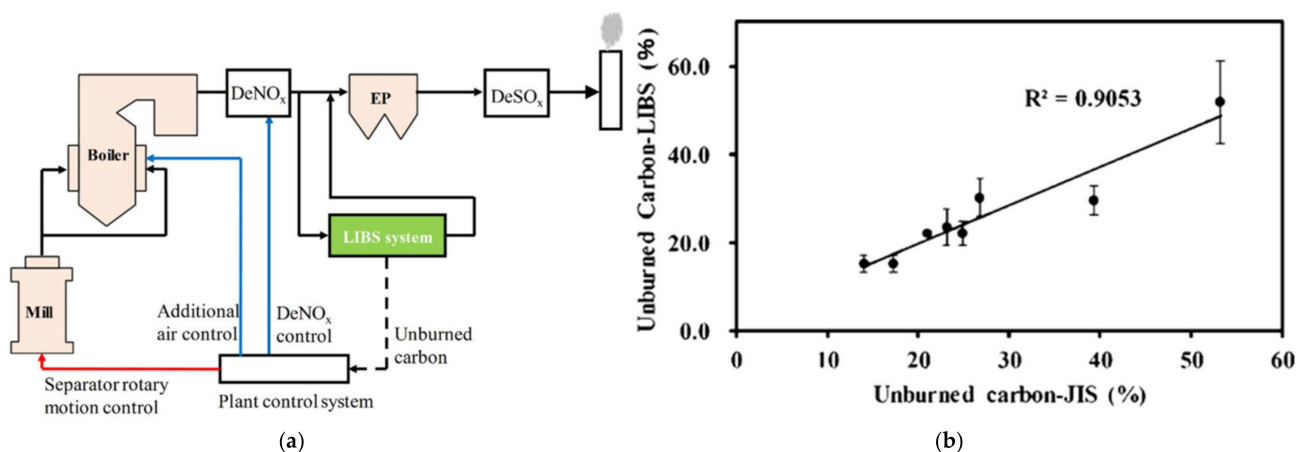

Figure 7. LIBS analysis of unburned carbon in coal fly ash. (**a**) Schematic of advanced control system using real-time LIBS measurements. (**b**) Unburned carbon content measured by LIBS and by standard chemical analysis method (JIS). Adapted from [106].

The unburned carbon content in different fly ash samples as measured by LIBS and by standard chemical analysis methods (Japanese Industrial Standards JIS) are compared in Figure 7b. For improved quantitative analysis the plasma temperature correction method was used. The results of measurements by LIBS and JIS method were consistent with $R^2 = 0.9052$ and RMSEP = 3.9% in the measurement range of 14.0 to 53.2% of unburned carbon. This demonstrates the feasibility of LIBS for real-time measurement of fly ash contents in power plants. Some earlier studies on the on-line analysis of unburned carbon in fly ash and of combustion products in industrial boilers and furnaces are reported in [454,455], respectively.

5.2. Metal Melts

The element analysis of metal melts in the production is usually performed off-line by laboratory-based analytical techniques such as XRF and spark OES. A liquid sample is taken and measured after cool-down and solidification. This is a time-consuming process, making the real-time monitoring of the melt composition impossible. With LIBS the melt can be measured directly, i.e., without sampling, and real-time analysis becomes feasible.

The chemical analysis of aluminum in a primary aluminum smelter has been reported recently [188]. The measurement system was installed at a casting launder system (Figure 8a). The melt temperature was around 730 °C. Fourteen trace elements (Fe, Si, Cu, Ni, Ti, Cr, Mn, Sn, V, Ga, Zn, Sb, Mg, Na) were measured in the melt and the results were correlated with laboratory measurements on corresponding solid samples. The trace elements Cu, Cr, Mn, and Sn were quantified down to ppm levels and volatile elements, e.g., Na, were measured in real-time down to ppm levels (Figure 8b). It was concluded that the in-line LIBS analysis of many technically important trace elements in the primary

aluminum melt was fully competitive with the off-line laboratory analysis of solid process samples in terms of accuracy and precision. Some earlier reports on the analysis of aluminum melts are [190–192].
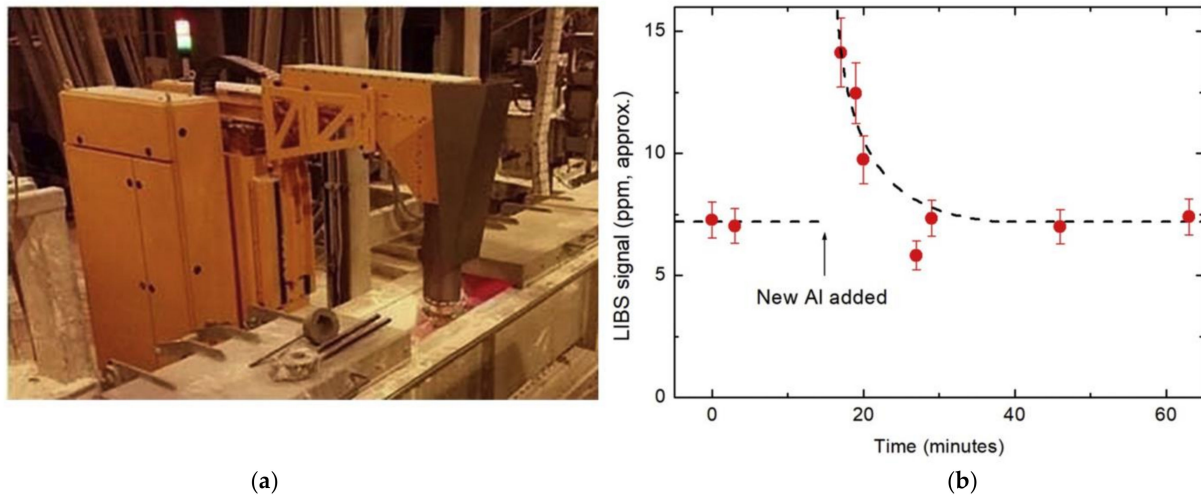

Figure 8. LIBS in-line measurement of molten aluminum. (**a**) LIBS device installed at a casting launder system in a primary aluminum smelter. (**b**) In-situ measurement of sodium concentration in the molten aluminum (dashed line: guide to the eye). Adapted from [188].

The LIBS analysis of molten steel has been reported by several groups, e.g., in [194,197–203]. In a recent publication, a hollow refractory lancet was immersed into the metal melt to pass the laser light through the surface slag layer onto the liquid steel underneath and to pass the optical radiation of the laser-induced plasma backwards to the optical detection system (using a Cassegrain telescope) and spectrometer (Figure 9a) [197]. The setup was designed to protect all optical and electronic equipment against the high-temperature environment near the steel ladle.
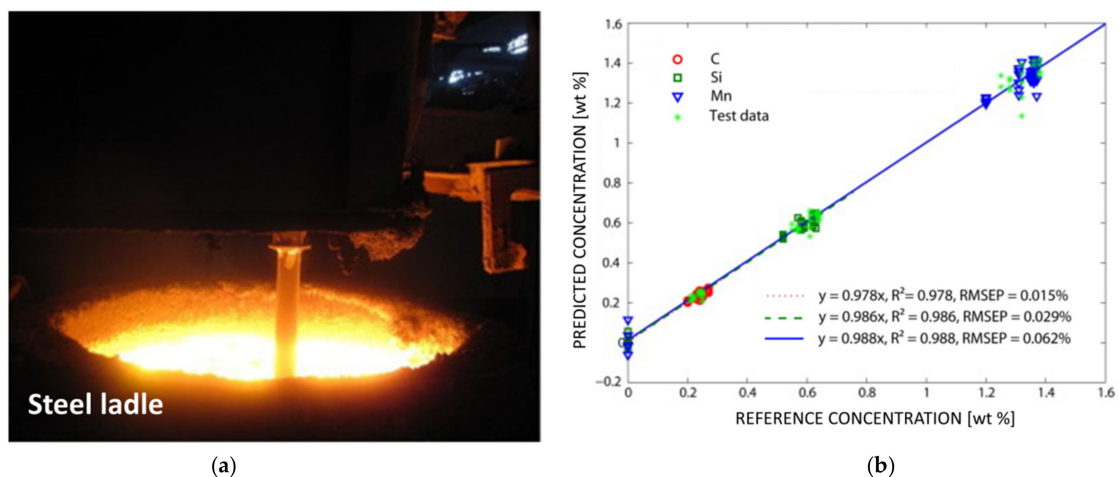
Figure 9. LIBS in-line measurement of molten steel. (**a**) Photograph of the LIBS system refractory lance that is immersed into the liquid steel in the ladle. (**b**) Calibration and test results for C, Si, and Mn of liquid steel in a steel plant (straight lines: linear fits to data). Adapted from [197].

In laboratory test runs the elements Si, Mn, Cr, Ni, and V in molten steel samples were measured. In the steel plant the elements C (0.21–0.27 wt%), Si (0.52–0.63 wt%), and Mn (1.20–1.38 wt%) were analyzed quantitatively by LIBS and by spark OES as reference. The predicted concentration of test samples was close to the reference concentration with small

relative root mean square errors of prediction RMSEP (Figure 9b). The results obtained in the steel plant were not as good as the results in the laboratory. However, the accuracy achieved in the in-line measurements approached the steel plant's requirements. From these results it was concluded that the developed LIBS system is promising for the in situ analysis of melt steel in the steelmaking industry. Immersion probes for LIBS analysis of liquid metals including steel were developed prior by other groups [199–201].

5.3. Minerals

For the exploration and efficient excavation of mineral quarries the composition of rock has to be measured during the drilling process. Analysis of minerals inside the drill hole is not feasible; however, the drill dust can be extracted with a dust hose and analyzed. Figure 10a shows a LIBS analyzer for continuous in-line analysis of the drill dust [102]. The LIBS system is mounted on a mobile drill rig.
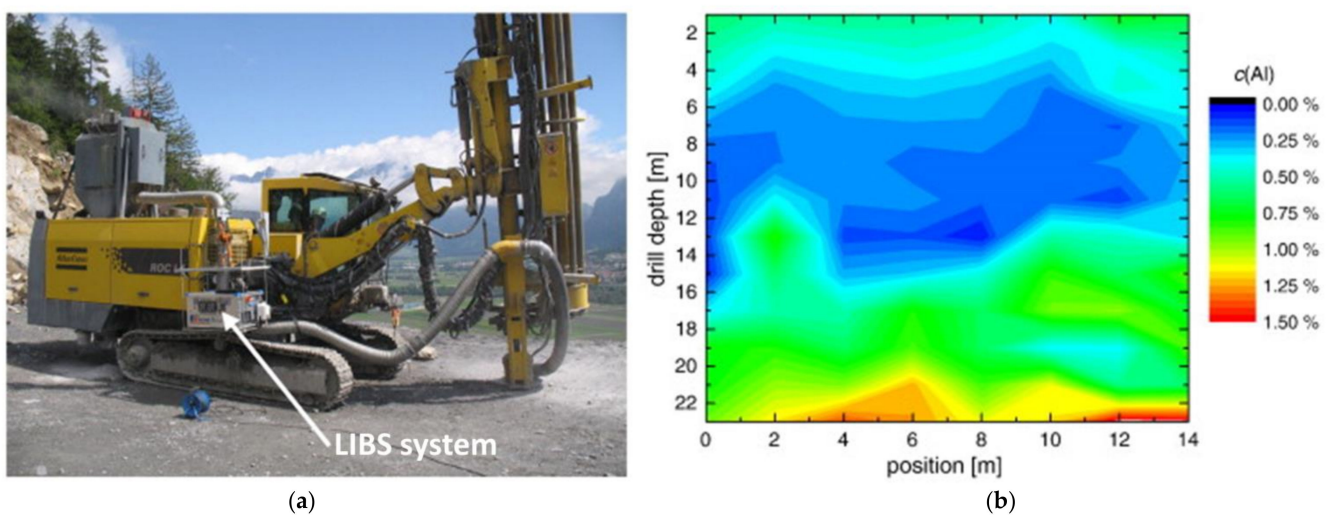

(**a**)　　　　　　　　　　　　　　　　　　　　　　　　　　　　(**b**)

Figure 10. LIBS in-line measurement of drill dust in a quarry. (**a**) LIBS system mounted on a drill rig. (**b**) Measured spatial variation of Aluminum concentration as a function of drill depth and horizontal position of the mobile drill rig. Adapted from [102].

The results from a LIBS measurement campaign in a quarry are shown in Figure 10b. Dust samples were collected at different horizontal positions of the drill rig and at various drill depths. The Aluminum concentration measured as a function of drill depth and horizontal position varied from 0 to 1.5 m%. From such elemental maps a spatial model of the mineral deposit can be determined, and the excavation process can be optimized.

In another study, the ability of LIBS to provide in-line analyses of phosphate ores under industrial conditions was demonstrated [233]. Impurities in the phosphate rock significantly affect the ability to efficiently recover phosphate from the rock in the production plant and produce on-grade products. The most significant variables are CaO, MgO, Fe_2O_3, and Al_2O_3. A rugged LIBS sensor was developed and installed above a conveyer belt in an open phosphate mine (Four Corners Mine, FL, USA). A photograph of the installed LIBS system is seen in Figure 11a. The system enabled automated measurements of several elements (Mg, Fe, Al, Si, Ca) and the on-belt evaluation of phosphate ores. The variation of LIBS-measured signals for MgO (square symbols), Fe_2O_3 (up triangle), bone phosphate lime (BPL, down triangle), and metal impurity ratio (MER, circle) over 27 h of a test run are shown in Figure 11b. During the test run two different rock portions were detected as evidenced by varying signals of MgO, Fe_2O_3, BPL, and MER. The real-time detection of unwanted material by LIBS enables removing this material from the conveyer before further processing.
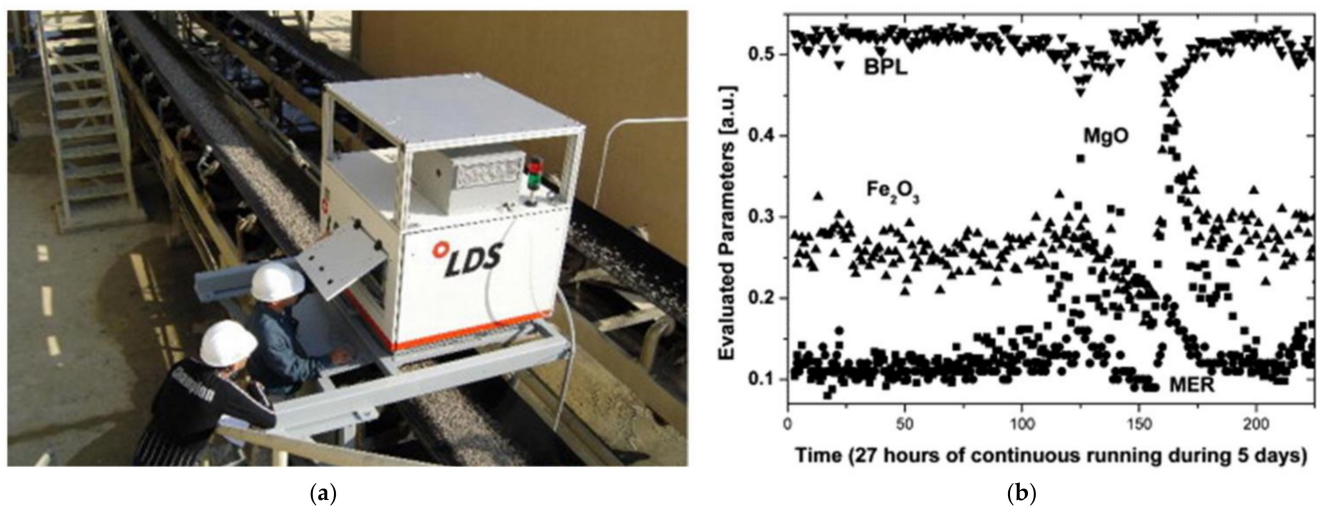
(**a**)   (**b**)

Figure 11. LIBS in-line measurement of phosphate minerals. (**a**) Photograph of LIBS sensor installed above a conveyor belt in the Four Corners Mine, Florida (USA). (**b**) MgO, Fe_2O_3, BPL, and MER measured by LIBS over several days. Adapted from [233].

5.4. Metal Scrap

Metal scrap is an important resource material for various industries. In 2017, approx. 57 million metric tons of selected metals were recycled from scrap in the U.S. (an amount equivalent to about 47% of the apparent supply of those metals). Iron and steel accounted for about 89% of the recycled metal and about 88% of the apparent supply [456]. The use of recycled scrap metals in place of virgin iron ore is beneficial to the environment (e.g., energy savings by 75%) and for every ton of new steel made from scrap steel approx. 1.1 tons of iron ore and 0.6 tons of coal are saved [457]. Aluminum is one of the few materials that is completely recyclable. The production of recycled aluminum is 92% more efficient than the production of new aluminum. Per year, 5 Mt of aluminum are recycled in the U.S. and Canada [458].

LIBS was applied for the in-line monitoring of steel scrap on a conveyor belt transporting the scrap metal to an electrical arc furnace (EAF) in a steel plant [102]. The real-time measurement of the content of key elements in the scrap allows stabilizing the process of furnace charging and steel making. The optical unit of the developed LIBS system was installed over the conveyor line (Figure 12a). The main components included a 3D scanner and a laser light section sensor to measure the geometry of the scrap pieces. The scanner optics directed and focused the laser beam onto the scrap in a wide field of the cross-section of the conveyor (1.2 m × 2 m, varying filling level). The charging operation of the EAF is controlled by determining the mass flow of key elements (e.g., Si) from the element concentration measured by LIBS (Figure 12b). Parameters such as the belt speed, the filling height, and the average scrap density have to be taken into account to determine the element mass flow. The availability of data in real-time enables to adjust the charging process before the charging is finished. LIBS analysis of steel scarp was reported by other groups as well [215].

The LIBS technique has been applied also to the inspection of aluminum scrap for metal recycling [6,209,210,214]. Wrought and cast Al alloy pieces have been identified using a belt conveyor sorting system by measuring the LIBS signals for Al, Ti, and Si achieving a mass throughput of up to 4 tons/hour [6]. In another study, scrap of Al alloys containing different amount of Mg and Si was sorted by LIBS. For Al scrap pieces of 40–110 mm size the sorting throughput was 3–5 metric tons per hour and the sorting purity was 98% [209].
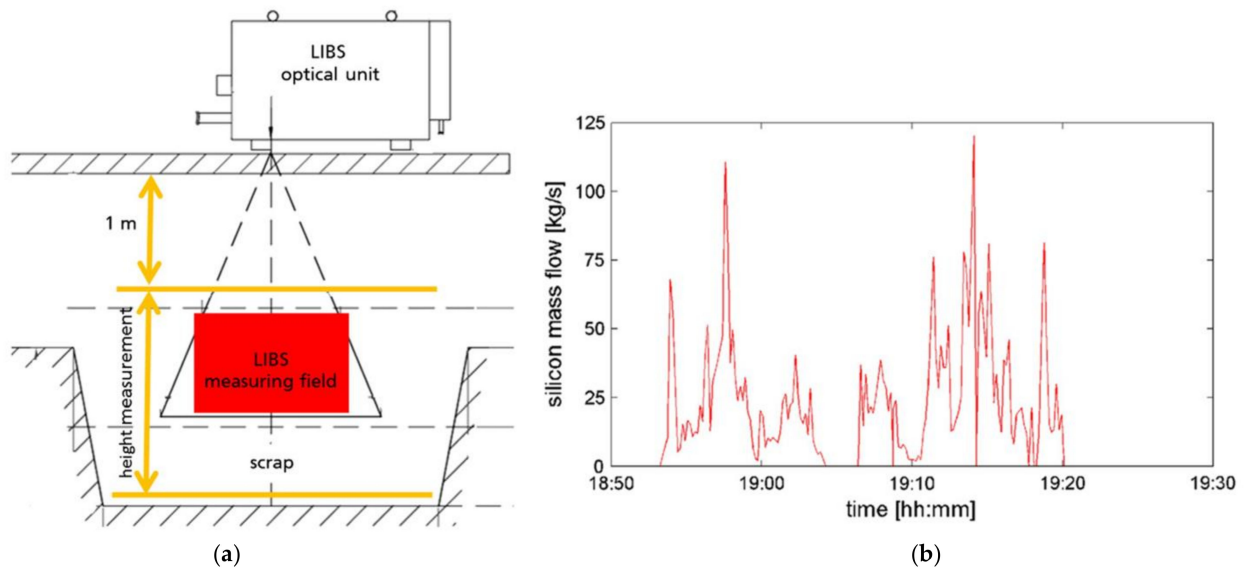
Figure 12. LIBS in-line measurement of steel scrap. (**a**) Schematic of LIBS sensor installed above a conveyor belt in a steel plant. (**b**) Variation of the silicon mass in the scrap on the conveyor as derived from the in-line LIBS measurements. Adapted from [102].

5.5. Nuclear Material

In the nuclear industry the analysis of nuclear and other materials before, during, and after production and utilization is required for safe and economic operation. This includes different processes in the nuclear fuel cycle such as mining of ore, fabrication of fuel, power plant operation, fuel reprocessing, and spent fuel storage (Figure 13a) [259]. Laser spectroscopy techniques such as LIBS, laser-induced fluorescence (LIF), and cavity-ring down spectroscopy (CRDS) are employed for analysis due to their elemental and molecular selectivity and high sensitivity. The inherent advantages of LIBS make it an efficient method for the analysis of hazardous samples in harsh environments. The nuclear industry is one of the fast-growing fields of LIBS application [248]. The development of stand-off LIBS systems enables for remote and in situ inspection of samples that are at large distance from the LIBS sensor (i.e., many meters).
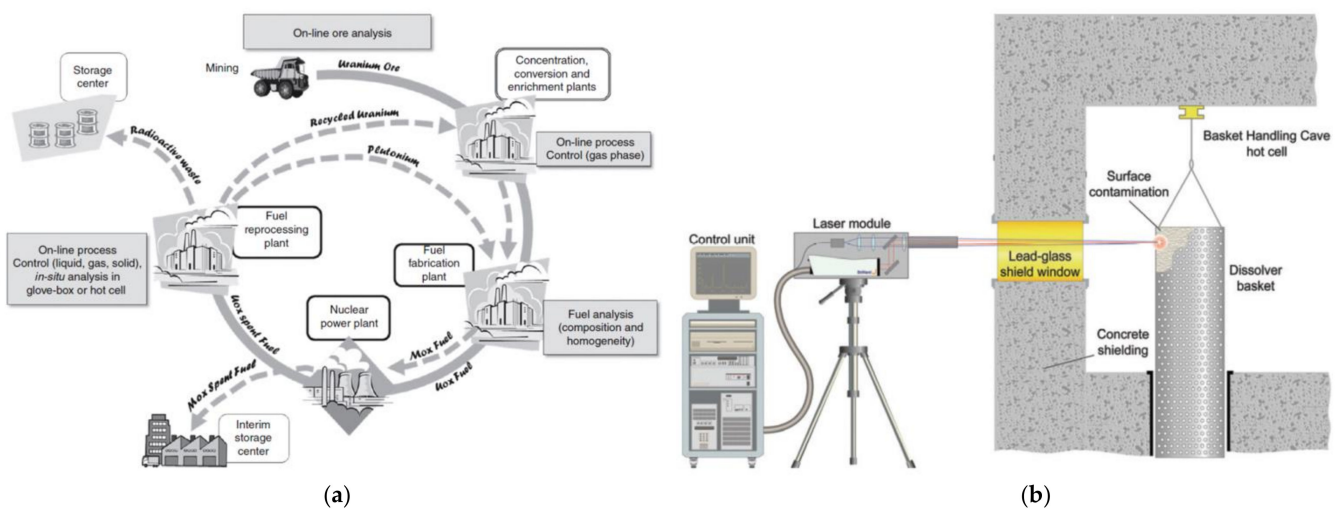

Figure 13. LIBS in nuclear materials analysis. (**a**) Potential applications of LIBS in nuclear fuel cycle. Adapted from [259]. (**b**) Schematic of a stand-off LIBS analyzer installed at the THORP nuclear plant in UK. Adapted from [263].

Figure 13b shows a stand-off LIBS system using an optical telescope for the characterization of high-level radioactive waste at the THORP nuclear reprocessing plant in UK [263]. Optical access to the material was possible via a 1 m thick lead-glass radiation shield window. The LIBS system was used for remote identification of an unknown solid material that accumulated on the basket surface. The perforated basket was used in the processing of spent fuel. Remote analysis of this surface contamination was necessary due to the difficulties in taking a sample from behind the radiation shield and the subsequent difficulties with laboratory analysis. The LIBS analysis showed that the contaminant material was rich in zirconium and molybdenum (mainly zirconium molybdate which forms during the reprocessing of spent fuel).

Remote analysis of materials in nuclear fusion reactors is another important application for stand-off LIBS [249,257]. During operation of a tokamak fusion reactor, the inner walls of fusion chambers and divertors (plasma-facing components, PFC) are severely interacting with the plasma. As a consequence, the PFCs are subject to erosion, re-deposition of eroded material, and retention of fuel. The performance of fusion tokamaks such as ITER [459] can be influenced by such processes. Figure 14a shows the schematic of a stand-off LIBS system installed at the Experimental Advanced Superconducting Tokamak (EAST) [257,460]. The Nd:YAG laser beam (1064 nm, 5 ns, 180 mJ) was focused on the wall surface on the high-magnetic-field side using a quartz lens (f = 3 m) mounted at port H of the EAST device. The emission of LIBS plasma was collected in a backward direction using an optical telescope. The LIBS spectra measured in situ showed spectral signals of multiple elements (D, H, Li, Mo, W, Ti, La, Fe, and Si). The signals of Mo, W, C, and La were from the substrate materials of tiles, the signals of D and H came from the fuel (H was used for isotope experiments). The Li signal was caused by Li wall conditioning and Ti, Fe, and Si were due to impurities in the Li co-deposited layer.
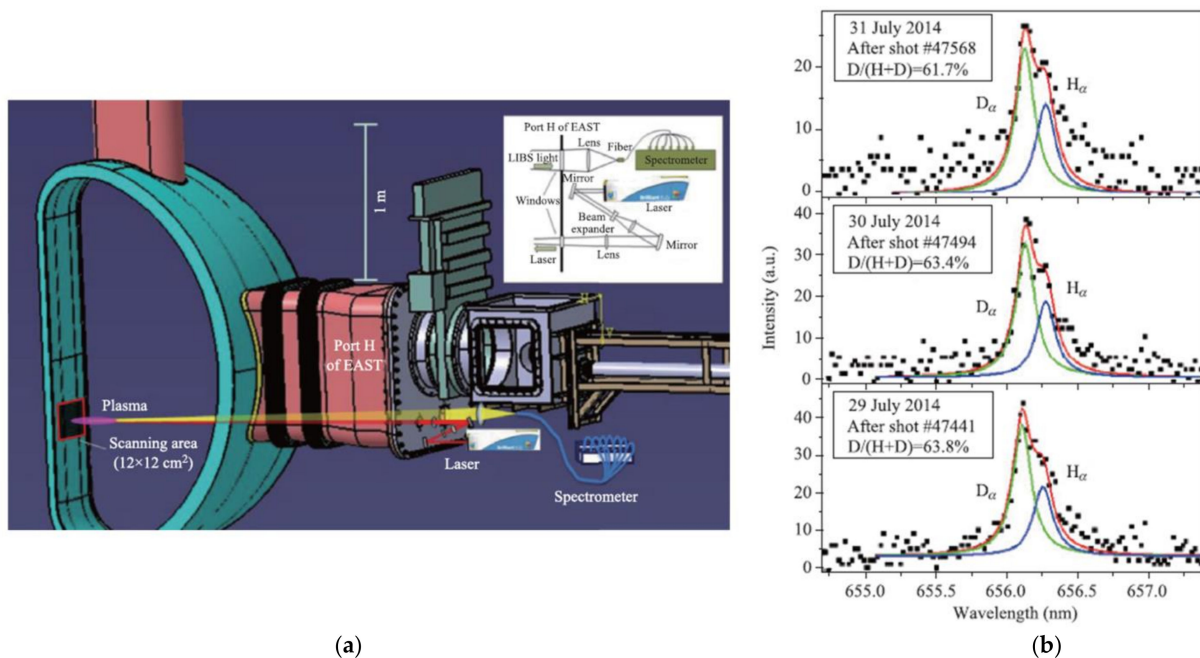
Figure 14. LIBS in fusion materials analysis. (**a**) Schematic of a stand-off LIBS system installed at the EAST tokamak in China. (**b**) In situ LIBS spectra with Hα and Dα lines measured on different days at EAST. Adapted from [257].

Figure 14b shows LIBS spectra with the Hα and Dα lines measured in situ at EAST on different days. From such measurements, the H/H + D ratio in the plasma phase can be determined. These results demonstrate the potential of LIBS for in situ characterization of D/H retention and Li co-deposition on the walls of the fusion reactor.

5.6. Refractory Materials

Many industrial processes at high temperature such as metal making, furnace annealing, and sintering require high-temperature stable refractory products such as bricks, etc. The reuse and recycling of spent refractory materials have high potential to reduce the production of waste and the consumption of primary raw materials. The estimated amount of spent refractories is up to 28 million tons per year [461]. For high-grade recycling, the different types of refractory materials have to be identified and sorted with respect to their chemical composition and impurities have to be removed. The refractory materials are modified on the surface due to the interaction with the high-temperature processed material (e.g., liquid steel). Therefore, the surface layer is not representative for the bulk. LIBS has been used for the analysis of spent refractory materials [353,354]. When several laser pulses are applied on the same position of the specimen the contamination layers on the surface can be removed and the composition of the bulk material retrieved [208].

A demonstrator of a LIBS-based spent refractory sorting machine is shown in Figure 15a. The LIBS sensor is installed above the conveyor belt. An end-of-life refractory brick with a modified surface layer and unmodified bulk is shown in Figure 15b. Three LIBS measurement spots are marked with a white rectangle.

(a)   (b)

Figure 15. LIBS on-site measurement of spent refractory materials. (**a**) Demonstrator of a LIBS-based sorting machine (Photo: Orbix). Adapted from [461]. (**b**) End-of-life refractory brick with a modified surface layer. LIBS measurement spots marked with white rectangle (Photo: Fraunhofer ILT). Adapted from [208].

The demonstrator succeeded in sorting 30 tons of mixed bricks (doloma, magnesia, and alumina) at a throughput of 10 tons/h (1 brick per second). The sorting accuracy was validated by analysis of the output fractions (magnesite and dolomite). For all oxides analyzed (CaO, MgO, SiO_2, Fe_2O_3, Al_2O_3) the targeted composition of sorted fractions was reached (small exceedance for SiO_2) [208].

5.7. Rubber

Rubber has outstanding material properties such as mechanical elasticity, viscoelasticity, dielectric strength, thermal stability, resisting power against chemicals, morphological flexibility, and durability, and is used in a wide range of applications. About 70% of the annual global production of rubber is used for tire production and retreading [462]. A key parameter for the fabrication of rubber is the concentration of the vulcanization agents Sulfur and Zinc oxide (ZnO). The properties of the material (e.g., elasticity, stiffness, wear) depend on the amount of S and ZnO, and for the production of rubber of high quality the concentrations have to be controlled precisely in the process.

XRF and PGNAA cannot be employed for in-line measurements in the rubber production due to radiation hazards and other techniques were not available. Recently, LIBS has been employed for the first time to quantify ZnO and S directly in the tire rubber

production [357]. The system was optimized to measure the optical emission of S and Zn from the rubber plasma in air (Figure 16a). Plasma excitation in collinear double-pulse geometry and detection of plasma emission with time-gated detectors was employed to resolve the weak sulfur lines in the near-infrared range.
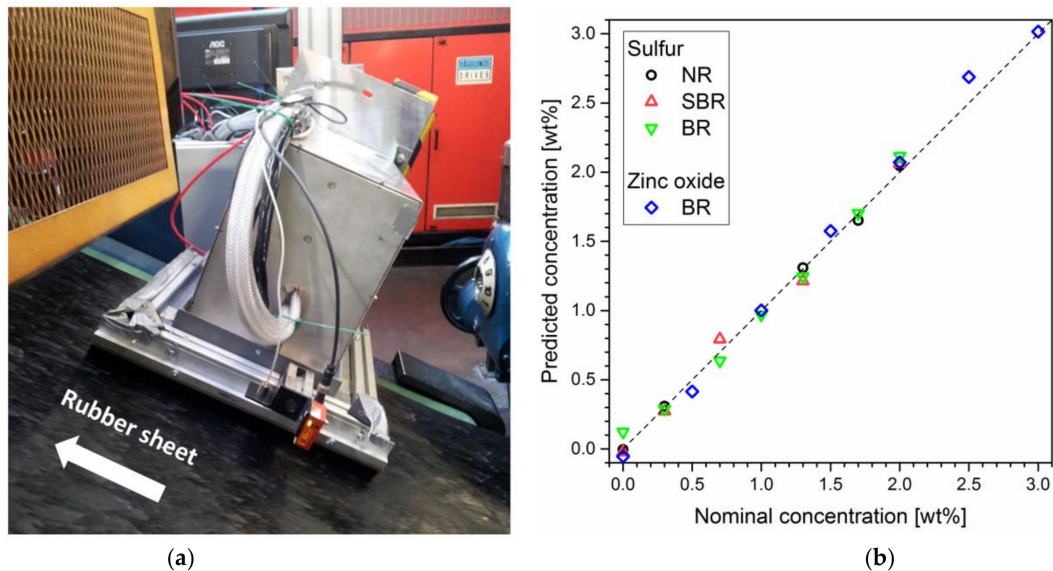

(**a**)   (**b**)

Figure 16. LIBS in-line measurement of tire rubber. (**a**) Photograph of the LIBS system installed at the tire rubber production line. (**b**) Validation of S and ZnO concentrations measured in different types of rubbers (dashed line: ideal match). Adapted from [357].

The element S and ZnO were quantified in three different sample materials (natural rubber NR, styrene-butadiene rubber SBR, and butadiene rubber BR) that were prepared from the most important polymers used in production (Figure 16b). The mean error of the prediction of concentrations RMSEP is $\leq$0.07 wt% for S and $\leq$0.33 wt% for ZnO for all polymer types. The results demonstrated that the vulcanizing system of rubber can be quantified under ambient conditions with a LIBS in-line sensor. Earlier attempts on tire rubber analysis by LIBS in the production are reported in [363,364].

5.8. Steel Grade Detection in Casting

In industrial steel production the casting of liquid steel into slabs, blooms, and billets is a frequently used process. The continuous casting of steel from different heats produces slabs that may have different chemical composition. The detection of different steel grades is important for the identification of the slabs. Moreover, the detection of transition zones from one steel grade to the other can improve productivity and cost-efficiency, e.g., by the reduction of steel waste. LIBS has been proposed for analyzing the chemical composition of cast steel and the at-line monitoring in the steel casting process has been successfully demonstrated [463–465].

The steel slabs are covered by different layers of varying thickness, which poses a substantial challenge for surface-analytical techniques such as LIBS. A schematic of LIBS at-line measurement of hot steel slabs in the continuous steel casting process is shown in Figure 17a. The bulk steel material (a) is covered by a scale (oxide) layer (c), mold powder (d), and dirt. The thickness of this surface layer can exceed several 100 μm. For LIBS analysis of the bulk material the surface layer has to be removed locally, e.g., by a sequence of laser pulses that precede the LIBS measurement and ablate the slab surface ("laser cleaning").
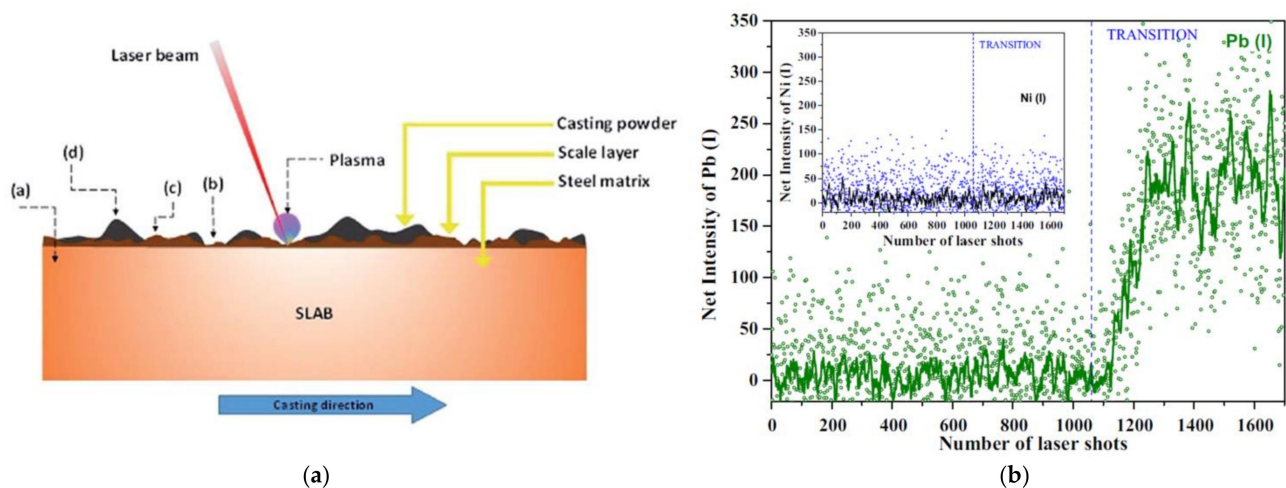
Figure 17. LIBS at-line measurement of hot steel slabs in the continuous steel casting process. (**a**) Schematic of a slab with steel matrix (a) and various surface layers (b–d). Adapted from [464]. (**b**) LIBS signal of Pb showing the transition between two different steel grades. The inset shows the signal for Ni. Solid lines are 25-point averages. Adapted from [463].

The LIBS signal of the Pb (I) line at 405.78 nm measured at-line on a hot steel slab in motion shows the transition from one steel grade to another (Figure 17b) [463]. The number of laser shots corresponds to the position of LIBS measurements on the steel slab along the casting direction (5 mm distance between two subsequent laser shots at pulse repetition frequency of 5 Hz). For comparison, the Ni (I) 341.47 nm line intensity did not change at the transition zone (inset of Figure 17b). The concentration of Pb in the two steel grades was 0 and 0.17 wt% (for Ni the concentration was 1.75 and 0.88 wt%). The LIBS signals obtained from the sample surface in real-time and the statistical analysis of signals allowed to discriminate special steel grades and to predict the distribution of elements in the intermixed transition zone of the cast slabs. The combination of LIBS measurements and Artificial Neural Network (ANN) methods for signal evaluation has also been used for the quantitative elemental analysis of cast steel along the slab length [465].

5.9. Steel Slags

Steel slags are multi-component oxide materials that are produced in large quantity in industrial steel production. For the control of the steelmaking processes and for the recycling of the metallurgical slag materials suitable analytical techniques are required. The standard method is XRF. However, LIBS requires less time for the analysis of slags than XRF [466]. For some applications the quantitative analysis of the major components of metallurgical slags is sufficient. This task can be accomplished by calibration-free LIBS (CF-LIBS) where the concentration of major elements is calculated directly from LIBS spectra of the samples without the need to measure reference materials. This approach is of interest if minor and trace elements are not relevant, analysis time is important, and reference materials are not available. The CF-LIBS method has been employed to analyze metals [467–470], rocks [471–473], and biological materials [474,475].

Figure 18a shows a LIBS system installed in the secondary metallurgy of a steel plant of voestalpine Stahl GmbH (Austria). The system measures the concentration of major oxides in solid slag by the CF-LIBS method [375,476]. The concentration of major oxides in various slag samples determined by CF-LIBS and the nominal concentration determined by reference analysis are shown in Figure 18b. The major oxides in the slag samples were CaO, Al_2O_3, MgO, SiO_2, FeO, and MnO with concentration values ranging from 5×10^{-3} wt% to 54 wt%. The concentration values by CF-LIBS (C_{CF}) match very closely the nominal concentrations (C_N). Deviations from the perfect match $C_{CF} = C_N$ (dashed line in Figure 18b) depend on type and concentration of oxide and are up to a few wt%.
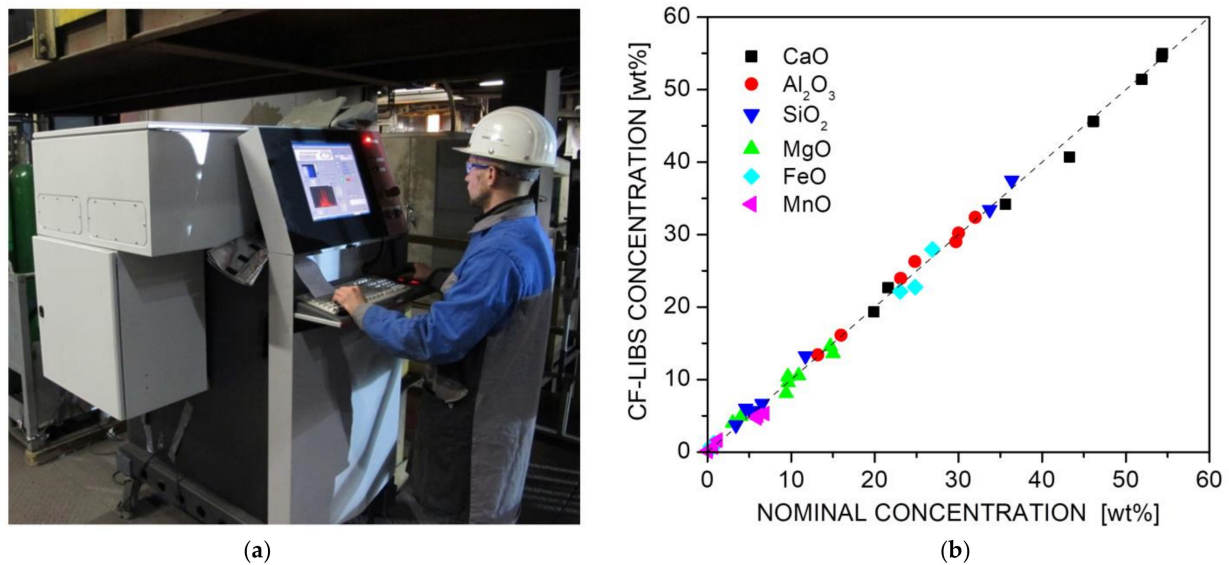
Figure 18. LIBS in-line measurement of solid steel slag in secondary metallurgy at voestalpine steel plant. (**a**) Photograph of the installed LIBS system. (**b**) Concentration of major oxides obtained by calibration-free (CF) analysis vs. nominal concentration (dashed line: ideal match). Adapted from [372].

The analysis of slag samples at high temperature is important when short time-to-analysis is required. In order to study the stability of CF-LIBS analysis against sample temperature, ceramic slag samples were heated in a box furnace to high temperature and measured during cool-down in air [374]. The calculated concentration values C_{CF} showed only weak variation with sample temperature up to 275 °C. Larger deviations in concentration were observed at higher sample temperature. The ablation rate, the self-absorption of radiation, the plasma expansion dynamics, and the plasma parameters may depend on the sample temperature [477]. The evaluation of data has led to the conclusion that the CF-LIBS method enables to quantify individual constituents with concentrations ≥ 1 wt%. This result agrees with the conclusions from theoretical investigations [371,478] that the inhomogeneity of plasma is a major limiting factor for the quantitation of smaller concentrations by CF-LIBS.

In the crude steel production (Linz-Donawitz process) converter slag is a by-product which can be used as raw material in other industrial branches, e.g., for road construction. The chemical composition of the slag is varying, and chemical analysis is required before further use of the material. An automated LIBS measurement system has been developed to analyze the major oxide components of the liquid slag (T = 600−1400 °C) while it is transported in a ladle to slag pits [373]. Figure 19a is a camera view into the slag ladle showing a solidified crust at the slag surface and the laser-induced plasma plume. A measuring probe guides the laser beam onto the slag surface and the plasma radiation from the liquid to the detection unit. The probe is moving across the slag surface during the LIBS measurement (2 min/meas.). The mass fraction of the major oxides was determined by calibration curves for approx. 50 slag ladles and compared to the XRF reference mass fraction (Figure 19b). Similar results were obtained for the liquid slag ($R^2 = 0.992$, Figure 19b) and solid pressed powder samples ($R^2 = 0.997$, data not shown). Stable operation during a three-month test run has demonstrated the potential of LIBS for in-line process analysis.
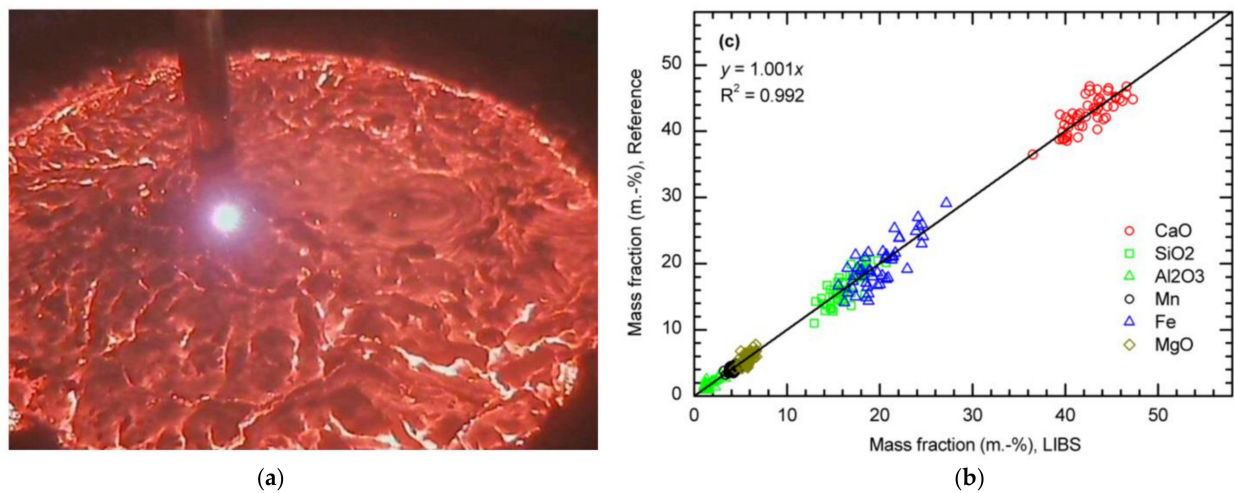
Figure 19. LIBS in-line measurement of liquid converter slag at voestalpine steel plant. (**a**) Photograph of the laser-induced plasma at the slag surface in the slag ladle. (**b**) Concentration of major oxides obtained by calibration-based analysis vs. reference concentration (dashed line: ideal match). Adapted from [373].

5.10. Waste Electrical and Electronic Equipment

The amount of waste electrical and electronic equipment (WEEE) produced per year has increased exponentially in the last 20 years, reaching 50 million metric tons in 2018 [479]. WEEE is mainly composed of iron/steel, plastics, non-ferrous metals, glass, and printed circuit boards (PCBs). For efficient recycling and recovery of valuable materials from this increasing waste, new technologies for fast and accurate chemical identification of WEEE components are needed [412].

Figure 20 shows an application of LIBS for the inspection of end-of-life PCBs from disassembled mobile phones [208].
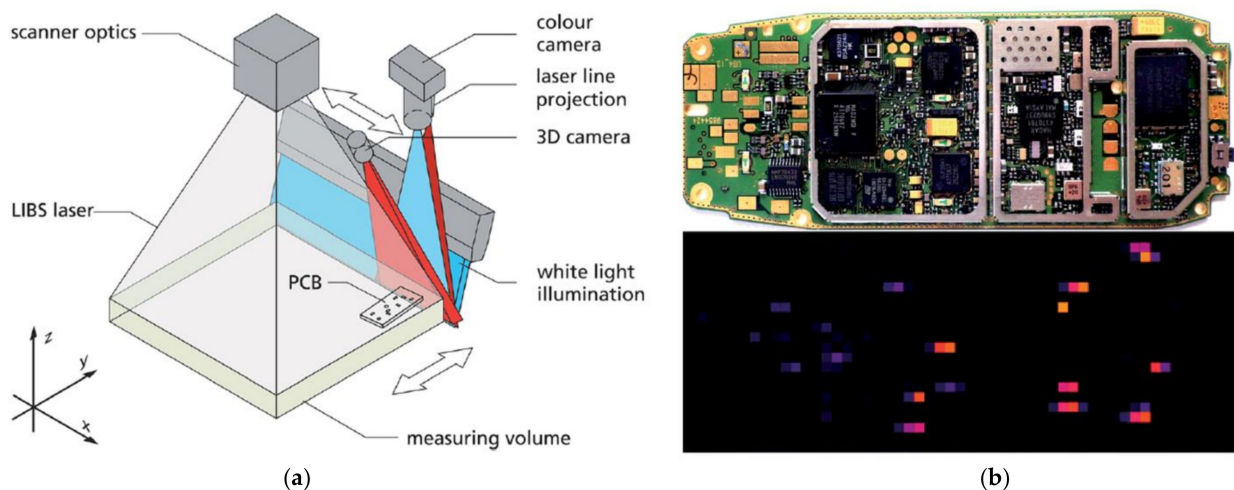
Figure 20. LIBS measurement of printed circuit boards (PCBs). (**a**) Schematic setup for optical inspection and LIBS analysis. (**b**) Photograph of PCB from a mobile phone (top); chemical image of Tantalum in the PCB measured by LIBS. Adapted from [208].

The optical sensors used for sample recognition within the measuring volume and the LIBS sensor (Figure 20a) were part of a large demonstrator system aiming at automated disassembly, separation, and recovery of valuable materials from WEEE [480]. The photograph of a PCB from a mobile phone (top) and a LIBS raster scan of the PCB with the obtained chemical image of Ta (bottom) are shown in Figure 20b. High intensities of Ta are represented by orange/red color. The LIBS scan of the complete PCB (108×42 mm^2) was

repeated several times to penetrate the housings of the electronic components and to access the bulk material. The chemical information gained by LIBS can be used in the next step for selective laser unsoldering and removal of the identified components (e.g., capacitors) from the PCB [208].

In related studies, LIBS sensors have been developed to control a hydrometallurgical Cu recovery process in discarded PCBs [412] and to analyze heavy metals and brominated flame retardants in polymers and WEEE pieces on a conveyor belt [347].

5.11. Waste Polymers

For the recycling of waste polymers and the use of polymer recyclates as secondary raw material, the identification of different types of polymers and the detection of contaminations such as surface layers and heavy metals is important. The polymer polyvinylchloride (PVC, monomer formula C_2H_3Cl) is used in different segments such as building and construction, packaging, automotive, electrical and electronic, and textile. PVC is among the top three materials by market share accounting for 10% of the total European demand for plastics (Figure 4). More than 42% of the collected post-consumer plastic waste in Europe is used for energy recovery. For the energy recovery, the PVC fraction has to be sorted out from the polymer waste to avoid the formation of HCl and other detrimental or toxic substances.

LIBS enables discriminating different types of polymers and detecting contaminations. PVC can be identified by measuring the Chlorine emission line, which is unique for this polymer type. However, this task is challenging because of the low emission rate (Figure 1) and rather high LOD values for Cl (Figure A4 in Appendix). The in-line measurement of waste polymers for the identification of PVC in an industrial waste materials sorting plant is shown in Figure 21a [343]. Material from municipal waste plastic collection containing different types of plastic pieces and impurities was measured on the conveyor belt.

(a) (b)
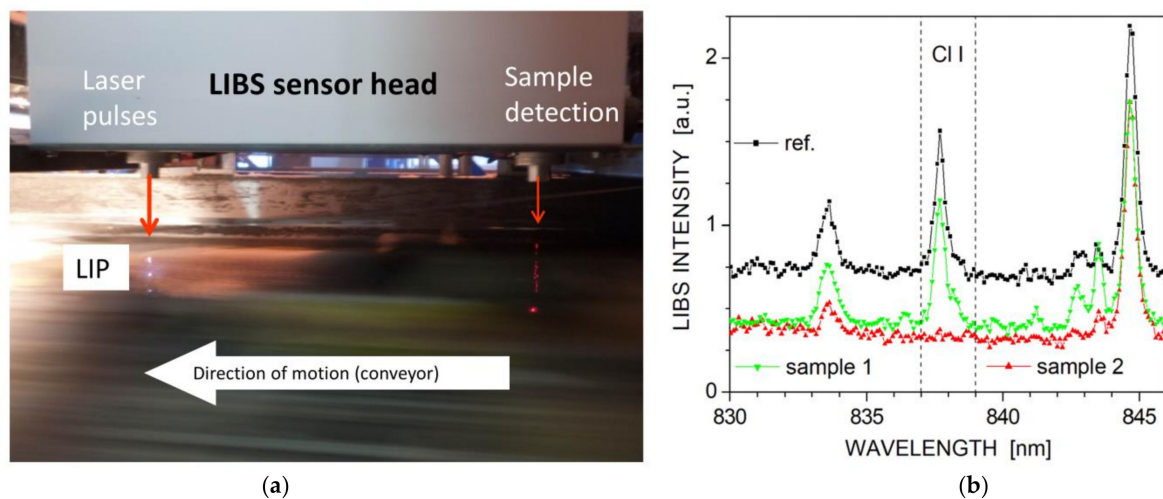
Figure 21. LIBS in-line measurement of waste polymers. (**a**) Photograph of the LIBS sensor head mounted above a conveyor belt in a waste sorting plant. (**b**) LIBS spectra of two polymer waste samples and a pure PVC reference sample. Chlorine emission line at 837.6 nm used for PVC detection. Adapted from [343].

The LIBS spectra (100 measurements/sec) were evaluated in real-time comparing the NIR range with the Cl emission line at around 837.6 nm. LIBS spectra of two different polymer waste samples measured in-line and of a pure PVC reference sample are shown in Figure 21b. PVC pieces were identified by a high correlation of spectra of the waste and reference materials (e.g., sample 1). Waste polymers of low optical reflectivity are difficult to measure by standard NIR reflectance sensors, but they are easy to measure with LIBS as this signal is largely independent of the sample color. Similar measurements were performed on polymer recyclate material to identify impurities such as PVC and surface

contaminations in recycled PET flakes [481]. LIBS analysis of heavy metals and halogens in waste polymers has been reported by several groups, e.g., [345,347,482,483].

In the production of plastics, new polymers are often diluted with recycled material. The properties (mechanical, color, chemical) of the diluted polymer should be monitored to keep it within specifications. This is a challenging task as the chemical and mechanical properties are usually tuned via a huge variety of additives such as inorganic coloring pigments, flame retardants, and various thermal and photochemical stabilizers. LIBS can be used for the elemental monitoring of recycled plastics in the production process. A demonstration of LIBS monitoring in polymer production is illustrated in Figure 22 [418]. The produced polymer material is measured at the extrusion orifice of an industrial extruder in a recycling plant (Figure 22a). In addition to the elemental analysis by LIBS, other parameters of the recycled material such as color and strength can also be measured.
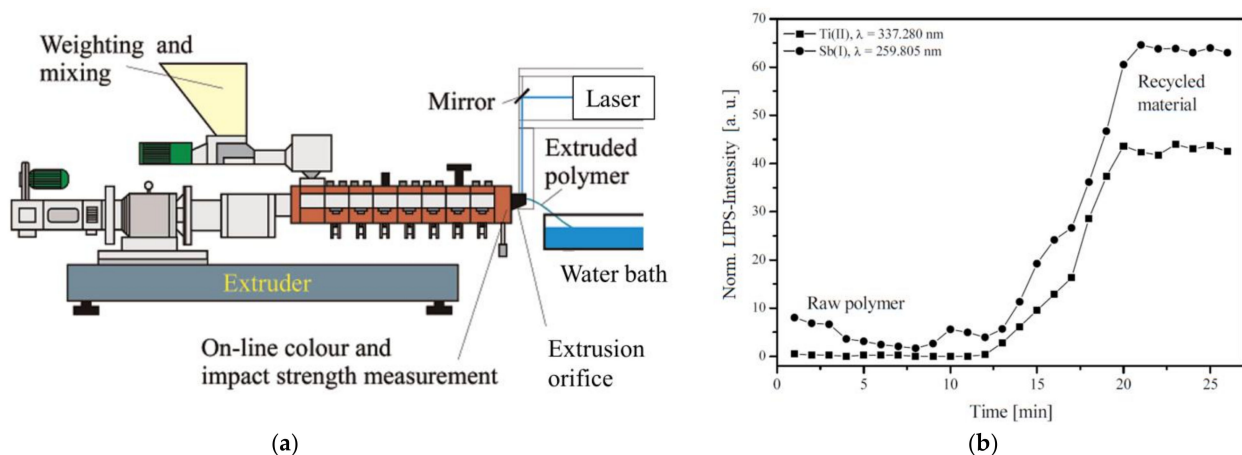

Figure 22. LIBS in-line measurement of polymers in a recycling plant. (**a**) Schematic of the LIBS sensor installed at a polymer extruder. (**b**) Detection of different types of polymer material at the extruder by means of LIBS intensities measured for Ti and Sb. Adapted from [418].

The monitoring of chemical composition of polymers is shown in Figure 22b. The measured LIBS intensities for Ti and Sb (from additives) are changing with extrusion time as the raw polymeric material (ABS) is increasingly replaced by recycled plastic material (granulate from casings of electronic waste) [418]. After completion of transition from raw to recycled material (at approx. 20 min time) the elemental signals reach a plateau level. The elemental monitoring allows to control the polymer composition and to automatically discard undesirable fractions of the recycled material.

5.12. Welds

Welding processes are one of the most commonly used joining technologies. Defects in the weld metal reduce the safety and integrity of a weldment. For the welding of stainless steel, the chemical composition of the weld metal determines the solidification of the steel and the weld metal quality. For the inspection of weld seams, various destructive and non-destructive methods are employed after completion of the welding process. Inspection during the welding process would save time and effort. LIBS can be used for in-situ weld pool monitoring during the welding process. Tungsten inert gas welding of austenitic stainless steel was monitored by LIBS to measure in-situ changes of the chemical composition [402]. Figure 23a shows the schematic of an in-situ LIBS monitor in a welding process.
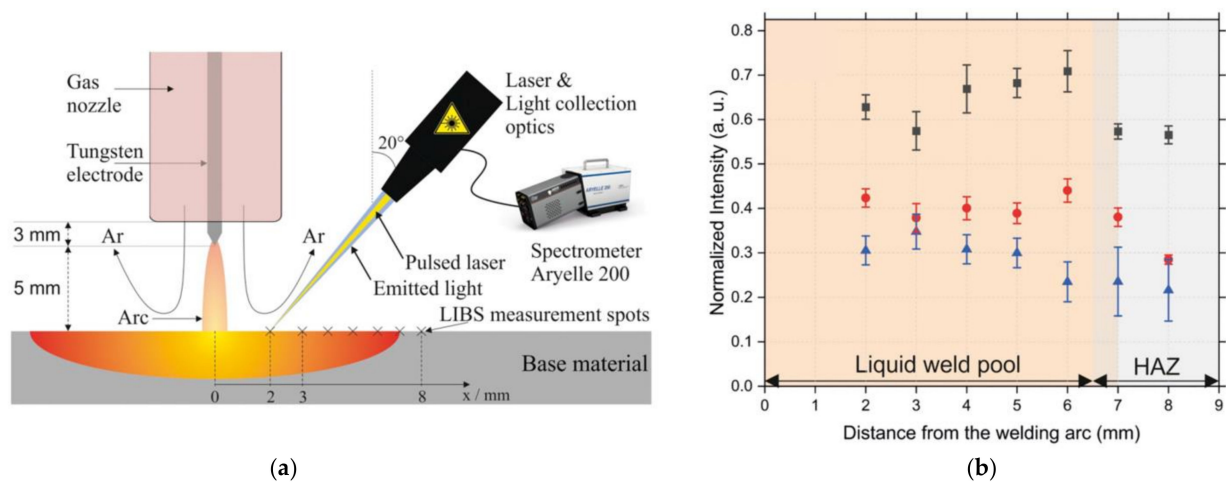
Figure 23. In-situ LIBS measurement of tungsten inert gas (TIG) stainless steel welding. (**a**) Experimental set-up of welding and LIBS equipment. (**b**) Intensities of Cr I/Fe I (black squares), Ni I/Fe I (red circles), and Mn I/Fe I (blue triangles) were measured at different distance to the welding arc (HAZ is heated affected zone). Adapted from [402].

The normalized intensities for elements Cr, Ni, and Mn recorded during welding at various positions on the weld metal are shown in Figure 23b. After solidification of the weld pool the intensity for Mn strongly dropped, whereas intensities for Cr and Ni were almost unchanged. The formation of Mn vapor above the weld pool and condensation of Mn on the weld metal surface was concluded from the measurements. The results proved that LIBS can be used in situ to inspect the TIG welding process.

6. Conclusions

The major strengths of LIBS from the application point of view are the versatility, the multi-element detection, and the field suitability of the method. LIBS enables for fast measurements without or with only little sample preparation reaching detection limits in the low ppm range, typically. The major limitation of LIBS is its rather low sensitivity ("ppm barrier"), which does not compete with laboratory-based laser analytical techniques such as LA-ICP-MS and LA-ICP-OES. These methods have better analytical performance in terms of LOD and LOQ reaching values in the ppb range, typically. However, the field suitability of LIBS enables to use LIBS-based sensors for in-line and at-line measurements in industrial production and for other applications under harsh conditions out of the laboratory. The ongoing rapid development of laser sources, efficient spectrometers, and sensitive light detection systems is a driving force for the further development of robust LIBS systems and of hand-held LIBS devices. New solid state lasers with high repetition rate and high average power, e.g., advanced fiber lasers and compact Nd:YAG lasers, are supporting this development. Fast element analysis of primary and secondary raw materials, of semi-finished workpieces, and of finished goods is an area with large growth potential. LIBS-based sensors can contribute to the efficient use of resource materials and the accurate chemical monitoring of materials in production. The progress in LIBS measurement technology and the increasing demands for efficient production processes will continue triggering the development of new in-line, at-line, and on-site applications of this laser-analytical method in the near future.

Author Contributions: Conceptualization, J.D.P.; methodology, J.D.P.; validation, S.T., S.G., N.G., S.E.-F. and J.H.; investigation, S.T., S.G., N.G., S.E.-F. and J.H.; resources, S.T., S.G., N.G., S.E.-F., and J.H.; writing—original draft preparation, J.D.P.; writing—review and editing, J.D.P.; funding acquisition, J.D.P. All authors have read and agreed to the published version of the manuscript.

Institutional Review Board Statement: Not applicable.

Informed Consent Statement: Not applicable.

Data Availability Statement: The datasets analyzed or generated during the study are not publicly archived. All datasets are compiled from data available in the cited references.

Conflicts of Interest: The authors declare no conflict of interest. The funders had no role in the design of the study; in the collection, analyses, or interpretation of data; in the writing of the manuscript, or in the decision to publish the results.

Appendix A

Figure A1 shows the annual number of scientific publications on LIBS as retrieved from the SCOPUS database in June 2021 using the search terms "laser induced breakdown spectroscopy" and "laser induced plasma spectroscopy" [484].
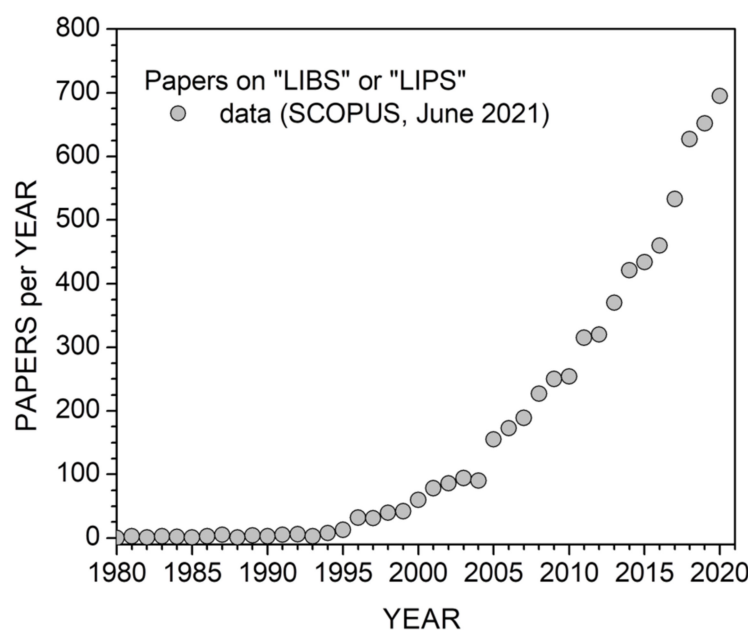
Figure A1. Number of scientific papers on LIBS or LIPS published per year (SCOPUS, June 2021) [484].

The distribution of country affiliations of LIBS papers published in years 2001–2010 and 2011–2020 is shown in Figure A2 (the 15 most frequent country affiliations). More than 80% of the papers are published by research groups in theses 15 countries.
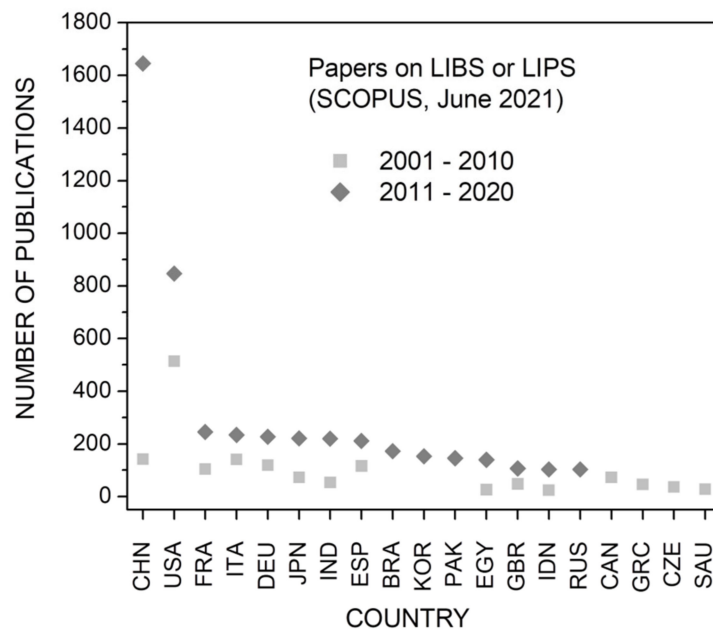
Figure A2. Fifteen top countries, i.e., most frequent country affiliations, regarding scientific papers on LIBS or LIPS published in years 2001–2010 and 2011–2020 (SCOPUS, June 2021) [484].

China and the United States account for more than 35% of the scientific publications on LIBS or LIPS.

Figure A3 shows the table of elements with the LOD values obtained by LIBS measurements of solid sample materials (data taken from www.LIBS-info.com [50]). For each element, the LOD values reported in several publications are averaged. The number above the atomic symbol is the number of publications used. For some elements only one publication was available. The number below the atomic symbol is the average LOD value in ppm.
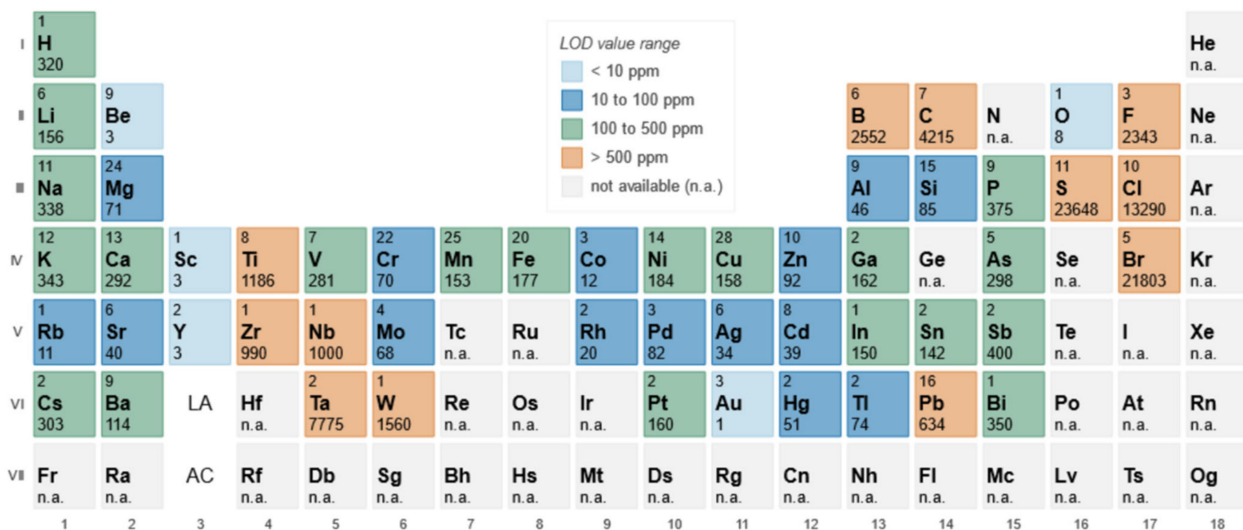
Figure A3. LOD values reported for LIBS analysis of solid materials (data: www.LIBS-info.com [50], accessed on 31 May 2021).

Figure A4 shows the correlation of reported LOD values [50] and calculated emission rate EMRA of elements (calculated for LTE plasma at temperature T_e = 10,000 K, average

over the most intense emission lines for each element). A higher EMRA favors lower LOD values for most of the elements (order of magnitude estimate).
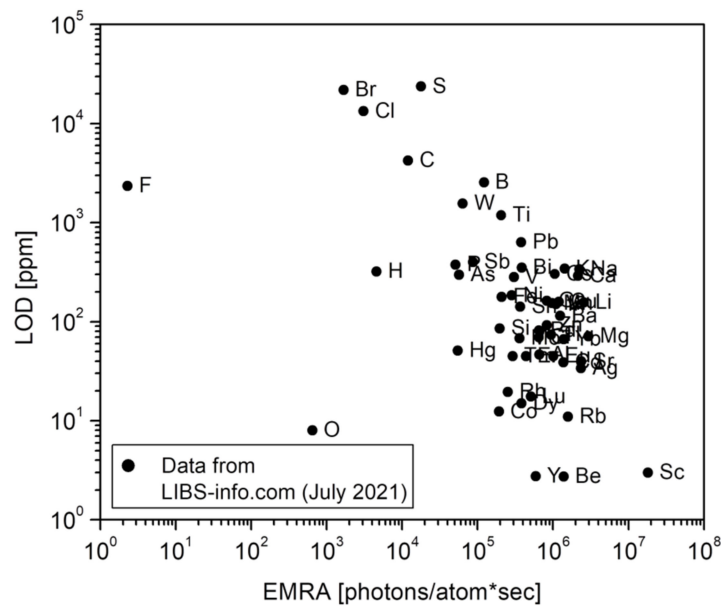
Figure A4. Correlation of reported LOD values for LIBS analysis of solid materials with calculated emission rate EMRA of LIBS plasma for various elements. The sign "*" stands for multiplication.

Figure A5 shows the total number of smartphones sold to end-users in the time period 2007 to 2021 (values for 2020 and 2021 are estimates) [432].
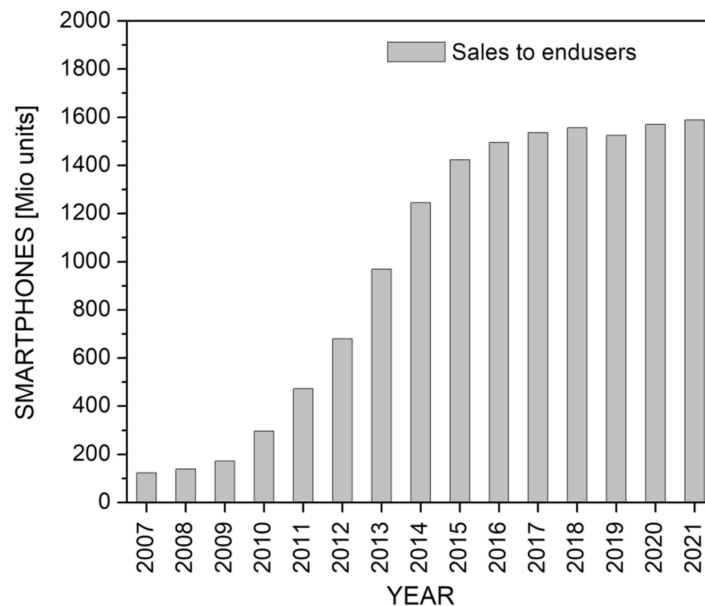
Figure A5. Global sales of smartphones to end-users from 2007 to 2021 [432].

References

1. Singh, J.P.; Thakur, S.N. *Laser-Induced Breakdown Spectroscopy*, 2nd ed.; Elsevier: Amsterdam, Netherlands, 2020.
2. Mussazzi, S.; Perini, U. *Laser-Induced Breakdown Spectroscopy: Theory and Applications*; Springer Series in Optical Sciences; Springer: Berlin/Heidelberg, Germany, 2014; Volume 182.

3. Hahn, D.W.; Omenetto, N. Laser-induced breakdown spectroscopy (LIBS), part I: Review of basic diagnostics and plasma particle interactions: Still-challenging issues within the analytical plasma community. *Appl. Spectrosc.* **2010**, *64*, 335A–366A. [CrossRef]

4. Hahn, D.W.; Omenetto, N. Laser-induced breakdown spectroscopy (LIBS), part II: Review of instrumental and methodological approaches to material analysis and applications to different fields. *Appl. Spectrosc.* **2012**, *66*, 347–419. [CrossRef]

5. Pathak, A.K.; Kumar, R.; Singh, V.K.; Agrawal, R.; Rai, S.; Rai, A.K. Assessment of LIBS for spectrochemical analysis: A review. *Appl. Spectrosc. Rev.* **2012**, *47*, 14–40. [CrossRef]

6. Noll, R. *Laser Induced Breakdown Spectroscopy, Fundamentals and Applications*; Springer: Berlin/Heidelberg, Germany, 2012.

7. Miziolek, A.W.; Palleschi, V.; Schechter, I. *Laser-Induced Breakdown Spectroscopy (LIBS), Fundamentals and Applications*; Cambridge University Press: Cambridge, UK, 2006.

8. Cremers, D.A.; Radziemski, L.J. *Handbook of Laser-Induced Breakdown Spectroscopy*; John Wiley & Sons Ltd.: Chichester, West Sussex, UK, 2006.

9. Carter, S.; Clough, R.; Fisher, A.; Gibson, B.; Russell, B.; Waack, J. Atomic spectrometry update: Review of advances in the analysis of metals, chemicals and materials. *J. Anal. At. Spectrom.* **2020**, *35*, 2410–2474. [CrossRef]

10. Christesen, S.D.; Fountain III, A.W.; Chyba, T.H.; Pearman, W.F.; Guicheteau, J.A. Laser spectroscopy for the detection of chemical, biological and explosive threats. In *Laser Spectroscopy for Sensing: Fundamentals, Techniques and Applications*; Baudelet, M., Ed.; Woodhead: Cambridge, UK, 2014; Chapter 13; pp. 393–420. [CrossRef]

11. Panya panya, S.N.; Galmed, A.H.; Maaza, M.; Mothudi, B.M.; Harith, M.A.; Kennedy, J. Laser-Induced Breakdown Spectroscopy (LIBS) on Geological Samples: Compositional Differentiation. *MRS Adv.* **2018**, *3*, 1969–1983. [CrossRef]

12. Qiao, S.; Ding, Y.; Tian, D.; Yao, L.; Yang, G. A Review of Laser-Induced Breakdown Spectroscopy for Analysis of Geological Materials. *Appl. Spectrosc. Rev.* **2015**, *50*, 1–26. [CrossRef]

13. Botto, A.; Campanella, B.; Legnaioli, S.; Lezzerini, M.; Lorenzetti, G.; Pagnotta, S.; Poggialini, F.; Palleschi, V. Applications of laser-induced breakdown spectroscopy in cultural heritage and archaeology: A critical review. *J. Anal. At. Spectrom.* **2019**, *34*, 81–103. [CrossRef]

14. Lazic, V.; Vadrucci, M.; Fantoni, R.; Chiari, M.; Mazzinghi, A.; Gorghinian, A. Applications of laser induced breakdown spectroscopy for cultural heritage: A comparison with XRF and PIXE techniques. *Spectrochim. Acta Part B* **2018**, *149*, 1–14. [CrossRef]

15. Rehse, S.J. A review of the use of laser-induced breakdown spectroscopy for bacterial classification, quantification, and identification. *Spectrochim. Acta Part B* **2019**, *154*, 50–69. [CrossRef]

16. Gaudiuso, R.; Melikechi, N.; Abdel-Salam, Z.A.; Harith, M.A.; Palleschi, V.; Motto-Ros, V.; Busser, B. Laser-induced breakdown spectroscopy for human and animal health: A review. *Spectrochim. Acta Part B* **2018**, *152*, 123–148. [CrossRef]

17. Singh, V.K.; Rai, A.K. Prospects for laser-induced breakdown spectroscopy for biomedical applications: A review. *Lasers Med. Sci.* **2011**, *26*, 673–687. [CrossRef]

18. Baudelet, M.; Guyon, L.; Yu, J.; Wolf, J.-P.; Amodeo, T.; Frájafon, E.; Laloi, P. Femtosecond time-resolved laser-induced breakdown spectroscopy for detection and identification of bacteria: A comparison to the nanosecond regime. *J. Appl. Phys.* **2006**, *99*, 084701. [CrossRef]

19. Fortes, F.J.; Guirado, S.; Metzinger, A.; Laserna, J.J. A study of underwater stand-off laser-induced breakdown spectroscopy for chemical analysis of objects in the deep ocean. *J. Anal. At. Spectrom.* **2015**, *30*, 1050–1056. [CrossRef]

20. Thornton, B.; Takahashi, T.; Sato, T.; Sakka, T.; Tamura, A.; Matsumoto, A.; Nozaki, T.; Ohki, T.; Ohki, K. Development of a deep-sea laser-induced breakdown spectrometer for in situ multi-element chemical analysis. *Deep Sea Res. Part I* **2015**, *95*, 20–36. [CrossRef]

21. Wiens, R.C.; Maurice, S.; Barraclough, B.; Saccoccio, M.; Barkley, W.C.; Bell III, J.F.; Bender, S.; Bernardin, J.; Blaney, D.; Blank, J.; et al. The chemcam instrument suite on the mars science laboratory (MSL) rover: Body unit and combined system tests. *Space Sci. Rev.* **2012**, *170*, 167–227. [CrossRef]

22. Nachon, M.; Clegg, S.M.; Mangold, N.; Schröder, S.; Kah, L.C.; Dromart, G.; Ollila, A.; Johnson, J.R.; Oehler, D.Z.; Bridges, J.C.; et al. Calcium sulfate veins characterized by chemcam/curiosity at gale crater, mars. *J. Geophys. Res. Planets* **2014**, *119*, 1991–2016. [CrossRef]

23. NASA, Mars Science Laboratory. Available online: http://www.nasa.gov/mission_pages/msl/index.html (accessed on 24 February 2021).

24. NASA, Mars Perseverance Rover. Available online: https://www.nasa.gov/perseverance (accessed on 24 February 2021).

25. Zhang, Y.; Zhang, T.; Li, H. Application of laser-induced breakdown spectroscopy (LIBS) in environmental monitoring. *Spectrochim. Acta Part B* **2021**, *181*, 106218. [CrossRef]

26. Gonçalves, D.A.; Senesi, G.S.; Nicolodelli, G. Laser-induced breakdown spectroscopy applied to environmental systems and their potential contaminants. An overview of advances achieved in the last few years. *Trends Environ. Anal. Chem.* **2021**, *30*, e00121. [CrossRef]

27. Zorov, N.B.; Popov, A.M.; Zaytsev, S.M.; Labutin, T.A. Qualitative and quantitative analysis of environmental samples by laser-induced breakdown spectrometry. *Russ. Chem. Rev.* **2015**, *84*, 1021–1050. [CrossRef]

28. Yu, X.; Li, Y.; Gu, X.; Bao, J.; Yang, H.; Sun, L. Laser-induced breakdown spectroscopy application in environmental monitoring of water quality: A review. *Environ. Monit. Assess.* **2014**, *186*, 8969–8980. [CrossRef] [PubMed]

29. Bäuerle, D. *Laser Processing and Chemistry*, 4th ed.; Springer: Berlin/Heidelberg, Germany, 2011.

30. Konjević, N.; Ivković, M.; Jovićević, S. Spectroscopic diagnostics of laser-induced plasmas. *Spectrochim. Acta Part B* **2010**, *65*, 593–602. [CrossRef]

31. Kautz, E.J.; Rönnebro, E.C.E.; Devaraj, A.; Senor, D.J.; Harilal, S.S. Detection of hydrogen isotopes in zircaloy-4 via femtosecond LIBS. *J. Anal. At. Spectrom.* **2021**, *36*, 1217–1227. [CrossRef]

32. Giannakaris, N.; Haider, A.; Ahamer, C.M.; Grünberger, S.; Trautner, S.; Pedarnig, J.D. Femtosecond single-pulse and orthogonal double-pulse laser-induced breakdown spectroscopy (LIBS): Femtogram mass detection and chemical imaging with micrometer spatial resolution. *Appl. Spectrosc.* **2021**. published online. [CrossRef]

33. He, X.; Chen, B.; Chen, Y.; Li, R.; Wang, F. Femtosecond laser-ablation spark-induced breakdown spectroscopy and its application to the elemental analysis of aluminum alloys. *J. Anal. At. Spectrom.* **2018**, *33*, 2203–2209. [CrossRef]

34. Ahamer, C.M.; Pedarnig, J.D. Femtosecond double pulse laser-induced breakdown spectroscopy: Investigation of the intensity enhancement. *Spectrochim. Acta Part B* **2018**, *148*, 23–30. [CrossRef]

35. Ahamer, C.M.; Riepl, K.M.; Huber, N.; Pedarnig, J.D. Femtosecond laser-induced breakdown spectroscopy: Elemental imaging of thin films with high spatial resolution. *Spectrochim. Acta Part B* **2017**, *136*, 56–65. [CrossRef]

36. Zhang, D.; Chen, A.; Wang, X.; Li, S.; Wang, Y.; Sui, L.; Jiang, Y.; Jin, M. Enhancement mechanism of femtosecond double-pulse laser-induced Cu plasma spectroscopy. *Opt. Laser Technol.* **2017**, *96*, 117–122. [CrossRef]

37. Labutin, T.A.; Lednev, V.N.; Ilyin, A.A.; Popov, A.M. Femtosecond laser-induced breakdown spectroscopy. *J. Anal. At. Spectrom.* **2016**, *31*, 90–118. [CrossRef]

38. Zorba, V.; Mao, X.; Russo, R.E. Femtosecond laser induced breakdown spectroscopy of Cu at the micron/sub-micron scale. *Spectrochim. Acta Part B* **2015**, *113*, 37–42. [CrossRef]

39. Harilal, S.S.; Brumfield, B.E.; LaHaye, N.L.; Hartig, K.C.; Phillips, M.C. Optical spectroscopy of laser-produced plasmas for standoff isotopic analysis. *Appl. Phys. Rev.* **2018**, *5*, 021301. [CrossRef]

40. Bol'shakov, A.A.; Mao, X.L.; Gonzalez, J.J.; Russo, R.E. Laser ablation molecular isotopic spectrometry (LAMIS): Current state of the art. *J. Anal. At. Spectrom.* **2016**, *31*, 119–134. [CrossRef]

41. Otto, M. *Chemometrics—Statistics and Computer Application in Analytical Chemistry*, 5th ed.; Wiley-VCH: Weinheim, Germany, 2019.

42. Torrione, R.; Collins, L.M.; Morton Jr, K.D. Multivariate analysis, chemometrics, and machine learning in laser spectroscopy. In *Laser Spectroscopy for Sensing: Fundamentals, Techniques And Applications*; Baudelet, M., Ed.; Woodhead: Cambridge, UK, 2014; Chapter 5; pp. 125–164. [CrossRef]

43. Poitrasson, F.; d'Abzac, F.-X. Femtosecond laser ablation inductively coupled plasma source mass spectrometry for elemental and isotopic analysis: Are ultrafast lasers worthwhile? *J. Anal. At. Spectrom.* **2017**, *32*, 1075–1091. [CrossRef]

44. LaHaye, N.L.; Phillips, M.C.; Duffin, A.M.; Eiden, G.C.; Harilal, S.S. The influence of ns- and fs-LA plume local conditions on the performance of a combined LIBS/LA-ICP-MS sensor. *J. Anal. At. Spectrom.* **2016**, *31*, 515–522. [CrossRef]

45. Koch, J.; Günther, D. Review of the State-of-the-Art of Laser Ablation Inductively Coupled Plasma Mass Spectrometry. *Appl. Spectrosc.* **2011**, *65*, 155A–162A. [CrossRef]

46. Knobel, R.; Behrens, H.; Schwarzburger, N.I.; Binnewies, M.; Horn, I. Kinetics of lithium intercalation in TiX_2 single crystals (X = S, Se, Te) under hydrostatic pressure. *Z. Phys. Chem.* **2015**, *229*, 1289–1312. [CrossRef]

47. Bian, Q.Z.; Koch, J.; Lindner, H.; Berndt, H.; Hergenröder, R.; Niemax, K. Non-matrix matched calibration using near-IR femtosecond laser ablation inductively coupled plasma optical emission spectrometry. *J. Anal. At. Spectrom.* **2005**, *20*, 736–740. [CrossRef]

48. Ciucci, A.; Corsi, M.; Palleschi, V.; Rastelli, S.; Salvetti, A.; Tognoni, E. New procedure for quantitative elemental analysis by laser induced plasma spectroscopy. *Appl. Spectrosc.* **1999**, *53*, 960–964. [CrossRef]

49. Tognoni, E.; Cristoforetti, G.; Legnaioli, S.; Palleschi, V.; Salvetti, A.; Mueller, M.; Panne, U.; Gornushkin, I. A numerical study of expected accuracy and precision in calibration-free laser-induced breakdown spectroscopy in the assumption of ideal analytical plasma. *Spectrochim. Acta Part B* **2007**, *62*, 1287–1302. [CrossRef]

50. LIBS Info (2021). And: Applied Photonics Ltd. (2019), Analytical Capabilities of LIBS. Available online: http://www.appliedphotonics.co.uk/Libs/capabilities_libs.htm (accessed on 23 January 2019).

51. Ahamer, C.M.; Eschlböck-Fuchs, S.; Kolmhofer, P.J.; Rössler, R.; Huber, N.; Pedarnig, J.D. Laser-induced breakdown spectroscopy of major and minor oxides in steel slags: Influence of detection geometry and signal normalization. *Spectrochim. Acta Part B* **2016**, *122*, 157–164. [CrossRef]

52. NIST Atomic Spectra Database. Available online: http://physics.nist.gov/PhysRefData/ASD/ (accessed on 14 July 2021).

53. Sansonetti, J.; Martin, W.; Young, S. Handbook of Basic Atomic Spectroscopic Data (version 1.1.2). 2005. Available online: http://physics.nist.gov/Handbook (accessed on 14 July 2021).

54. IUPAC, International Union of Pure and Applied Chemistry. 2021. Available online: https://iupac.org/ (accessed on 14 July 2021).

55. Eschlböck-Fuchs, S.; Demidov, A.; Gornushkin, I.B.; Schmid, T.; Rössler, R.; Huber, N.; Panne, U.; Pedarnig, J.D. Tomography of homogenized laser-induced plasma by Radon transform technique. *Spectrochim. Acta Part B* **2016**, *123*, 59–67. [CrossRef]

56. Ctvrtníkova, T.; Cabalín, L.M.; Laserna, J.; Kanický, V. Comparison of double-pulse and single-pulse laser-induced breakdown spectroscopy techniques in the analysis of powdered samples of silicate raw materials for the brick-and-tile industry. *Spectrochim. Acta Part B* **2008**, *63*, 42–50. [CrossRef]

57. St-Onge, L.; Sabsabi, M.; Cielo, P. Analysis of solids using laser-induced plasma spectroscopy in double-pulse mode. *Spectrochim. Acta Part B* **1998**, *53*, 407–415. [CrossRef]

58. Babushok, V.I.; DeLucia, F.C., Jr.; Gottfried, J.L.; Munson, C.A.; Miziolek, A.W. Double pulse laser ablation and plasma: Laser induced breakdown spectroscopy signal enhancement. *Spectrochim. Acta Part B* **2006**, *61*, 999–1014. [CrossRef]

59. Viskup, R.; Praher, B.; Linsmeyer, T.; Scherndl, H.; Pedarnig, J.D.; Heitz, J. Influence of pulse-to-pulse delay for 532 nm double-pulse laser-induced breakdown spectroscopy of technical polymers. *Spectrochim. Acta Part B* **2010**, *65*, 935–942. [CrossRef]

60. Windom, B.C.; Hahn, D.W. Laser ablation—laser induced breakdown spectroscopy (LA-LIBS): A means for overcoming matrix effects leading to improved analyte response. *J. Anal. At. Spectrom.* **2009**, *24*, 1665–1675. [CrossRef]

61. Heilbrunner, H.; Huber, N.; Wolfmeir, H.; Arenholz, E.; Pedarnig, J.D.; Heitz, J. Double-pulse laser-induced breakdown spectroscopy for trace element analysis in sintered iron oxide ceramics. *Appl. Phys. A: Mater. Sci. Process.* **2012**, *106*, 15–23. [CrossRef]

62. Grünberger, S.; Eschlböck-Fuchs, S.; Hofstadler, J.; Pissenberger, A.; Duchaczek, H.; Trautner, S.; Pedarnig, J.D. Analysis of minor elements in steel and chemical imaging of micro-patterned polymer by laser ablation-spark discharge-optical emission spectroscopy and laser-induced breakdown spectroscopy. *Spectrochim. Acta Part B* **2020**, *169*, 105884. [CrossRef]

63. Grünberger, S.; Watzl, G.; Huber, N.; Eschlböck-Fuchs, S.; Hofstadler, J.; Pissenberger, A.; Duchaczek, H.; Trautner, S.; Pedarnig, J.D. Chemical imaging with Laser Ablation—Spark Discharge—Optical Emission Spectroscopy (LA-SD-OES) and Laser-Induced Breakdown Spectroscopy (LIBS). *Opt. Laser Technol.* **2020**, *123*, 105944. [CrossRef]

64. Kexue, L.I.; Zhou, W.; Shen, Q.; Shao, J.; Qian, H. Signal enhancement of lead and arsenic in soil using laser ablation combined with fast electric discharge. *Spectrochim. Acta Part B* **2010**, *65*, 420–424. [CrossRef]

65. Chen, Y.; Zhang, Q.; Li, G.; Li, R.; Zhou, J. Laser ignition assisted spark-induced breakdown spectroscopy for the ultra-sensitive detection of trace mercury ions in aqueous solutions. *J. Anal. At. Spectrom.* **2010**, *25*, 1969–1973. [CrossRef]

66. Deng, W.; Liu, Y.; Wei, G.; Li, X.; Tu, X.; Xie, L.; Zhang, H.; Sun, W. High-precision analysis of Sr/Ca and Mg/Ca ratios in corals by laser ablation inductively coupled plasma optical emission spectrometry. *J. Anal. At. Spectrom.* **2010**, *25*, 84–87. [CrossRef]

67. Pedarnig, J.D.; Heitz, J.; Ionita, E.R.; Dinescu, G.; Praher, B.; Viskup, R. Combination of RF—plasma jet and Laser—induced plasma for breakdown spectroscopy analysis of complex materials. *Appl. Surf. Sci.* **2011**, *257*, 5452–5455. [CrossRef]

68. Iqbal, A.; Sun, Z.; Wall, M.; Alwahabi, Z.T. Sensitive elemental detection using microwave-assisted laser-induced breakdown imaging. *Spectrochim. Acta Part B* **2017**, *136*, 16–22. [CrossRef]

69. Ikeda, Y.; Moon, A.; Kaneko, M. Development of microwave-enhanced spark-induced breakdown spectroscopy. *Appl. Opt.* **2010**, *49*, C95–C100. [CrossRef]

70. Liu, Y.; Baudelet, M.; Richardson, M. Elemental analysis by microwave-assisted laser-induced breakdown spectroscopy: Evaluation on ceramics. *J. Anal. At. Spectrom.* **2010**, *25*, 1316–1323. [CrossRef]

71. Liu, J.; Shen, X.-J.; Xu, P.; Cui, F.-P.; Shi, X.-X.; Li, X.-P.; Wang, H.-Z. Research on on-line classification system of aluminum alloy for laser-induced breakdown spectrum. *Spectrosc. Spectr. Analysis.* **2020**, *40*, 3901–3905.

72. Piorek, S. Rapid sorting of aluminum alloys with handheld μLIBS analyzer. *Mater. Today Proc.* **2019**, *10*, 348–354. [CrossRef]

73. Aragón, C.; Aguilera, J.A. Direct analysis of aluminum alloys by CSigma laser-induced breakdown spectroscopy. *Anal. Chim. Acta* **2018**, *1009*, 12–19. [CrossRef]

74. Bennett, B.N.; Martin, M.Z.; Leonard, D.N.; Garlea, E. Calibration curves for commercial copper and aluminum alloys using handheld laser-induced breakdown spectroscopy. *Appl. Phys. B Lasers Opt.* **2018**, *124*, 42. [CrossRef]

75. Sun, D.; Ma, Y.; Wang, Y.; Su, M.; Lu, Q.; Dong, C. Determination of the limits of detection for aluminum-based alloys by spatially resolved single-and double-pulse laser-induced breakdown spectroscopy. *Anal. Methods* **2018**, *10*, 2595–2603. [CrossRef]

76. Doucet, F.R.; Belliveau, T.F.; Fortier, J.-L.; Hubert, J. Use of chemometrics and laser-induced breakdown spectroscopy for quantitative analysis of major and minor elements in aluminium alloys. *Appl. Spectrosc.* **2007**, *61*, 327–332. [CrossRef]

77. Campanella, B.; Grifoni, E.; Legnaioli, S.; Lorenzetti, G.; Pagnotta, S.; Sorrentino, F.; Palleschi, V. Classification of wrought aluminum alloys by ANN evaluation of LIBS spectra from aluminum scrap samples. *Spectrochim. Acta Part B* **2017**, *134*, 52–57. [CrossRef]

78. Zivkovic, S.; Savovic, J.; Trtica, M.; Mutic, J.; Momcilovic, M. Elemental analysis of aluminum alloys by laser induced breakdown spectroscopy based on TEA CO_2 laser. *J. Alloy. Compd.* **2017**, *700*, 175–184. [CrossRef]

79. Cristoforetti, G.; Legnaioli, S.; Palleschi, V.; Salvetti, A.; Tognoni, E.; Benedetti, P.A.; Brioschi, F.; Ferrario, F. Quantitative analysis of aluminium alloys by low-energy, high-repetition rate laser-induced breakdown spectroscopy. *J. Anal. At. Spectrom.* **2006**, *21*, 697–702. [CrossRef]

80. Kaufmann, H.; Fragner, W.; Uggowitzer, P.J. Influence of variations in alloy composition on castability and process stability. Part 2: Semi-solid casting processes. *Int. J. Cast Met. Res.* **2005**, *18*, 279–285. [CrossRef]

81. Völker, T.; Millar, S.; Strangfeld, C.; Wilsch, G. Identification of type of cement through laser-induced breakdown spectroscopy. *Constr. Build. Mater.* **2020**, *258*, 120345. [CrossRef]

82. Mateo, J.; Quintero, M.C.; Fernández, J.M.; García, M.C.; Rodero, A. Application of LIBS technology for determination of Cl concentrations in mortar samples. *Constr. Build. Mater.* **2019**, *204*, 716–726. [CrossRef]

83. Dietz, T.; Klose, J.; Kohns, P.; Ankerhold, G. Quantitative determination of chlorides by molecular laser-induced breakdown spectroscopy. *Spectrochim. Acta Part B* **2019**, *152*, 59–67. [CrossRef]

84. Millar, S.; Gottlieb, C.; Günther, T.; Sankat, N.; Wilsch, G.; Kruschwitz, S. Chlorine determination in cement-bound materials with laser-induced breakdown spectroscopy (LIBS)—A review and validation. *Spectrochim. Acta Part B* **2018**, *147*, 1–8. [CrossRef]

85. Yin, H.; Hou, Z.; Zhang, L.; Zhang, X.; Wang, Z.; Li, Z. Cement raw material quality analysis using laser-induced breakdown spectroscopy. *J. Anal. At. Spectrom.* **2016**, *31*, 2384–2390. [CrossRef]

86. Xia, H.; Bakker, M.C.M. Reliable classification of moving waste materials with LIBS in concrete recycling. *Talanta* **2014**, *120*, 239–247. [CrossRef] [PubMed]

87. Labutin, T.A.; Popov, A.M.; Raikov, S.N.; Zaytsev, S.M.; Labutina, N.A.; Zorov, N.B. Determination of chlorine in concrete by laser-induced breakdown spectroscopy in air. *J. Appl. Spectrosc.* **2013**, *80*, 315–318. [CrossRef]

88. Mansoori, A.; Roshanzadeh, B.; Khalaji, M.; Tavassoli, S.H. Quantitative analysis of cement powder by laser induced breakdown spectroscopy. *Opt. Lasers Eng.* **2011**, *49*, 318–323. [CrossRef]

89. Gondal, M.A.; Yamani, Z.H.; Hussain, T.; Al-Amoudi, O.S.B. Determination of chloride content in different types of cement using laser-induced breakdown spectroscopy. *Spectrosc. Lett.* **2009**, *42*, 171–177. [CrossRef]

90. Gehlen, C.D.; Wiens, E.; Noll, R.; Wilsch, G.; Reichling, K. Chlorine detection in cement with laser-induced breakdown spectroscopy in the infrared and ultraviolet spectral range. *Spectrochim. Acta Part B* **2009**, *64*, 1135–1140. [CrossRef]

91. Weritz, F.; Schaurich, D.; Wilsch, G. Detector comparison for sulfur and chlorine detection with laser induced breakdown spectroscopy in the near-infrared-region. *Spectrochim. Acta Part B* **2007**, *62*, 1504–1511. [CrossRef]

92. Guo, L.-B.; Zhang, D.; Sun, L.-X.; Yao, S.-C.; Zhang, L.; Wang, Z.-Z.; Wang, Q.-Q.; Ding, H.-B.; Lu, Y.; Hou, Z.-Y.; et al. Development in the application of laser-induced breakdown spectroscopy in recent years: A review. *Front. Phys.* **2021**, *16*, 22500. [CrossRef]

93. Zhang, W.; Zhuo, Z.; Lu, P.; Tang, J.; Tang, H.; Lu, J.; Xing, T.; Wang, Y. LIBS analysis of the ash content, volatile matter, and calorific value in coal by partial least squares regression based on ash classification. *J. Anal. At. Spectrom.* **2020**, *35*, 1621–1631. [CrossRef]

94. Zhang, Y.; Dong, M.; Cheng, L.; Wei, L.; Cai, J.; Lu, J. Improved measurement in quantitative analysis of coal properties using laser induced breakdown spectroscopy. *J. Anal. At. Spectrom.* **2020**, *35*, 810–818. [CrossRef]

95. Sheta, S.; Afgan, M.S.; Hou, Z.; Yao, S.-C.; Zhang, L.; Li, Z.; Wang, Z. Coal analysis by laser-induced breakdown spectroscopy: A tutorial review. *J. Anal. At. Spectrom.* **2019**, *34*, 1047–1082. [CrossRef]

96. Li, W.; Lu, J.; Dong, M.; Lu, S.; Yu, J.; Li, S.; Huang, J.; Liu, J. Quantitative analysis of calorific value of coal based on spectral preprocessing by laser-induced breakdown spectroscopy (LIBS). *Energy Fuels* **2018**, *32*, 24–32. [CrossRef]

97. Yan, C.; Qi, J.; Liang, J.; Zhang, T.; Li, H. Determination of coal properties using laser-induced breakdown spectroscopy combined with kernel extreme learning machine and variable selection. *J. Anal. At. Spectrom.* **2018**, *33*, 2089–2097. [CrossRef]

98. Yao, S.; Mo, J.; Zhao, J.; Li, Y.; Zhang, X.; Lu, W.; Lu, Z. Development of a rapid coal analyzer using laser-induced breakdown spectroscopy (LIBS). *Appl. Spectrosc.* **2018**, *72*, 1225–1233. [CrossRef]

99. He, Y.; Whiddon, R.; Wang, Z.; Liu, Y.; Zhu, Y.; Liu, J.; Cen, K. Inhibition of sodium release from zhundong coal via the addition of mineral additives: Online combustion measurement with laser-induced breakdown spectroscopy (LIBS). *Energy Fuels* **2017**, *31*, 1082–1090. [CrossRef]

100. Redoglio, D.; Golinelli, E.; Musazzi, S.; Perini, U.; Barberis, F. A large depth of field LIBS measuring system for elemental analysis of moving samples of raw coal. *Spectrochim. Acta Part B* **2016**, *116*, 46–50. [CrossRef]

101. Dong, M.; Oropeza, D.; Chirinos, J.; González, J.J.; Lu, J.; Mao, X.; Russo, R.E. Elemental analysis of coal by tandem laser induced breakdown spectroscopy and laser ablation inductively coupled plasma time of flight mass spectrometry. *Spectrochim. Acta Part B* **2015**, *109*, 44–50. [CrossRef]

102. Noll, R.; Fricke-Begemann, C.; Brunk, M.; Connemann, S.; Meinhardt, C.; Scharun, M.; Sturm, V.; Makowe, J.; Gehlen, C. Laser-induced breakdown spectroscopy expands into industrial applications. *Spectrochim. Acta Part B* **2014**, *93*, 41–51. [CrossRef]

103. Wang, Z.; Yuan, T.-B.; Hou, Z.-Y.; Zhou, W.-D.; Lu, J.-D.; Ding, H.-B.; Zeng, X.-Y. Laser-induced breakdown spectroscopy in China. *Front. Phys.* **2014**, *9*, 419–438. [CrossRef]

104. Zhang, L.; Hu, Z.-Y.; Yin, W.-B.; Huang, D.; Ma, W.-G.; Dong, L.; Wu, H.-P.; Li, Z.-X.; Xiao, L.-T.; Jia, S.-T. Recent progress on laser-induced breakdown spectroscopy for the monitoring of coal quality and unburned carbon in fly ash. *Front. Phys.* **2012**, *7*, 690–700. [CrossRef]

105. Romero, C.E.; De Saro, R.; Craparo, J.; Weisberg, A.; Moreno, R.; Yao, Z. Laser-induced breakdown spectroscopy for coal characterization and assessing slagging propensity. *Energy Fuels* **2010**, *24*, 510–517. [CrossRef]

106. Wang, Z.; Liu, R.; Deguchi, Y.; Tanaka, S.; Tainaka, K.; Tanno, K.; Watanabe, H.; Yan, J.; Liu, J. Detection improvement of unburned carbon content in fly ash flow using LIBS with a two-stage cyclone measurement system. *Energy Fuels* **2019**, *33*, 7805–7812. [CrossRef]

107. Zhang, T.; Yan, C.; Qi, J.; Tang, H.; Li, H. Classification and discrimination of coal ash by laser-induced breakdown spectroscopy (LIBS) coupled with advanced chemometric methods. *J. Anal. At. Spectrom.* **2017**, *32*, 1960–1965. [CrossRef]

108. Sanghapi, H.K.; Ayyalasomayajula, K.K.; Yueh, F.Y.; Singh, J.P.; McIntyre, D.L.; Jain, J.C.; Nakano, J. Analysis of slags using laser-induced breakdown spectroscopy. *Spectrochim. Acta Part B* **2016**, *115*, 40–45. [CrossRef]

109. Ctvrtnickova, T.; Mateo, M.P.; Yañez, A.; Nicolas, G. Laser induced breakdown spectroscopy application for ash characterisation for a coal fired power plant. *Spectrochim. Acta Part B* **2010**, *65*, 734–737. [CrossRef]

110. Gaft, M.; Dvir, E.; Modiano, H.; Schone, U. Laser induced breakdown spectroscopy machine for online ash analyses in coal. *Spectrochim. Acta Part B* **2008**, *63*, 1177–1182. [CrossRef]

111. Badawy, T.; Hamza, M.; Mansour, M.S.; Abdel-Hafez, A.-H.H.; Imam, H.; Abdel-Raheem, M.A.; Wang, C.; Lattimore, T. Lean partially premixed turbulent flame equivalence ratio measurements using laser-induced breakdown spectroscopy. *Fuel* **2019**, *237*, 320–334. [CrossRef]

112. Jun, H.M.; Kim, J.H.; Lee, S.H.; Yoh, J.J. Towards simplified monitoring of instantaneous fuel concentration in both liquid and gas fueled flames using a combustor injectable LIBS plug. *Energy* **2018**, *160*, 225–232. [CrossRef]

113. McGann, B.; Carter, C.D.; Ombrello, T.; Do, H. Direct spectrum matching of laser-induced breakdown for concentration and gas density measurements in turbulent reacting flows. *Combust. Flame* **2015**, *162*, 4479–4485. [CrossRef]

114. Letty, C.; Pastore, A.; Mastorakos, E.; Balachandran, R.; Couris, S. Comparison of electrical and laser spark emission spectroscopy for fuel concentration measurements. *Exp. Therm. Fluid Sci.* **2010**, *34*, 338–345. [CrossRef]

115. Phuoc, T.X. Laser-induced spark for simultaneous ignition and fuel-to-air ratio measurements. *Opt. Lasers Eng.* **2006**, *44*, 520–534. [CrossRef]

116. Shin, S.; Moon, Y.; Lee, J.; Jang, H.; Hwang, E.; Jeong, S. Signal processing for real-time identification of similar metals by laser-induced breakdown spectroscopy. *Plasma Sci. Technol.* **2019**, *21*, 034011. [CrossRef]

117. He, X.; Li, R.; Wang, F. Elemental analysis of copper alloy by high repetition rate LA-SIBS using compact fiber spectrometer. *Plasma Sci. Technol.* **2019**, *21*, 034005. [CrossRef]

118. Jiang, Y.; Li, R.; Chen, Y. Elemental analysis of copper alloys with laser-Ablation spark-induced breakdown spectroscopy based on a fiber laser operated at 30 kHz pulse repetition rate. *J. Anal. At. Spectrom.* **2019**, *34*, 1838–1845. [CrossRef]

119. Mal, E.; Junjuri, R.; Gundawar, M.K.; Khare, A. Optimization of temporal window for application of calibration free-laser induced breakdown spectroscopy (CF-LIBS) on copper alloys in air employing a single line. *J. Anal. At. Spectrom.* **2019**, *34*, 319–330. [CrossRef]

120. Tang, Z.; Zhou, R.; Hao, Z.; Ma, S.; Zhang, W.; Liu, K.; Li, X.; Zeng, X.; Lu, Y. Micro-destructive analysis with high sensitivity using double-pulse resonant laser-induced breakdown spectroscopy. *J. Anal. At. Spectrom.* **2019**, *34*, 1198–1204. [CrossRef]

121. Zhao, S.; Zhang, L.; Hou, J.; Zhao, Y.; Yin, W.; Ma, W.; Dong, L.; Xiao, L.; Jia, S. Accurate quantitative CF-LIBS analysis of both major and minor elements in alloys via iterative correction of plasma temperature and spectral intensity. *Plasma Sci. Technol.* **2018**, *20*, 035502. [CrossRef]

122. Guarnaccio, A.; Parisi, G.P.; Mollica, D.; De Bonis, A.; Teghil, R.; Santagata, A. Fs-ns double-pulse laser induced breakdown spectroscopy of copper-based-alloys: Generation and elemental analysis of nanoparticles. *Spectrochim. Acta Part B* **2014**, *101*, 261–268. [CrossRef]

123. De Giacomo, A.; Dell'Aglio, M.; De Pascale, O.; Gaudiuso, R.; Santagata, A.; Teghil, R. Laser induced breakdown spectroscopy methodology for the analysis of copper-based-alloys used in ancient artworks. *Spectrochim. Acta Part B* **2008**, *63*, 585–590. [CrossRef]

124. Imashuku, S.; Taguchi, H.; Fujieda, S.; Suzuki, S.; Wagatsuma, K. Three-dimensional lithium mapping of graphite anode using laser-induced breakdown spectroscopy. *Electrochim. Acta* **2019**, *293*, 78–83. [CrossRef]

125. Cheng, L.; Hou, H.; Lux, S.; Kostecki, R.; Davis, R.; Zorba, V.; Mehta, A.; Doeff, M. Enhanced lithium ion transport in garnet-type solid state electrolytes. *J. Electroceram.* **2017**, *38*, 168–175. [CrossRef]

126. Wang, Y.; Yu, J.; Wu, J.; Wang, Z. Rapid analysis of platinum and nafion loadings using laser induced breakdown spectroscopy. *J. Electrochem. Soc.* **2017**, *164*, F1294–F1300. [CrossRef]

127. Smyrek, P.; Pröll, J.; Seifert, H.J.; Pfleging, W. Laser-induced breakdown spectroscopy of laser-structured Li(NiMnCo)O2 electrodes for lithium-ion batteries. *J. Electrochem. Soc.* **2016**, *163*, A19–A26. [CrossRef]

128. Hou, H.; Cheng, L.; Richardson, T.; Chen, G.; Doeff, M.; Zheng, R.; Russo, R.; Zorba, V. Three-dimensional elemental imaging of Li-ion solid-state electrolytes using fs-laser induced breakdown spectroscopy (LIBS). *J. Anal. At. Spectrom.* **2015**, *30*, 2295–2302. [CrossRef]

129. Peng, L.; Sun, D.; Su, M.; Han, J.; Dong, C. Rapid analysis on the heavy metal content of spent zinc-manganese batteries by laser-induced breakdown spectroscopy. *Opt. Laser Technol.* **2012**, *44*, 2469–2475. [CrossRef]

130. Dib, S.R.; Nespeca, M.G.; Santos Junior, D.; Ribeiro, C.A.; Crespi, M.S.; Gomes Neto, J.A.; Ferreira, E.C. CN diatomic emission for N determination by LIBS. *Microchem. J.* **2020**, *157*, 105107. [CrossRef]

131. Nicolodelli, G.; Cabral, J.; Menegatti, C.R.; Marangoni, B.; Senesi, G.S. Recent advances and future trends in LIBS applications to agricultural materials and their food derivatives: An overview of developments in the last decade (2010–2019). Part I. Soils and fertilizers. *TrAC Trends Anal. Chem.* **2019**, *115*, 70–82. [CrossRef]

132. de Morais, C.P.; Barros, A.I.; Bechlin, M.A.; Silva, T.V.; Júnior, D.S.; Senesi, G.S.; Crespi, M.S.; Ribeiro, C.A.; Gomes Neto, J.A.; Ferreira, E.C. Laser-induced breakdown spectroscopy determination of K in biochar-based fertilizers in the presence of easily ionizable element. *Talanta* **2018**, *188*, 199–202. [CrossRef]

133. Jull, H.; Künnemeyer, R.; Schaare, P. Nutrient quantification in fresh and dried mixtures of ryegrass and clover leaves using laser-induced breakdown spectroscopy. *Precis. Agric.* **2018**, *19*, 823–839. [CrossRef]

134. Liao, S.-Y.; Wu, X.-L.; Li, G.-H.; Wei, M.; Zhang, M. Quantitative Analysis of P in fertilizer by laser-induced breakdown spectroscopy with multivariate nonlinear method. *Spectrosc. Spectr. Anal.* **2018**, *38*, 271–275.

135. Sha, W.; Niu, P.; Zhen, C.; Lu, C.; Jiang, Y. Analysis of phosphorus in fertilizer using laser-induced breakdown spectroscopy. *J. Appl. Spectrosc.* **2018**, *85*, 653–658. [CrossRef]

136. Andrade, D.F.; Sperança, M.A.; Pereira-Filho, E.R. Different sample preparation methods for the analysis of suspension fertilizers combining LIBS and liquid-to-solid matrix conversion: Determination of essential and toxic elements. *Anal. Methods* **2017**, *9*, 5156–5164. [CrossRef]

137. Senesi, G.S.; Romano, R.A.; Marangoni, B.S.; Nicolodelli, G.; Villas-Boas, P.R.; Benites, V.M.; Milori, D.M.B.P. Laser-induced breakdown spectroscopy associated with multivariate analysis applied to discriminate fertilizers of different nature. *J. Appl. Spectrosc.* **2017**, *84*, 923–928. [CrossRef]

138. Nunes, L.C.; De Carvalho, G.G.A.; Santos, D., Jr.; Krug, F.J. Determination of Cd, Cr and Pb in phosphate fertilizers by laser-induced breakdown spectroscopy. *Spectrochim. Acta Part B* **2014**, *97*, 42–48. [CrossRef]

139. Lu, W.; Lu, J.; Yao, S.; Chen, K. Synchronization detection of nitrogen phosphorus potassium in compound fertilizer with laser induced breakdown spectroscopy. *Chin. J. Lasers* **2011**, *38*, 1008003.

140. Groisman, Y.; Gaft, M. Online analysis of potassium fertilizers by laser-induced breakdown spectroscopy. *Spectrochim. Acta Part B* **2010**, *65*, 744–749. [CrossRef]

141. Yao, S.; Lu, J.; Li, J.; Chen, K.; Li, J.; Dong, M. Multi-elemental analysis of fertilizer using laser-induced breakdown spectroscopy coupled with partial least squares regression. *J. Anal. At. Spectrom.* **2010**, *25*, 1733–1738. [CrossRef]

142. Hussain, T.; Gondal, M.A.; Yamani, Z.H.; Baig, M.A. Measurement of nutrients in green house soil with laser induced breakdown spectroscopy. *Environ. Monit. Assess.* **2007**, *124*, 131–139. [CrossRef]

143. Akin, P.A.; Sezer, B.; Bean, S.R.; Peiris, K.; Tilley, M.; Apaydin, H.; Boyaci, I.H. Analysis of corn and sorghum flour mixtures using laser-induced breakdown spectroscopy. *J. Sci. Food. Agric.* **2021**, *101*, 1076–1084. [CrossRef] [PubMed]

144. Tian, Y.; Chen, Q.; Lin, Y.; Lu, Y.; Li, Y.; Lin, H. Quantitative determination of phosphorus in seafood using laser-induced breakdown spectroscopy combined with machine learning. *Spectrochim. Acta Part B* **2021**, *175*, 106027. [CrossRef]

145. Costa, V.C.; Amorim, F.A.C.; de Babos, D.V.; Pereira-Filho, E.R. Direct determination of Ca, K, Mg, Na, P, S, Fe and Zn in bivalve mollusks by wavelength dispersive X-ray fluorescence (WDXRF) and laser-induced breakdown spectroscopy (LIBS). *Food Chem.* **2019**, *273*, 91–98. [CrossRef] [PubMed]

146. Yang, P.; Zhou, R.; Zhang, W.; Yi, R.; Tang, S.; Guo, L.; Hao, Z.; Li, X.; Lu, Y.; Zeng, X. High-sensitivity determination of cadmium and lead in rice using laser-induced breakdown spectroscopy. *Food Chem.* **2019**, *272*, 323–328. [CrossRef]

147. Alfarraj, B.A.; Sanghapi, H.K.; Bhatt, C.R.; Yueh, F.Y.; Singh, J.P. Qualitative analysis of dairy and powder milk using laser-induced breakdown spectroscopy (LIBS). *Appl. Spectrosc.* **2018**, *72*, 89–101. [CrossRef] [PubMed]

148. Atta, B.M.; Saleem, M.; Haq, S.U.; Ali, H.; Ali, Z.; Qamar, M. Determination of zinc and iron in wheat using laser-induced breakdown spectroscopy. *Laser Phys. Lett.* **2018**, *15*, 125603. [CrossRef]

149. Chen, C.-T.; Banaru, D.; Sarnet, T.; Hermann, J. Two-step procedure for trace element analysis in food via calibration-free laser-induced breakdown spectroscopy. *Spectrochim. Acta Part B* **2018**, *150*, 77–85. [CrossRef]

150. Sezer, B.; Bilge, G.; Boyaci, I.H. Capabilities and limitations of LIBS in food analysis. *TrAC Trends Anal. Chem.* **2017**, *97*, 345–353. [CrossRef]

151. Peng, J.; Liu, F.; Zhou, F.; Song, K.; Zhang, C.; Ye, L.; He, Y. Challenging applications for multi-element analysis by laser-induced breakdown spectroscopy in agriculture: A review. *TrAC Trends Anal. Chem.* **2016**, *85*, 260–272. [CrossRef]

152. Barnett, C.; Bell, C.; Vig, K.; Akpovo, A.C.; Johnson, L.; Pillai, S.; Singh, S. Development of a LIBS assay for the detection of salmonella enterica serovar typhimurium from food. *Anal. Bioanal. Chem.* **2011**, *400*, 3323–3330. [CrossRef]

153. Lei, W.Q.; El Haddad, J.; Motto-Ros, V.; Gilon-Delepine, N.; Stankova, A.; Ma, Q.L.; Bai, X.S.; Zheng, L.J.; Zeng, H.P.; Yu, J. Comparative measurements of mineral elements in milk powders with laser-induced breakdown spectroscopy and inductively coupled plasma atomic emission spectroscopy. *Anal. Bioanal. Chem.* **2011**, *400*, 3303–3313. [CrossRef] [PubMed]

154. Augusto, A.S.; Castro, J.P.; Sperança, M.A.; Pereira-Filho, E.R. Combination of multi-energy calibration (MEC) and laser-induced breakdown spectroscopy (LIBS) for dietary supplements analysis and determination of Ca, Mg and K. *J. Braz. Chem. Soc.* **2019**, *30*, 804–812. [CrossRef]

155. dos Santos Augusto, A.; Barsanelli, P.L.; Pereira, F.M.V.; Pereira-Filho, E.R. Calibration strategies for the direct determination of Ca, K, and Mg in commercial samples of powdered milk and solid dietary supplements using laser-induced breakdown spectroscopy (LIBS). *Food Res. Int.* **2017**, *94*, 72–78. [CrossRef]

156. Agrawal, R.; Kumar, R.; Rai, S.; Pathak, A.K.; Rai, A.K.; Rai, G.K. LIBS: A quality control tool for food supplements. *Food Biophys.* **2011**, *6*, 527–533. [CrossRef]

157. Parigger, C.G. Review of spatiotemporal analysis of laser-induced plasma in gases. *Spectrochim. Acta Part B* **2021**, *179*, 106122. [CrossRef]

158. Chan, G.C.-Y.; Martin, L.R.; Trowbridge, L.D.; Zhu, Z.; Mao, X.; Russo, R.E. Analytical characterization of laser induced plasmas towards uranium isotopic analysis in gaseous uranium hexafluoride. *Spectrochim. Acta Part B* **2021**, *176*, 106036. [CrossRef]

159. McGann, B.; Ombrello, T.M.; Peterson, D.M.; Hassan, E.; Hammack, S.D.; Carter, C.D.; Lee, T.; Do, H. Lean fuel detection with nanosecond-gated laser-induced breakdown spectroscopy. *Combust. Flame* **2021**, *224*, 209–218. [CrossRef]

160. Yang, G.; Liu, L.; Wang, T.; Fan, L.; Huang, X.; Tian, D.; Jiang, L.; Silvain, J.-F.; Lu, Y. Laser-induced breakdown spectroscopy of ammonia gas with resonant vibrational excitation. *Opt. Express* **2020**, *28*, 1197–1205. [CrossRef] [PubMed]

161. Zhang, Z.; Li, T.; Xue, X.; Huang, S. Simultaneous measurements of fuel concentration and temperature in gas jets by laser induced breakdown spectroscopy. *Spectrochim. Acta Part B* **2019**, *161*, 105706. [CrossRef]

162. Deguchi, Y.; Kamimoto, T.; Wang, Z.Z.; Yan, J.J.; Liu, J.P.; Watanabe, H.; Kurose, R. Applications of laser diagnostics to thermal power plants and engines. *Appl. Therm. Eng.* **2014**, *73*, 1453–1464. [CrossRef]

163. Eseller, K.; Yueh, F.; Singh, J.; Melikechi, N. Helium detection in gas mixtures by LIBS. *Appl. Opt.* **2012**, *51*, B171–B175. [CrossRef]

164. Sturm, V.; Brysch, A.; Noll, R. Online multielement analysis of the top gas of a blast furnace by laser-induced breakdown spectroscopy (LIBS). *Berg. Huettenmaenn. Monatsh.* **2007**, *152*, 28–32. [CrossRef]

165. D'Ulivo, A.; Onor, M.; Pitzalis, E.; Spiniello, R.; Lampugnani, L.; Cristoforetti, G.; Legnaioli, S.; Palleschi, V.; Salvetti, A.; Tognoni, E. Determination of the deuterium/hydrogen ratio in gas reaction products by laser-induced breakdown spectroscopy. *Spectrochim. Acta Part B* **2006**, *61*, 797–802. [CrossRef]

166. Ferioli, F.; Puzinauskas, P.V.; Buckley, S.G. Laser-induced breakdown spectroscopy for on-line engine equivalence ratio measurements. *Appl. Spectrosc.* **2003**, *57*, 1183–1189. [CrossRef]

167. Haisch, C.; Niessner, R.; Matveev, O.I.; Panne, U.; Omenetto, N. Element-specific determination of chlorine in gases by Laser-Induced-Breakdown-Spectroscopy (LIBS). *Fresenius' J. Anal. Chem.* **1996**, *356*, 21–26. [CrossRef] [PubMed]

168. Corzo, R.; Hoffman, T.; Ernst, T.; Trejos, T.; Berman, T.; Coulson, S.; Weis, P.; Stryjnik, A.; Dorn, H.; Pollock, E.; et al. An interlaboratory study evaluating the interpretation of forensic glass evidence using refractive index measurements and elemental composition. *Forensic Chem.* **2021**, *22*, 100307. [CrossRef]

169. Gerhard, C.; Taleb, A.; Pelascini, F.; Hermann, J. Quantification of surface contamination on optical glass via sensitivity-improved calibration-free laser-induced breakdown spectroscopy. *Appl. Surf. Sci.* **2021**, *537*, 147984. [CrossRef]

170. Devangad, P.; Unnikrishnan, V.K.; Yogesha, M.; Kulkarni, S.D.; Chidangil, S. Plasma spectroscopy + chemometrics: An ideal approach for the spectrochemical analysis of iron phosphate glass samples. *J. Chemom.* **2020**, *34*, e3310. [CrossRef]

171. Teklemariam, T.A.; Gotera, J. Application of laser induced breakdown spectroscopy in food container glass discrimination. *Spectrochim. Acta Part B* **2019**, *155*, 34–43. [CrossRef]

172. Skruibis, J.; Balachninaite, O.; Butkus, S.; Vaicaitis, V.; Sirutkaitis, V. Multiple-pulse Laser-induced breakdown spectroscopy for monitoring the femtosecond laser micromachining process of glass. *Opt. Laser Technol.* **2019**, *111*, 295–302. [CrossRef]

173. Chappell, J.; Martinez, M.; Baudelet, M. Statistical evaluation of spectral interferences in laser-induced breakdown spectroscopy. *Spectrochim. Acta Part B* **2018**, *149*, 167–175. [CrossRef]

174. Ewusi-Annan, E.; Surmick, D.M.; Melikechi, N.; Wiens, R.C. Simulated laser-induced breakdown spectra of graphite and synthetic shergottite glass under martian conditions. *Spectrochim. Acta Part B* **2018**, *148*, 31–43. [CrossRef]

175. Motto-Ros, V.; Syvilay, D.; Bassel, L.; Negre, E.; Trichard, F.; Pelascini, F.; El Haddad, J.; Harhira, A.; Moncayo, S.; Picard, J.; et al. Critical aspects of data analysis for quantification in laser-induced breakdown spectroscopy. *Spectrochim. Acta Part B* **2018**, *140*, 54–64. [CrossRef]

176. Sánchez-Aké, C.; García-Fernández, T.; Benítez, J.L.; de la Mora, M.B.; Villagrán-Muniz, M. Intensity enhancement of LIBS of glass by using Au thin films and nanoparticles. *Spectrochim. Acta Part B* **2018**, *146*, 77–83. [CrossRef]

177. Devangad, P.; Unnikrishnan, V.K.; Tamboli, M.M.; Shameem, K.M.M.; Nayak, R.; Choudhari, K.S.; Santhosh, C. Quantification of Mn in glass matrices using laser induced breakdown spectroscopy (LIBS) combined with chemometric approaches. *Anal. Methods* **2016**, *8*, 7177–7184. [CrossRef]

178. Klus, J.; Pořízka, P.; Prochazka, D.; Novotný, J.; Novotný, K.; Kaiser, J. Effect of experimental parameters and resulting analytical signal statistics in laser-induced breakdown spectroscopy. *Spectrochim. Acta Part B* **2016**, *126*, 6–10. [CrossRef]

179. Bridge, C.M.; Powell, J.; Steele, K.L.; Williams, M.; MacInnis, J.M.; Sigman, M.E. Characterization of automobile float glass with laser-induced breakdown spectroscopy and laser ablation inductively coupled plasma mass spectrometry. *Appl. Spectrosc.* **2006**, *60*, 1181–1187. [CrossRef] [PubMed]

180. Matiaske, A.-M.; Gornushkin, I.B.; Panne, U. Double-pulse laser-induced breakdown spectroscopy for analysis of molten glass. *Anal. Bioanal. Chem.* **2012**, *402*, 2597–2606. [CrossRef]

181. Craparo, J.C.; Weisberg, A.; De Saro, R. Measurements of batch and cullet using laser induced breakdown spectroscopy. *Ceram. Eng. Sci. Proc.* **2006**, *27*, 105–118. [CrossRef]

182. Yun, J.-I.; Klenze, R.; Kim, R. Laser-induced breakdown spectroscopy for the on-line multielement analysis of highly radioactive glass melt simulants. Part II: Analyses of molten glass samples. *Appl. Spectrosc.* **2002**, *56*, 852–858. [CrossRef]

183. Dawood, A.; Bashir, S. Characterizing laser induced plasma and ablation of Mg-alloy in the presence and absence of magnetic field. *Optik* **2018**, *170*, 353–367. [CrossRef]

184. Xin, Y.; Sun, L.-X.; Yang, Z.-J.; Zeng, P.; Cong, Z.-B.; Qi, L.-F. In situ analysis of magnesium alloy using a standoff and double-pulse laser-induced breakdown spectroscopy system. *Front. Phys.* **2016**, *11*, 115207. [CrossRef]

185. Qi, L.; Sun, L.; Xin, Y.; Cong, Z.; Li, Y.; Yu, H. Application of stand-off double-pulse laser-induced breakdown spectroscopy in elemental analysis of magnesium alloy. *Plasma Sci. Technol.* **2015**, *17*, 676–681. [CrossRef]

186. Latkoczy, C.; Ghislain, T. Simultaneous LIBS and LA-ICP-MS analysis of industrial samples. *J. Anal. At. Spectrom.* **2006**, *21*, 1152–1160. [CrossRef]

187. Gesing, A.; Torek, P.; Dalton, R.; Wolanski, R. Assuring recyclability of automotive magnesium alloys: Chemical composition-based sorting of magnesium shredded scrap. *TMS Annu. Meet.* **2003**, 15–23.

188. Gudmundsson, S.H.; Matthiasson, J.; Björnsson, B.M.; Gudmundsson, H.; Leosson, K. Quantitative in-situ analysis of impurity elements in primary aluminum processing using laser-induced breakdown spectroscopy. *Spectrochim. Acta Part B* **2019**, *158*, 105646. [CrossRef]

189. Xin, Y.; Li, Y.; Cai, Z.-R.; Yang, M.; Yang, Z.-J.; Sun, L.-X. On-line monitoring of elemental composition in molten aluminum by laser-induced breakdown spectroscopy online analyzer for liquid metal composition. *Metall. Anal.* **2019**, *39*, 15–20.

190. Hudson, S.W.; Craparo, J.; Desaro, R.; Apelian, D. Inclusion detection in aluminum alloys via laser-induced breakdown spectroscopy. *Metall. Mater. Trans. B* **2018**, *49*, 658–665. [CrossRef]

191. Rai, A.K.; Yueh, F.-Y.; Singh, J.P. Laser-induced breakdown spectroscopy of molten aluminum alloy. *Appl. Opt.* **2003**, *42*, 2078–2084. [CrossRef]

192. Paksy, L.; Nemet, B.; Lengyel, A.; Kozma, L. Production control of metal alloys by laser spectroscopy of the molten metals. Part I. Preliminary investigations. *Spectrochim. Acta Part B* **1996**, *51*, 279–290. [CrossRef]

193. Maury, C.; Sirven, J.-B.; Tabarant, M.; L'Hermite, D.; Courouau, J.-L.; Gallou, C.; Caron, N.; Moutiers, G.; Cabuil, V. Analysis of liquid sodium purity by laser-induced breakdown spectroscopy. Modeling and correction of signal fluctuation prior to quantitation of trace elements. *Spectrochim. Acta Part B* **2013**, *82*, 28–35. [CrossRef]

194. Cui, M.; Deguchi, Y.; Yao, C.; Wang, Z.; Tanaka, S.; Zhang, D. Carbon detection in solid and liquid steel samples using ultraviolet long-short double pulse laser-induced breakdown spectroscopy. *Spectrochim. Acta Part B* **2020**, *167*, 105839. [CrossRef]

195. Lednev, V.N.; Grishin, M.Y.; Sdvizhenskii, P.A.; Asyutin, R.D.; Tretyakov, R.S.; Stavertiy, A.Y.; Pershin, S.M. Sample temperature effect on laser ablation and analytical capabilities of laser induced breakdown spectroscopy. *J. Anal. At. Spectrom.* **2019**, *34*, 607–615. [CrossRef]

196. Zhao, T.; Fan, Z.; Lian, F.; Liu, Y.; Lin, W.; Mo, Z.; Nie, S.; Wang, P.; Xiao, H.; Li, X.; et al. Using laser-induced breakdown spectroscopy on vacuum alloys-production process for elements concentration analysis. *Spectrochim. Acta Part B* **2017**, *137*, 64–69. [CrossRef]

197. Sun, L.; Yu, H.; Cong, Z.; Xin, Y.; Li, Y.; Qi, L. In situ analysis of steel melt by double-pulse laser-induced breakdown spectroscopy with a cassegrain telescope. *Spectrochim. Acta Part B* **2015**, *112*, 40–48. [CrossRef]

198. Tusset, V. Future of the online control of molten metal. *Metall. Anal.* **2013**, *33*, 13–20.

199. Mathy, G.; Monfort, G.; Vanderheyden, B.; Tusset, V. Measurement of composition and temperature in blast furnace runners by using laser induced breakdown spectroscopy. *Metall. Anal.* **2011**, *31*, 21–23.

200. Gruber, J.; Heitz, J.; Arnold, N.; Bäuerle, D.; Ramaseder, N.; Meyer, W.; Hochörtler, J.; Koch, F. In situ analysis of metal melts in metallurgic vacuum devices by laser-induced breakdown spectroscopy. *Appl. Spectrosc.* **2004**, *58*, 457–462. [CrossRef]

201. Peter, L.; Sturm, V.; Noll, R. Liquid steel analysis with laser-induced breakdown spectrometry in the vacuum ultraviolet. *Appl. Opt.* **2003**, *42*, 6199–6204. [CrossRef] [PubMed]

202. Aragón, C.; Aguilera, J.A.; Campos, J. Determination of carbon content in molten steel using laser-induced breakdown spectroscopy. *Appl. Spectrosc.* **1993**, *47*, 606–608. [CrossRef]

203. Carlhoff, C.; Kirchhoff, S. Laser-induced emission spectroscopy for on-line analysis of molten metal in a steel converter. *Laser Und Optoelektron.* **1991**, *23*, 50–52.

204. Tecnar. Available online: https://www.tecnar.com/online-chemistry-analyser/ (accessed on 12 February 2021).

205. Sabsabi, M.; St-Onge, L.; Detalle, V.; Lucas, J.M. Laser-Induced Breakdown Spectroscopy: A New Tool for Process Control. In Proceedings of the 16th World Conference on Non Destructive Testing, H2Z 1H2, Montreal, QC, Canada, August 30 – September 3 2004; Available online: http://www.ndt.net/article/wcndt2004/pdf/in-process_ndt-nde/679_sabsabi.pdf (accessed on 14 July 2021).

206. Guo, M.-T.; Sun, L.-X.; Dong, W.; Wang, J.-C.; Cong, Z.-B.; Zheng, L.-M. Classification and identification of scrap metals based on laser-induced breakdown spectroscopy. *Metall. Anal.* **2020**, *40*, 72–78. [CrossRef]

207. Shin, S.; Moon, Y.; Lee, J.; Kwon, E.; Park, K.; Jeong, S. Improvement in classification accuracy of stainless steel alloys by laser-induced breakdown spectroscopy based on elemental intensity ratio analysis. *Plasma Sci. Technol.* **2020**, *22*, 074011. [CrossRef]

208. Noll, R.; Fricke-Begemann, C.; Connemann, S.; Meinhardt, C.; Sturm, V. LIBS analyses for industrial applications-an overview of developments from 2014 to 2018. *J. Anal. At. Spectrom.* **2018**, *33*, 945–956. [CrossRef]

209. Bauer, A.J.R.; Laska, C. LIBS for Automated Aluminum Scrap Sorting. Application Note LIBS-028 (US), 2018. 2018. Available online: www.tsi.com (accessed on 25 June 2021).

210. Bohling, C.; Feierabend, A.; Günther, J.-U.; John, A.; Singer, A.; Cordts, L. Operation of LIBS elemental analysers for inline analysis of aluminium scrap and industrial products. In Proceedings of the 9th European Metallurgical Conference (EMC 2017), Leipzig, Germany, 25–28 June 2017; Volume 4, pp. 1819–1830.

211. Grifoni, E.; Legnaioli, S.; Lorenzetti, G.; Pagnotta, S.; Palleschi, V. Applying LIBS to metals processing. *Spectroscopy* **2015**, *30*, 20–31. Available online: https://www.spectroscopyonline.com/view/applying-libs-metals-processing (accessed on 28 January 2019).

212. Kashiwakura, S.; Wagatsuma, K. Rapid sorting of stainless steels by open-air laser-induced breakdown spectroscopy with detecting chromium, nickel, and molybdenum. *ISIJ Int.* **2015**, *55*, 2391–2396. [CrossRef]

213. Merk, S.; Scholz, C.; Florek, S.; Mory, D. Increased identification rate of scrap metal using laser induced breakdown spectroscopy echelle spectra. *Spectrochim. Acta Part B* **2015**, *112*, 10–15. [CrossRef]

214. Noharet, B.; Sterner, C.; Irebo, T.; Gurell, J.; Bengtson, A.; Vainik, R.; Karlsson, H.; Illy, E. A compact LIBS system for industrial applications. *SPIE-Int. Soc. Opt. Eng. Proc.* **2015**, *9369*, 936904. [CrossRef]

215. Gurell, J.; Bengtson, A.; Falkenström, M.; Hansson, B.A.M. Laser induced breakdown spectroscopy for fast elemental analysis and sorting of metallic scrap pieces using certified reference materials. *Spectrochim. Acta Part B* **2012**, *74–75*, 46–50. [CrossRef]

216. Sturm, V.; Eilers, D.; Werheit, P.; Noll, R.; Chiarotti, U.; Volponi, V.; Moroli, V.; DeMiranda, U.; Zanforlin, M.; Zani, M.; et al. Elemental monitoring of steel scrap loading an electrical arc furnace. In Proceedings of the 8th International Workshop on Progress in Analytical Chemistry & Materials Characterisation in the Steel and Metals Industries, Luxembourg City, Luxembourg, 17–19 May 2011; pp. 55–61.

217. Cabalín, L.M.; González, A.; Ruiz, J.; Laserna, J.J. Assessment of statistical uncertainty in the quantitative analysis of solid samples in motion using laser-induced breakdown spectroscopy. *Spectrochim. Acta Part B* **2010**, *65*, 680–687. [CrossRef]

218. Vieitez, M.O.; Hedberg, J.; Launila, O.; Berg, L.-E. Elemental analysis of steel scrap metals and minerals by laser-induced breakdown spectroscopy. *Spectrochim. Acta Part B* **2005**, *60*, 920–925. [CrossRef]

219. Lawley, C.J.M.; Somers, A.M.; Kjarsgaard, B.A. Rapid geochemical imaging of rocks and minerals with handheld laser induced breakdown spectroscopy (LIBS). *J. Geochem. Explor.* **2021**, *222*, 106694. [CrossRef]

220. Müller, S.; Meima, J.A.; Rammlmair, D. Detecting REE-rich areas in heterogeneous drill cores from storkwitz using LIBS and a combination of k-means clustering and spatial raster analysis. *J. Geochem. Explor.* **2021**, *221*, 106697. [CrossRef]

221. Wiens, R.C.; Maurice, S.; Robinson, S.H.; Nelson, A.E.; ·Cais, P.; ·Bernardi, P.; Newell, R.T.; ·Clegg, S.; Sharma, S.K.; ·Storms, S.; et al. The supercam instrument suite on the NASA mars 2020 rover: Body unit and combined system tests. *Space Sci. Rev.* **2021**, *217*, 4. [CrossRef]

222. Fabre, C. Advances in laser-induced breakdown spectroscopy analysis for geology: A critical review. *Spectrochim. Acta Part B* **2020**, *166*, 105799. [CrossRef]

223. Harmon, R.S.; Lawley, C.J.M.; Watts, J.; Harraden, C.L.; Somers, A.M.; Hark, R.R. Laser-induced breakdown spectroscopy—An emerging analytical tool for mineral exploration. *Minerals* **2019**, *9*, 718. [CrossRef]

224. Díaz, D.; Molina, A.; Hahn, D. Effect of laser irradiance and wavelength on the analysis of gold- and silver-bearing minerals with laser-induced breakdown spectroscopy. *Spectrochim. Acta Part B* **2018**, *145*, 86–95. [CrossRef]

225. Fabre, C.; Devismes, D.; Moncayo, S.; Pelascini, F.; Trichard, F.; Lecomte, A.; Bousquet, B.; Cauzid, J.; Motto-Ros, V. Elemental imaging by laser-induced breakdown spectroscopy for the geological characterization of minerals. *J. Anal. At. Spectrom.* **2018**, *33*, 1345–1353. [CrossRef]

226. McMillan, N.J.; Curry, A.J.; Dutrow, B.L.; Henry, D.J. Identification of the host lithology of tourmaline using laser-induced breakdown spectroscopy for application in sediment provenance and mineral exploration. *Can. Mineral.* **2018**, *56*, 393–410. [CrossRef]

227. Rifai, K.; Laflamme, M.; Constantin, M.; Vidal, F.; Sabsabi, M.; Blouin, A.; Bouchard, P.; Fytas, K.; Castello, M.; Kamwa, B.N. Analysis of gold in rock samples using laser-induced breakdown spectroscopy: Matrix and heterogeneity effects. *Spectrochim. Acta Part B* **2017**, *134*, 33–41. [CrossRef]

228. Yang, G.; Han, X.; Wang, C.; Ding, Y.; Liu, K.; Tian, D.; Yao, L. The basicity analysis of sintered ore using laser-induced breakdown spectroscopy (LIBS) combined with random forest regression (RFR). *Anal. Methods* **2017**, *9*, 5365–5370. [CrossRef]

229. Kuhn, K.; Meima, J.A.; Rammlmair, D.; Ohlendorf, C. Chemical mapping of mine waste drill cores with laser-induced breakdown spectroscopy (LIBS) and energy dispersive X-ray fluorescence (EDXRF) for mineral resource exploration. *J. Geochem. Explor.* **2015**, *161*, 72–84. [CrossRef]

230. Senesi, G.S. Laser-Induced Breakdown Spectroscopy (LIBS) applied to terrestrial and extraterrestrial analogue geomaterials with emphasis to minerals and rocks. *Earth-Sci. Rev.* **2014**, *139*, 231–267. [CrossRef]

231. Gaft, M.; Nagli, L.; Gornushkin, I.; Groisman, Y. Doubly ionized ion emission in laser-induced breakdown spectroscopy in air. *Anal. Bioanal. Chem.* **2011**, *400*, 3229–3237. [CrossRef] [PubMed]

232. Fricke-Begemann, C.; Noll, R.; Wotruba, H.; Schmitz, C. Laser-based material analysis for sorting of minerals. In *Applications of Sensor-Based Sorting in the Raw Material Industry*; Schriftenreihe zur Aufbereitung und Veredlung, Pretz, T., Quicker, P., Wotruba, H., Eds.; Shaker: Aachen, Germany, 2011; Volume 42, pp. 65–70. ISBN1 978-3-8440-0585-1. Available online: https://www.shaker.eu/en/index.asp?lang=en (accessed on 18 June 2017)ISBN2 978-3-8440-0585-1.

233. Gaft, M.; Sapir-Sofer, I.; Modiano, H.; Stana, R. Laser induced breakdown spectroscopy for bulk minerals online analyses. *Spectrochim. Acta Part B* **2007**, *62*, 1496–1503. [CrossRef]

234. McMillan, N.J.; Harmon, R.S.; De Lucia, F.C.; Miziolek, A.M. Laser-induced breakdown spectroscopy analysis of minerals: Carbonates and silicates. *Spectrochim. Acta Part B* **2007**, *62*, 1528–1536. [CrossRef]

235. Rosenwasser, S.; Asimellis, G.; Bromley, B.; Hazlett, R.; Martin, J.; Pearce, T.; Zigler, A. Development of a method for automated quantitative analysis of ores using LIBS. *Spectrochim. Acta Part B* **2001**, *56*, 707–714. [CrossRef]

236. Payré, V.; Siebach, K.L.; Dasgupta, R.; Udry, A.; Rampe, E.B.; Morrison, S.M. Constraining ancient magmatic evolution on mars using crystal chemistry of detrital igneous minerals in the sedimentary bradbury group, gale crater, mars. *J. Geophys. Res.: Planets* **2020**, *125*, e2020JE006467. [CrossRef]

237. Laville, S.; Sabsabi, M.; Doucet, F.R. Multi-elemental analysis of solidified mineral melt samples by laser-induced breakdown spectroscopy coupled with a linear multivariate calibration. *Spectrochim. Acta Part B* **2007**, *62*, 1557–1566. [CrossRef]

238. Abdul Kalam, S.; Balaji Manasa Rao, S.V.; Jayananda, M.; Venugopal Rao, S. Standoff femtosecond filament-induced breakdown spectroscopy for classification of geological materials. *J. Anal. At. Spectrom.* **2020**, *35*, 3007–3020. [CrossRef]

239. Fahad, M.; Ali, S.; Iqbal, Y. Plasma diagnostics by optical emission spectroscopy on manganese ore in conjunction with XRD, XRF and SEM-EDS. *Plasma Sci. Technol.* **2019**, *21*, 08550. [CrossRef]

240. Bhatt, C.R.; Jain, J.C.; Goueguel, C.L.; McIntyre, D.L.; Singh, J.P. Determination of rare earth elements in geological samples using laser-induced breakdown spectroscopy (LIBS). *Appl. Spectrosc.* **2018**, *72*, 114–121. [CrossRef] [PubMed]
241. Khajehzadeh, N.; Haavisto, O.; Koresaar, L. On-stream mineral identification of tailing slurries of an iron ore concentrator using data fusion of LIBS, reflectance spectroscopy and XRF measurement techniques. *Miner. Eng.* **2017**, *113*, 83–94. [CrossRef]
242. Romppanen, S.; Häkkänen, H.; Kaski, S. Singular value decomposition approach to the yttrium occurrence in mineral maps of rare earth element ores using laser-induced breakdown spectroscopy. *Spectrochim. Acta Part B* **2017**, *134*, 69–74. [CrossRef]
243. Pořízka, P.; Demidov, A.; Kaiser, J.; Keivanian, J.; Gornushkin, I.; Panne, U.; Riedel, J. Laser-induced breakdown spectroscopy for in situ qualitative and quantitative analysis of mineral ores. *Spectrochim. Acta Part B* **2014**, *101*, 155–163. [CrossRef]
244. Michaud, D.; Leclerc, R.; Proulx, E. Influence of particle size and mineral phase in the analysis of iron ore slurries by laser-induced breakdown spectroscopy. *Spectrochim. Acta Part B* **2007**, *62*, 1575–1581. [CrossRef]
245. Coffey, P.; Smith, N.; Lennox, B.; Kijne, G.; Bowen, B.; Davis-Johnston, A.; Martin, P.A. Robotic arm material characterisation using LIBS and Raman in a nuclear hot cell decommissioning environment. *J. Hazard. Mater.* **2021**, *412*, 125193. [CrossRef] [PubMed]
246. Rollin, E.; Musset, O.; Cardona, D.; Sirven, J.-B. Laser-induced breakdown spectroscopy of uranium in the vacuum ultraviolet range. *Spectrochim. Acta Part B* **2020**, *166*, 105796. [CrossRef]
247. Ararat-Ibarguen, C.E.; Lucia, A.; Corvalan, C.; Di Lalla, N.; Iribarren, M.J.; Rinaldi, C.A.; Pérez, R. Laser induced breakdown spectroscopy application to reaction-diffusion studies in nuclear materials. *Spectrochim. Acta Part B* **2020**, *166*, 105798. [CrossRef]
248. Wu, J.; Qiu, Y.; Li, X.; Yu, H.; Zhang, Z.; Qiu, A. Progress of laser-induced breakdown spectroscopy in nuclear industry applications. *J. Phys. D Appl. Phys.* **2020**, *53*, 023001. [CrossRef]
249. Maurya, G.S.; Marín-Roldán, A.; Veis, P.; Pathak, A.K.; Sen, P. A review of the LIBS analysis for the plasma-facing components diagnostics. *J. Nucl. Mater.* **2020**, *541*, 152417. [CrossRef]
250. Horsfall, J.P.O.; Trivedi, D.; Smith, N.T.; Martin, P.A.; Coffey, P.; Tourniere, S.; Banford, A.; Li, L.; Whitehead, D.; Lang, A.; et al. A new analysis workflow for discrimination of nuclear grade graphite using laser-induced breakdown spectroscopy. *J. Environ. Radioact.* **2019**, *199–200*, 45–57. [CrossRef]
251. Bhatt, B.; Hudson Angeyo, K.; Dehayem-Kamadjeu, A. LIBS development methodology for forensic nuclear materials analysis. *Anal. Methods* **2018**, *10*, 791–798. [CrossRef]
252. Manard, B.T.; Wylie, E.M.; Willson, S.P. Analysis of rare earth elements in uranium using handheld laser-induced breakdown spectroscopy (HH LIBS). *Appl. Spectrosc.* **2018**, *72*, 1653–1660. [CrossRef]
253. Xiaolin, L.; Zhixing, G.; Hongzhi, S. Experimental condition optimization for plutonium oxide surrogate by LIBS. *Laser Optoelectron. Prog.* **2018**, *55*, 121408. [CrossRef]
254. Williams, A.; Phongikaroon, S. Laser-induced breakdown spectroscopy (LIBS) measurement of uranium in molten salt. *Appl. Spectrosc.* **2018**, *72*, 1029–1039. [CrossRef]
255. Choi, D.; Han, B.-Y.; Park, S.H.; Kim, H.-D.; Park, G.-I.; Ku, J.-H. Effect of radiation on the transmission rate of emission intensity of optical fiber cable used in a nuclear material facility. *Nucl. Technol.* **2017**, *197*, 320–328. [CrossRef]
256. Manard, B.T.; Derrick Quarles, C.; Wylie, E.M.; Xu, N. Laser ablation-inductively couple plasma-mass spectrometry/laser induced break down spectroscopy: A tandem technique for uranium particle characterization. *J. Anal. At. Spectrom.* **2017**, *32*, 1680–1687. [CrossRef]
257. Li, C.; Feng, C.-L.; Oderji, H.Y.; Luo, G.-N.; Ding, H.-B. Review of LIBS application in nuclear fusion technology. *Front. Phys.* **2016**, *11*, 114214. [CrossRef]
258. Skrodzki, P.J.; Becker, J.R.; Diwakar, P.K.; Harilal, S.S.; Hassanein, A. A comparative study of single-pulse and double-pulse laser-induced breakdown spectroscopy with uranium-containing samples. *Appl. Spectrosc.* **2016**, *70*, 467–473. [CrossRef] [PubMed]
259. Mauchien, P.; Pailloux, A.; Vercouter, T. Applications of laser spectroscopy in the nuclear research and industry. In *Laser Spectroscopy for Sensing: Fundamentals, Techniques and Applications*, 1st ed.; Baudelet, M., Ed.; Woodhead: Cambridge, UK, 2014; pp. 522–543. [CrossRef]
260. Judge, E.J.; Barefield II, J.E.; Berg, J.M.; Clegg, S.M.; Havrilla, G.J.; Montoya, V.M.; Le, L.A.; Lopez, L.N. Laser-induced breakdown spectroscopy measurements of uranium and thorium powders and uranium ore. *Spectrochim. Acta Part B* **2013**, *83–84*, 28–36. [CrossRef]
261. Martin, M.Z.; Allman, S.; Brice, D.J.; Martin, R.C.; Andre, N.O. Exploring laser-induced breakdown spectroscopy for nuclear materials analysis and in-situ applications. *Spectrochim. Acta Part B* **2012**, *74–75*, 177–183. [CrossRef]
262. Chinni, R.C.; Cremers, D.A.; Radziemski, L.J.; Bostian, M.; Navarro-Northrup, C. Detection of uranium using laser-induced breakdown spectroscopy. *Appl. Spectrosc.* **2009**, *63*, 1238–1250. [CrossRef] [PubMed]
263. Whitehouse, A.I. Laser-induced breakdown spectroscopy and its application to the remote characterisation of hazardous materials. *Spectrosc. Eur.* **2006**, *18*, 14–21. [CrossRef]
264. Whitehouse, A.I.; Young, J.; Botheroyd, I.M.; Lawson, S.; Evans, C.P.; Wright, J. Remote material analysis of nuclear power station steam generator tubes by laser-induced breakdown spectroscopy. *Spectrochim. Acta Part B* **2001**, *56*, 821–830. [CrossRef]
265. Vinić, M.; Aruffo, E.; Andreoli, F.; Ivković, M.; Lazic, V. Quantification of heavy metals in oils with μL volume by laser induced breakdown spectroscopy and minimazing of the matrix effect. *Spectrochim. Acta Part B* **2020**, *164*, 105765. [CrossRef]
266. Ding, Y.; Xia, G.; Ji, H.; Xiong, X. Accurate quantitative determination of heavy metals in oily soil by laser induced breakdown spectroscopy (LIBS) combined with interval partial least squares (IPLS). *Anal. Methods* **2019**, *11*, 3657–3664. [CrossRef]

267. Aints, M.; Paris, P.; Laan, M.; Piip, K.; Riisalu, H.; Tufail, I. Determination of heating value of estonian oil shale by laser-induced breakdown spectroscopy. *J. Spectrosc.* **2018**, *2018*, 4605925. [CrossRef]

268. Harhira, A.; El Haddad, J.; Blouin, A.; Sabsabi, M. Rapid determination of bitumen content in athabasca oil sands by laser-induced breakdown spectroscopy. *Energy Fuels* **2018**, *32*, 3189–3193. [CrossRef]

269. Rendón-Sauz, F.G.; Flores-Reyes, T.; Costa, C. Laser induced breakdown spectroscopy (LIBS) for express identification of crude oils. *Rev. Cuba. Fis.* **2018**, *35*, 19–23.

270. Xiu, J.-S.; Liu, Y.-Y.; Dong, L.-L.; Qin, H. The detection of trace wear elements in engine oil using indirect ablation-laser induced breakdown spectroscopy. *Spectrosc. Spectr. Anal.* **2017**, *37*, 2885–2890.

271. Trichard, F.; Forquet, V.; Gilon, N.; Lienemann, C.-P.; Baco-Antoniali, F. Detection and quantification of sulfur in oil products by laser-induced breakdown spectroscopy for on-line analysis. *Spectrochim. Acta Part B* **2016**, *118*, 72–80. [CrossRef]

272. Fichet, P.; Mauchien, P.; Wagner, J.-F.; Moulin, C. Quantitative elemental determination in water and oil by laser induced breakdown spectroscopy. *Anal. Chim. Acta* **2001**, *429*, 269–278. [CrossRef]

273. Hassan, M.; Abdelhamid, M.; Nassef, O.A.; Abdel Harith, M. Spectrochemical analytical follow up of phytoremediation of oil-contaminated soil. *Soil Sediment. Contam.* **2018**, *27*, 485–500. [CrossRef]

274. Rehan, I.; Gondal, M.A.; Rehan, K. Determination of lead content in drilling fueled soil using laser induced spectral analysis and its cross validation using ICP/OES method. *Talanta* **2018**, *182*, 443–449. [CrossRef]

275. Khumaeni, A.; Budi, W.S.; Wardaya, A.Y.; Hedwig, R.; Kurniawan, K.H. Rapid detection of oil pollution in soil by using laser-induced breakdown spectroscopy. *Plasma Sci. Technol.* **2016**, *18*, 1186–1191. [CrossRef]

276. Fortes, F.J.; Ctvrtníčková, T.; Mateo, M.P.; Cabalín, L.M.; Nicolas, G.; Laserna, J.J. Spectrochemical study for the in situ detection of oil spill residues using laser-induced breakdown spectroscopy. *Anal. Chim. Acta* **2010**, *683*, 52–57. [CrossRef]

277. Gondal, M.A.; Hussain, T.; Yamani, Z.H.; Baig, M.A. Detection of heavy metals in Arabian crude oil residue using laser induced breakdown spectroscopy. *Talanta* **2006**, *69*, 1072–1078. [CrossRef] [PubMed]

278. Shakeel, H.; Haq, S.U.; Contreras, V.; Abbas, Q.; Nadeem, A. Analysis of alloy and solar cells with double-pulse calibration-free laser-induced breakdown spectroscopy. *Optik* **2020**, *211*, 164627. [CrossRef]

279. Banerjee, S.P.; Sarnet, T.; Siozos, P.; Loulakis, M.; Anglos, D.; Sentis, M. Characterization of organic photovoltaic devices using femtosecond laser induced breakdown spectroscopy. *Appl. Surf. Sci.* **2017**, *418*, 542–547. [CrossRef]

280. Diego-Vallejo, D.; Ashkenasi, D.; Lemke, A.; Eichler, H.J. Selective ablation of copper-indium-diselenide solar cells monitored by laser-induced breakdown spectroscopy and classification methods. *Spectrochim. Acta Part B* **2013**, *87*, 92–99. [CrossRef]

281. Sarkar, A.; Aggarwal, S.K.; Alamelu, D. Laser induced breakdown spectroscopy for rapid identification of different types of paper for forensic application. *Anal. Methods* **2010**, *2*, 32–36. [CrossRef]

282. Trejos, T.; Flores, A.; Almirall, J.R. Micro-spectrochemical analysis of document paper and gel inks by laser ablation inductively coupled plasma mass spectrometry and laser induced breakdown spectroscopy. *Spectrochim. Acta Part B* **2010**, *65*, 884–895. [CrossRef]

283. Häkkänen, H.; Houni, J.; Kaski, S.; Korppi-Tommola, J.E.I. Analysis of paper by laser-induced plasma spectroscopy. *Spectrochim. Acta Part B* **2001**, *56*, 737–742. [CrossRef]

284. Purohit, P.; Fortes, F.J.; Laserna, J.J. Optical trapping as a morphologically selective tool for in situ LIBS elemental characterization of single nanoparticles generated by laser ablation of bulk targets in air. *Anal. Chem.* **2021**, *93*, 2635–2643. [CrossRef] [PubMed]

285. Niu, C.; Cheng, X.; Zhang, T.; Wang, X.; He, B.; Zhang, W.; Feng, Y.; Bai, J.; Li, H. Novel method based on hollow laser trapping-libs-machine learning for simultaneous quantitative analysis of multiple metal elements in a single microsized particle in air. *Anal. Chem.* **2021**, *93*, 2281–2290. [CrossRef]

286. Ji, H.; Ding, Y.; Zhang, L.; Hu, Y.; Zhong, X. Review of aerosol analysis by laser-induced breakdown spectroscopy. *Appl. Spectros. Rev.* **2021**, *56*, 193–220. [CrossRef]

287. Girón, D.; Delgado, T.; Ruiz, J.; Cabalín, L.M.; Laserna, J.J. In-situ monitoring and characterization of airborne solid particles in the hostile environment of a steel industry using stand-off LIBS. *Meas. J. Int. Meas. Confed.* **2018**, *115*, 1–10. [CrossRef]

288. O'Neil, M.; Niemiec, N.A.; Demko, A.R.; Petersen, E.L.; Kulatilaka, W.D. Laser-induced-breakdown-spectroscopy-based detection of metal particles released into the air during combustion of solid propellants. *Appl. Opt.* **2018**, *57*, 1910–1917. [CrossRef]

289. Redoglio, D.A.; Palazzo, N.; Migliorini, F.; Dondè, R.; De Iuliis, S. Laser-induced breakdown spectroscopy analysis of lead aerosol in nitrogen and air atmosphere. *Appl. Spectrosc.* **2018**, *72*, 584–590. [CrossRef] [PubMed]

290. Boudhib, M.; Hermann, J.; Dutouquet, C. Compositional analysis of aerosols using calibration-free laser-induced breakdown spectroscopy. *Anal. Chem.* **2016**, *88*, 4029–4035. [CrossRef] [PubMed]

291. Xiong, G.; Li, S.; Zhang, Y.; Buckley, S.G.; Tse, S.D. Phase-selective laser-induced breakdown spectroscopy of metal-oxide nanoparticle aerosols with secondary resonant excitation during flame synthesis. *J. Anal. At. Spectrom.* **2016**, *31*, 482–491. [CrossRef]

292. Yoshiie, R.; Yamamoto, Y.; Uemiya, S.; Kambara, S.; Moritomi, H. Simple and rapid analysis of heavy metals in sub-micron particulates in flue gas. *Powder Technol.* **2008**, *180*, 135–139. [CrossRef]

293. Rusak, D.A.; Clara, M.; Austin, E.E.; Visser, K.; Niessner, R.; Smith, B.W.; Winefordner, J.D. Investigation of the effect of target water content on a laser-induced plasma. *Appl. Spectrosc.* **1997**, *51*, 1628–1631. [CrossRef]

294. Oki, H.; Suyanto, H.; Kurniawan, H.; Lie, T.J.; Lee, Y.I.; Sakan, F.; Idris, N.; Kagawa, K. Water analysis by laser-induced shock wave plasma spectroscopy using re-crystallized KBr powder confined in a cylindrical tube. *Jpn. J. Appl. Phys.* **2004**, *43*, 1036–1037. [CrossRef]

295. Liangying, Y.; Jidong, L.; Wen, C.; Ge, W.; Kai, S.; Wei, F. Analysis of pulverized coal by laser-induced breakdown spectroscopy. *Plasma Sci. Technol.* **2005**, *7*, 3041–3044. [CrossRef]

296. Pedarnig, J.D.; Haslinger, M.J.; Bodea, M.A.; Huber, N.; Wolfmeir, H.; Heitz, J. Sensitive detection of chlorine in iron oxide by single pulse and dual pulse laser-induced breakdown spectroscopy. *Spectrochim. Acta Part B* **2014**, *101*, 183–190. [CrossRef]

297. Díaz, D.; Hahn, D.W.; Molina, A. Evaluation of laser-induced breakdown spectroscopy (LIBS) as a measurement technique for evaluation of total elemental concentration in soils. *Appl. Spectrosc.* **2012**, *66*, 99–106. [CrossRef]

298. Asgill, M.E.; Brown, M.S.; Frische, K.; Roquemore, W.M.; Hahn, D.W. Double-pulse and single-pulse laser-induced breakdown spectroscopy for distinguishing between gaseous and particulate phase analytes. *Appl. Opt.* **2010**, *49*, C110–C119. [CrossRef]

299. Strauss, N.; Fricke-Begemann, C.; Noll, R. Size-resolved analysis of fine and ultrafine particulate matter by laser-induced breakdown spectroscopy. *J. Anal. At. Spectrom.* **2010**, *25*, 867–874. [CrossRef]

300. Stehrer, T.; Praher, B.; Viskup, R.; Jasik, J.; Wolfmeir, H.; Arenholz, E.; Heitz, J.; Pedarnig, J.D. Laser-induced breakdown spectroscopy of iron oxide powder. *J. Anal. At. Spectrom.* **2009**, *24*, 973–978. [CrossRef]

301. Viskup, R.; Praher, B.; Stehrer, T.; Jasik, J.; Wolfmeir, H.; Arenholz, E.; Pedarnig, J.D.; Heitz, J. Plasma plume photography and spectroscopy of Fe—Oxide materials. *Appl. Surf. Sci.* **2009**, *255*, 5215–5219. [CrossRef]

302. Lasheras, R.-J.; Paules, D.; Escudero, M.; Anzano, J.; Legnaioli, S.; Pagnotta, S.; Palleschi, V. Quantitative analysis of major components of mineral particulate matter by calibration free laser-induced breakdown spectroscopy. *Spectrochim. Acta Part B* **2020**, *171*, 105918. [CrossRef]

303. Viskup, R.; Wolf, C.; Baumgartner, W. Qualitative and quantitative characterisation of major elements in particulate matter from in-use diesel engine passenger vehicles by LIBS. *Energies* **2020**, *13*, 368. [CrossRef]

304. Viskup, R.; Baumgartner, W. Measurement of the main compounds present in the diesel particulate matter exhaust emissions generated from the real Diesel combustion engine passenger vehicles. *SPIE-Int. Soc. Opt. Eng., Proc.* **2018**, *10680*, 1068017. [CrossRef]

305. Williams, A.; Bryce, K.; Phongikaroon, S. Measurement of cerium and gadolinium in solid lithium chloride–potassium chloride salt using laser-induced breakdown spectroscopy (LIBS). *Appl. Spectrosc.* **2017**, *71*, 2302–2312. [CrossRef] [PubMed]

306. Purohit, P.; Fortes, F.J.; Laserna, J.J. Atomization efficiency and photon yield in laser-induced breakdown spectroscopy analysis of single nanoparticles in an optical trap. *Spectrochim. Acta Part B* **2017**, *130*, 75–81. [CrossRef]

307. Saari, S.; Järvinen, S.; Reponen, T.; Mensah-Attipoe, J.; Pasanen, P.; Toivonen, J.; Keskinen, J. Identification of single microbial particles using electro-dynamic balance assisted laser-induced breakdown and fluorescence spectroscopy. *Aerosol Sci. Technol.* **2016**, *50*, 126–132. [CrossRef]

308. Ahmed, N.; Liaqat, U.; Rafique, M.; Baig, M.A.; Tawfik, W. Detection of toxicity in some oral antidiabetic drugs using LIBS and LA-TOF-MS. *Microchem. J.* **2020**, *155*, 104679. [CrossRef]

309. Smith, J.P.; Zou, L.; Liu, Y.; Bu, X. Investigation of minor elemental species within tablets using in situ depth profiling via laser-induced breakdown spectroscopy hyperspectral imaging. *Spectrochim. Acta Part B* **2020**, *165*, 105769. [CrossRef]

310. Aldakheel, R.K.; Rehman, S.; Almessiere, M.A.; Khan, F.A.; Gondal, M.A.; Mostafa, A.; Baykal, A. Bactericidal and in vitro cyto-toxicity of moringa oleifera seed extract and its elemental analysis using laser-induced breakdown spectroscopy. *Pharmaceuticals* **2020**, *13*, 193. [CrossRef] [PubMed]

311. Zou, L.; Stenslik, M.J.; Giles, M.B.; Ormes, J.D.; Marsales, M.; Santos, C.; Kassim, B.; Smith, J.P.; Gonzalez, J.J.; Bu, X. Direct visualization of drug release in injectable implant by laser induced breakdown spectroscopy (LIBS). *J. Anal. At. Spectrom.* **2019**, *34*, 1351–1354. [CrossRef]

312. Nisar, S.; Dastgeer, G.; Shafiq, M.; Usman, M. Qualitative and semi-quantitative analysis of health-care pharmaceutical products using laser-induced breakdown spectroscopy. *J. Pharm. Anal.* **2019**, *9*, 20–24. [CrossRef]

313. Lednev, V.N.; Pershin, S.M.; Sdvizhenskii, P.A.; Grishin, M.Y.; Fedorov, A.N.; Bukin, V.V.; Oshurko, V.B.; Shchegolikhin, A.N. Combining Raman and laser induced breakdown spectroscopy by double pulse lasing. *Anal. Bioanal. Chem.* **2018**, *410*, 277–286. [CrossRef]

314. Tiwari, P.K.; Awasthi, S.; Kumar, R.; Anand, R.K.; Rai, P.K.; Rai, A.K. Rapid analysis of pharmaceutical drugs using LIBS coupled with multivariate analysis. *Lasers Med. Sci.* **2018**, *33*, 263–270. [CrossRef] [PubMed]

315. Zou, L.; Kassim, B.; Smith, J.P.; Ormes, J.D.; Liu, Y.; Tu, Q.; Bu, X. In situ analytical characterization and chemical imaging of tablet coatings using laser induced breakdown spectroscopy (LIBS). *Analyst* **2018**, *143*, 5000–5007. [CrossRef]

316. Yang, C.S.C.; Jin, F.; Swaminathan, S.R.; Patel, S.; Ramer, E.D.; Trivedi, S.B.; Brown, E.E.; Hommerich, U.; Samuels, A.C. Comprehensive study of solid pharmaceutical tablets in visible, near infrared (NIR), and longwave infrared (LWIR) spectral regions using a rapid simultaneous ultraviolet/visible/NIR (UVN) + LWIR laser-induced breakdown spectroscopy linear arrays detection system and a fast acousto-optic tunable filter NIR spectrometer. *Opt. Express* **2017**, *25*, 26885–26897. [CrossRef] [PubMed]

317. de Carvalho, G.G.A.; Nunes, L.C.; de Souza, P.F.; Krug, F.J.; Alegre, T.C.; Santos, D., Jr. Evaluation of laser induced breakdown spectrometry for the determination of macro and micronutrients in pharmaceutical tablets. *J. Anal. At. Spectrom.* **2010**, *25*, 803–809. [CrossRef]

318. Dubey, A.; Keyvan, G.; Hsia, R.; Saranteas, K.; Brone, D.; Misra, T.; Muzzio, F.J. Analysis of pharmaceutical tablet coating uniformity by laser-induced breakdown spectroscopy (LIBS). *J. Pharm. Innov.* **2011**, *6*, 77–87. [CrossRef]

319. St-Onge, L.; Kwong, E.; Sabsabi, M.; Vadas, E.B. Quantitative analysis of pharmaceutical products by laser-induced breakdown spectroscopy. *Spectrochim. Acta Part B* **2002**, *57*, 1131–1140. [CrossRef]

320. Zeng, Q.; Sirven, J.-B.; Gabriel, J.-C.P.; Tay, C.Y.; Lee, J.-M. Laser induced breakdown spectroscopy for plastic analysis. *TrAC Trends Anal. Chem.* **2021**, *140*, 116280. [CrossRef]

321. Chamradová, I.; Pořízka, P.; Kaiser, J. Laser-induced breakdown spectroscopy analysis of polymers in three different atmospheres. *Polym. Test.* **2021**, *96*, 107079. [CrossRef]

322. Costa, V.C.; de Mello, M.L.; Babos, D.V.; Castro, J.P.; Pereira-Filho, E.R. Calibration strategies for determination of Pb content in recycled polypropylene from car batteries using laser-induced breakdown spectroscopy (LIBS). *Microchem. J.* **2020**, *159*, 105558. [CrossRef]

323. Ledesma, R.; Palmieri, F.; Connell, J. Laser induced breakdown spectroscopy of polymer matrix composites for real-time analysis of trace surface contaminants: A review. *Int. J. Adhes. Adhes.* **2020**, *98*, 102528. [CrossRef]

324. Brunnbauer, L.; Mayr, M.; Larisegger, S.; Nelhiebel, M.; Pagnin, L.; Wiesinger, R.; Schreiner, M.; Limbeck, A. Combined LA-ICP-MS/LIBS: Powerful analytical tools for the investigation of polymer alteration after treatment under corrosive conditions. *Sci. Rep.* **2020**, *10*, 12513. [CrossRef]

325. Liu, K.; Tian, D.; Li, C.; Li, Y.; Yang, G.; Ding, Y. A review of laser-induced breakdown spectroscopy for plastic analysis. *TrAC Trends Anal. Chem.* **2019**, *110*, 327–334. [CrossRef]

326. Bonta, M.; Limbeck, A. Metal analysis in polymers using tandem LA-ICP-MS/LIBS: Eliminating matrix effects using multivariate calibration. *J. Anal. At. Spectrom.* **2018**, *33*, 1631–1637. [CrossRef]

327. Guo, Y.; Tang, Y.; Du, Y.; Tang, S.; Guo, L.; Li, X.; Lu, Y.; Zeng, X. Cluster analysis of polymers using laser-induced breakdown spectroscopy with K-means. *Plasma Sci. Technol.* **2018**, *20*, 065505. [CrossRef]

328. Lazic, V.; Filella, M.; Turner, A. Determination of antimony concentrations in widely used plastic objects by laser induced breakdown spectroscopy (LIBS). *J. Anal. At. Spectrom.* **2018**, *33*, 1917–1924. [CrossRef]

329. Ledesma, R.; Palmieri, F.; Connell, J.; Yost, W.; Fitz-Gerald, J. Surface characterization of carbon fiber reinforced polymers by picosecond laser induced breakdown spectroscopy. *Spectrochim. Acta Part B* **2018**, *140*, 5–12. [CrossRef]

330. Tang, Y.; Guo, Y.; Sun, Q.; Tang, S.; Li, J.; Guo, L.; Duan, J. Industrial polymers classification using laser-induced breakdown spectroscopy combined with self-organizing maps and K-means algorithm. *Optik* **2018**, *165*, 179–185. [CrossRef]

331. Negre, E.; Motto-Ros, V.; Pelascini, F.; Yu, J. Classification of plastic materials by imaging laser-induced ablation plumes. *Spectrochim. Acta Part B* **2016**, *122*, 132–141. [CrossRef]

332. Grégoire, S.; Boudinet, M.; Pelascini, F.; Surma, F.; Detalle, V.; Holl, Y. Laser-induced breakdown spectroscopy for polymer identification. *Anal. Bioanal. Chem.* **2011**, *400*, 3331–3340. [CrossRef]

333. Lasheras, R.J.; Bello-Gálvez, C.; Anzano, J. Identification of polymers by libs using methods of correlation and normalized coordinates. *Polym. Test.* **2010**, *29*, 1057–1064. [CrossRef]

334. Khachatrian, A.; Dagdigian, P.J. Laser-induced breakdown spectroscopy with laser irradiation on mid-infrared hydride stretch transitions: Polystyrene. *Appl. Phys. B: Lasers Opt.* **2009**, *97*, 243–248. [CrossRef]

335. Wang, Q.; Jander, P.; Fricke-Begemann, C.; Noll, R. Comparison of 1064 nm and 266 nm excitation of laser-induced plasmas for several types of plastics and one explosive. *Spectrochim. Acta Part B* **2008**, *63*, 1011–1015. [CrossRef]

336. Sattmann, R.; Monch, I.; Krause, H.; Noll, R.; Couris, S.; Hatziapostolou, A.; Mavromanolakis, A.; Fotakis, C.; Larrauri, E.; Miguel, R. Laser-induced breakdown spectroscopy for polymer identification. *Appl. Spectrosc.* **1998**, *52*, 456–461. [CrossRef]

337. Kim, E.; Choi, W.Z. Real-time identification of plastics by types using laser-induced breakdown spectroscopy. *J. Mater. Cycles Waste Manag.* **2019**, *21*, 176–180. [CrossRef]

338. Liang, D.; Du, C.; Ma, F.; Shen, Y.; Wu, K.; Zhou, J. Degradation of polyacrylate in the outdoor agricultural soil measured by FTIR-PAS and LIBS. *Polymers* **2018**, *10*, 1296. [CrossRef]

339. Roh, S.-B.; Park, S.-B.; Oh, S.-K.; Park, E.-K.; Choi, W.Z. Development of intelligent sorting system realized with the aid of laser-induced breakdown spectroscopy and hybrid preprocessing algorithm-based radial basis function neural networks for recycling black plastic wastes. *J. Mater. Cycles Waste Manag.* **2018**, *20*, 1934–1949. [CrossRef]

340. Vahid Dastjerdi, M.; Mousavi, S.J.; Soltanolkotabi, M.; Nezarati Zadeh, A. Identification and sorting of PVC polymer in recycling process by laser-induced breakdown spectroscopy (LIBS) combined with support vector machine (SVM) model. *Iran. J. Sci. Technol. Trans. A Sci.* **2018**, *42*, 959–965. [CrossRef]

341. Shameem, K.M.M.; Choudhari, K.S.; Bankapur, A.; Kulkarni, S.D.; Unnikrishnan, V.K.; George, S.D.; Kartha, V.B.; Santhosh, C. A hybrid LIBS–Raman system combined with chemometrics: An efficient tool for plastic identification and sorting. *Anal. Bioanal. Chem.* **2017**, *409*, 3299–3308. [CrossRef]

342. Aquino, F.W.B.; Paranhos, C.M.; Pereira-Filho, E.R. Method for the production of acrylonitrile-butadiene-styrene (ABS) and polycarbonate (PC)/ABS standards for direct Sb determination in plastics from e-waste using laser-induced breakdown spectroscopy. *J. Anal. At. Spectrom.* **2016**, *31*, 1228–1233. [CrossRef]

343. Huber, N.; Eschlböck-Fuchs, S.; Scherndl, H.; Freimund, A.; Heitz, J.; Pedarnig, J.D. In-line measurements of chlorine containing polymers in an industrial waste sorting plant by laser-induced breakdown spectroscopy. *Appl. Surf. Sci.* **2014**, *302*, 280–285. [CrossRef]

344. Boudinet, M.; Grégoire, S.; Pelascini, F.; Surma, F.; Detalle, V.; Holl, Y. Identification of plastics in WEEE (waste electric and electronic equipment) by laser induced breakdown spectroscopy. In Proceedings of the 6th Euro Mediterranean Symposium on Laser Induced Breakdown Spectroscopy, Izmir, Turkey, 11–15 September 2011.

345. Huber, N.; Viskup, R.; Linsmeyer, T.; Scherndl, H.; Heitz, J.; Pedarnig, J.D. Detection of heavy metals in waste polymers by laser-induced breakdown spectroscopy: A comparison of UV and IR lasers as ablation source. *SPIE-Int. Soc. Opt. Eng. Proc.* **2010**, *7726*, 77260G. [CrossRef]

346. Gondal, M.A.; Siddiqu, M.N. Identification of different kinds of plastics using laser induced breakdown spectroscopy for waste management. *J. Environ. Sci. Health Part A* **2007**, *42*, 1989–1997. [CrossRef] [PubMed]

347. Stepputat, M.; Noll, R. On-line detection of heavy metals and brominated flame retardants in technical polymers with laser-induced breakdown spectrometry. *Appl. Opt.* **2003**, *42*, 6210–6220. [CrossRef]

348. Fink, H.; Panne, U.; Niessner, R. Analysis of recycled thermoplasts from consumer electronics by laser-induced plasma spectroscopy. *Anal. Chim. Acta* **2001**, *440*, 17–25. [CrossRef]

349. Murakami, Y.; Matsuzaki, Y.; Kamimura, T.; Nishiura, T.; Masuda, K.; Shibayama, A.; Inoue, R. Erosion mechanism of refractories in a pyro-processing furnace for recycling lithium-ion secondary batteries. *Ceram. Int.* **2020**, *46*, 9281–9288. [CrossRef]

350. Feierabend, A.; Stissel, S. Operation of LIBS elemental analyzers for inline analysis of mineral resources and industrial products. In Proceedings of the 7th Sensor-Based Sorting & Control, Aachen, Germany, 23–24 February 2016; pp. 93–104.

351. Günther, J.-U.; Schilder, C.; Feierabend, A.; Bohling, C. Laser-induced breakdown spectroscopy (LIBS) in recycling of refractory material outbreak. In Proceedings of the Mineral Recycling Forum, Rotterdam, The Netherlands, 14–15 March 2016.

352. Baryshnikov, A.; Groisman, Y.; Eliezer, N.; Gaft, M.; Akselrod, L.; Savchenko, A. Laser-induced breakdown spectroscopy as a powerful tool for online quality control in the refractory industry. *China's Refract.* **2016**, *25*, 32–38.

353. Knapp, H.; Horckmans, L.; Bouillot, F.; Fricke-Begemann, C.; Connemann, S.; Makowe, J.; Ducastel, A.; Stark, A. Sensor-based sorting of spent refractory bricks. In Proceedings of the 28th International Mineral Processing Congress (IMPC 2016), Québec City, QC, Canada, 11–15 September 2016.

354. Gumpenberger, T.; Gruber, J.; Huber, N.; Dallinger, M. Sorting of refractory materials—A unique laser-based solution. In *Applications of Sensor-Based Sorting in the Raw Material Industry, Schriftenreihe zur Aufbereitung und Veredlung*; Pretz, T., Wotruba, H., Nienhaus, K., Eds.; Shaker: Aachen, Germany, 2011; Volume 42, pp. 227–239.

355. Lucchi, J.; Gluck, D.; Rials, S.; Tang, L.; Baudelet, M. Tire classification by elemental signatures using laser-induced breakdown spectroscop. *Appl. Spectrosc.* **2021**, *75*, 747–752. [CrossRef]

356. Kokkinaki, O.; Klini, A.; Polychronaki, M.; Mavrikakis, N.C.; Siderakis, K.G.; Koudoumas, E.; Pylarinos, D.; Thalassinakis, E.; Kalpouzos, K.; Anglos, D. Assessing the type and quality of high voltage composite outdoor insulators by remote laser-induced breakdown spectroscopy analysis: A feasibility study. *Spectrochim. Acta Part B* **2020**, *165*, 105768. [CrossRef]

357. Trautner, S.; Lackner, J.; Spendelhofer, W.; Huber, N.; Pedarnig, J.D. Quantification of the vulcanizing system of rubber in industrial tire rubber production by laser-induced breakdown spectroscopy (LIBS). *Anal. Chem.* **2019**, *91*, 5200–5206. [CrossRef] [PubMed]

358. Vinod, P.; Desai, B.M.A.; Sarathi, R.; Kornhuber, S. Investigation on the electrical, thermal and mechanical properties of silicone rubber nanocomposites. *IEEE Trans. Dielectr. Electr. Insul.* **2019**, *26*, 1876–1884. [CrossRef]

359. Lin, Z.; Han, W.; Xiao, H.; Wang, X.; Jia, Z. Study of silicone rubber used at external insulation of high voltage with laser-induced breakdown spectroscopy (LIBS). In Proceedings of the 2016 IEEE International Power Modulator and High Voltage Conference (IPMHVC), San Francisco, CA, USA, 6–9 July 2016. [CrossRef]

360. Trautner, S.; Jasik, J.; Parigger, C.G.; Pedarnig, J.D.; Spendelhofer, W.; Lackner, J.; Veis, P.; Heitz, J. Laser-induced optical breakdown spectroscopy of polymer materials based on evaluation of molecular emission bands. *Spectrochim. Acta Part A* **2017**, *174*, 331–338. [CrossRef] [PubMed]

361. Wang, X.; Hong, X.; Chen, C.; Wang, H.; Jia, Z.; Zou, L.; Li, R. Elemental analysis of RTV and HTV silicone rubber with laser-induced breakdown spectroscopy. In Proceedings of the 2017 IEEE Electrical Insulation Conference (EIC), Baltimore, MD, USA, 11–14 June 2017. [CrossRef]

362. Prochazka, D.; Bilík, M.; Prochazková, P.; Klus, J.; Pořízka, P.; Novotný, J.; Novotný, K.; Ticová, B.; Bradáč, A.; Semela, M.; et al. Detection of tire tread particles using laser-induced breakdown spectroscopy. *Spectrochim. Acta Part B* **2015**, *108*, 1–7. [CrossRef]

363. Keuter, H.; Ackfeld, D.; Limper, A. RELMA—A quality assurance device in the mixing room. *Kautsch. Gummi Kunstst. KGK* **2000**, *53*, 566–573.

364. Lorenzen, C.J.; Carlhoff, C.; Hahn, U.; Jogwich, M. Applications of laser-induced emission spectral analysis for industrial process and quality control. *J. Anal. At. Spectrom.* **1992**, *7*, 1029–1035. [CrossRef]

365. Davari, S.A.; Taylor, P.A.; Standley, R.W.; Mukherjee, D. Detection of interstitial oxygen contents in Czochralski grown silicon crystals using internal calibration in laser-induced breakdown spectroscopy (LIBS). *Talanta* **2019**, *193*, 192–198. [CrossRef] [PubMed]

366. Patatut, L.; Serasset, M.; Lignier, H.; Pelletier, D.; Bouchard, P.; Sabsabi, M.; Benmansour, M. In-situ chemical analysis of molten photovoltaic silicon by laser induced breakdown spectroscopy. In Proceedings of the 2015 IEEE 42nd Photovoltaic Specialist Conference (PVSC 2015), New Orleans, LA, USA, 14–19 June 2015; Available online: http://toc.proceedings.com/28560webtoc.pdf (accessed on 28 January 2019).

367. Darwiche, S.; Benmansour, M.; Eliezer, N.; Morvan, D. Laser-induced breakdown spectroscopy for photovoltaic silicon wafer analysis. *Prog. Photovolt. Res. Appl.* **2012**, *20*, 463–471. [CrossRef]

368. Romero, D.; Laserna, J.J. Surface and tomographic distribution of carbon impurities in photonic-grade silicon using laser-induced breakdown spectrometry. *J. Anal. At. Spectrom.* **1998**, *13*, 557–560. [CrossRef]

369. Petersson, J.; Gilbert-Gatty, M.; Bengtson, A. Rapid chemical analysis of steel slag by laser-induced breakdown spectroscopy for near-the-line applications. *J. Anal. At. Spectrom.* **2020**, *35*, 1848–1858. [CrossRef]

370. Gornushkin, I.B.; Völker, T.; Kazakov, A.Y. Extension and investigation by numerical simulations of algorithm for calibration-free laser induced breakdown spectroscopy. *Spectrochim. Acta Part B* **2018**, *147*, 149–163. [CrossRef]

371. Demidov, A.; Eschlböck-Fuchs, S.; Kazakov, A.Y.; Gornushkin, I.B.; Kolmhofer, P.J.; Pedarnig, J.D.; Huber, N.; Heitz, J.; Schmid, T.; Rössler, R.; et al. Monte carlo standardless approach for laser induced breakdown spectroscopy based on massive parallel graphic processing unit computing. *Spectrochim. Acta Part B* **2016**, *125*, 97–102. [CrossRef]

372. Kolmhofer, P.J.; Eschlböck-Fuchs, S.; Huber, N.; Rössler, R.; Heitz, J.; Pedarnig, J.D. Calibration-free analysis of steel slag by laser-induced breakdown spectroscopy with combined UV and VIS spectra. *Spectrochim. Acta Part B* **2015**, *106*, 67–74. [CrossRef]

373. Sturm, V.; Fleige, R.; De Kanter, M.; Leitner, R.; Pilz, K.; Fischer, D.; Hubmer, G.; Noll, R. Laser-induced breakdown spectroscopy for 24/7 automatic liquid slag analysis at a steel works. *Anal. Chem.* **2014**, *86*, 9687–9692. [CrossRef]

374. Pedarnig, J.D.; Kolmhofer, P.; Huber, N.; Praher, B.; Heitz, J.; Rössler, R. Element analysis of complex materials by calibration-free laser-induced breakdown spectroscopy. *Appl. Phys. A Mater. Sci. Process.* **2013**, *112*, 105–111. [CrossRef]

375. Praher, B.; Rössler, R.; Arenholz, E.; Heitz, J.; Pedarnig, J.D. Quantitative determination of element concentrations in industrial oxide materials by laser-induced breakdown spectroscopy. *Anal. Bioanal. Chem.* **2011**, *400*, 3367–3375. [CrossRef]

376. Sturm, V.; Schmitz, H.-U.; Reuter, T.; Fleige, R.; Noll, R. Fast vacuum slag analysis in a steel works by laser-induced breakdown spectroscopy. *Spectrochim. Acta Part B* **2008**, *63*, 1167–1170. [CrossRef]

377. Palagas, C.; Stavropoulos, P.; Couris, S.; Angelopoulos, G.N.; Kolm, I.; Papamantellos, D.C. Investigation of the parameters influencing the accuracy of rapid slag analysis with laser-induced breakdown spectroscopy. *Steel Res. Int.* **2007**, *78*, 693–703. [CrossRef]

378. Zhang, W.; Zhou, R.; Liu, K.; Li, Q.; Tang, Z.; Zhu, C.; Li, X.; Zeng, X.; He, C. Silicon determination in steel with molecular emission using laser-induced breakdown spectroscopy combined with laser-induced molecular fluorescence. *J. Anal. At. Spectrom.* **2021**, *36*, 375–379. [CrossRef]

379. Zhang, Y.; Sun, C.; Gao, L.; Yue, Z.; Shabbir, S.; Xu, W.; Wu, M.; Yu, J. Determination of minor metal elements in steel using laser-induced breakdown spectroscopy combined with machine learning algorithms. *Spectrochim. Acta Part B* **2020**, *166*, 105802. [CrossRef]

380. Cui, M.; Deguchi, Y.; Wang, Z.; Tanaka, S.; Fujita, Y.; Zhao, S. Improved analysis of manganese in steel samples using collinear long–short double pulse laser-induced breakdown spectroscopy (LIBS). *Appl. Spectrosc.* **2019**, *73*, 152–162. [CrossRef]

381. Lednev, V.N.; Dormidonov, A.E.; Sdvizhenskii, P.A.; Ya Grishin, M.; Fedorov, A.N.; Savvin, A.D.; Safronova, E.S.; Pershin, S.M. Compact diode-pumped Nd:YAG laser for remote analysis of low-alloy steels by laser-induced breakdown spectroscopy. *J. Anal. At. Spectrom.* **2018**, *33*, 294–303. [CrossRef]

382. Wang, Z.; Deguchi, Y.; Shiou, F.; Yan, J.; Liu, J. Application of laser-induced breakdown spectroscopy to real-time elemental monitoring of iron and steel making processes. *ISIJ Int.* **2016**, *56*, 723–735. [CrossRef]

383. Li, C.; Hao, Z.; Zou, Z.; Zhou, R.; Li, J.; Guo, L.; Li, X.; Lu, Y.; Zeng, X. Determinations of trace boron in superalloys and steels using laser-induced breakdown spectroscopy assisted with laser-induced fluorescence. *Opt. Express* **2016**, *24*, 7850–7857. [CrossRef]

384. Boué-Bigne, F. Laser-induced breakdown spectroscopy and multivariate statistics for the rapid identification of oxide inclusions in steel products. *Spectrochim. Acta Part B* **2016**, *119*, 25–35. [CrossRef]

385. Meinhardt, C.; Sturm, V.; Fleige, R.; Fricke-Begemann, C.; Noll, R. Laser-induced breakdown spectroscopy of scaled steel samples taken from continuous casting blooms. *Spectrochim. Acta Part B* **2016**, *123*, 171–178. [CrossRef]

386. Pořízka, P.; Klus, J.; Prochazka, D.; Képeš, E.; Hrdlička, A.; Novotný, J.; Novotný, K.; Kaiser, J. Laser-induced breakdown spectroscopy coupled with chemometrics for the analysis of steel: The issue of spectral outliers filtering. *Spectrochim. Acta Part B* **2016**, *123*, 114–120. [CrossRef]

387. Zeng, Q.; Guo, L.; Li, X.; Shen, M.; Zhu, Y.; Li, J.; Yang, X.; Li, K.; Duan, J.; Zeng, X.; et al. Quantitative analyses of Mn, V, and Si elements in steels using a portable laser-induced breakdown spectroscopy system based on a fiber laser. *J. Anal. At. Spectrom.* **2016**, *31*, 767–772. [CrossRef]

388. Zhang, T.; Xia, D.; Tang, H.; Yang, X.; Li, H. Classification of steel samples by laser-induced breakdown spectroscopy and random forest. *Chemom. Intell. Lab. Syst.* **2016**, *157*, 196–201. [CrossRef]

389. Li, J.; Guo, L.; Zhao, N.; Yang, X.; Yi, R.; Li, K.; Zeng, Q.; Li, X.; Zeng, X.; Lu, Y. Determination of cobalt in low-alloy steels using laser-induced breakdown spectroscopy combined with laser-induced fluorescence. *Talanta* **2016**, *151*, 234–238. [CrossRef] [PubMed]

390. Li, K.; Guo, L.; Li, C.; Li, X.; Shen, M.; Zheng, Z.; Yu, Y.; Hao, R.; Hao, Z.; Zeng, Q.; et al. Analytical-performance improvement of laser-induced breakdown spectroscopy for steel using multi-spectral-line calibration with an artificial neural network. *J. Anal. At. Spectrom.* **2015**, *30*, 1623–1628. [CrossRef]

391. Li, C.M.; Zou, Z.M.; Yang, X.Y.; Hao, Z.Q.; Guo, L.B.; Li, X.Y.; Lu, Y.F.; Zeng, X.Y. Quantitative analysis of phosphorus in steel using laser-induced breakdown spectroscopy in air atmosphere. *J. Anal. At. Spectrom.* **2014**, *29*, 1432–1437. [CrossRef]

392. Liang, L.; Zhang, T.; Wang, K.; Tang, H.; Yang, X.; Zhu, X.; Duan, Y.; Li, H. Classification of steel materials by laser-induced breakdown spectroscopy coupled with support vector machines. *Appl. Opt.* **2014**, *53*, 544–552. [CrossRef] [PubMed]

393. Zaytsev, S.M.; Popov, A.M.; Chernykh, E.V.; Voronina, R.D.; Zorov, N.B.; Labutin, T.A. Comparison of single- and multivariate calibration for determination of Si, Mn, Cr and Ni in high-alloyed stainless steels by laser-induced breakdown spectrometry. *J. Anal. At. Spectrom.* **2014**, *29*, 1417–1424. [CrossRef]

394. Zhang, T.; Liang, L.; Wang, K.; Tang, H.; Yang, X.; Duan, Y.; Li, H. A novel approach for the quantitative analysis of multiple elements in steel based on laser-induced breakdown spectroscopy (LIBS) and random forest regression (RFR). *J. Anal. At. Spectrom.* **2014**, *29*, 2323–2329. [CrossRef]

395. Khater, M.A. Laser-induced breakdown spectroscopy for light elements detection in steel: State of the art. *Spectrochim. Acta Part B* **2013**, *81*, 1–10. [CrossRef]

396. Noll, R.; Sturm, V.; Aydin, Ü.; Eilers, D.; Gehlen, C.; Höhne, M.; Lamott, A.; Makowe, J.; Vrenegor, J. Laser-induced breakdown spectroscopy—From research to industry, new frontiers for process control. *Spectrochim. Acta Part B* **2008**, *63*, 1159–1166. [CrossRef]

397. Boué-Bigne, F. Analysis of oxide inclusions in steel by fast laser-induced breakdown spectroscopy scanning: An approach to quantification. *Appl. Spectrosc.* **2007**, *61*, 333–337. [CrossRef]

398. Lopez-Moreno, C.; Amponsah-Manager, K.; Smith, B.W.; Gornushkin, I.B.; Omenetto, N.; Palanco, S.; Laserna, J.J.; Winefordner, J.D. Quantitative analysis of low-alloy steel by microchip laser induced breakdown spectroscopy. *J. Anal. At. Spectrom.* **2005**, *20*, 552–556. [CrossRef]

399. Bulajic, D.; Cristoforetti, G.; Corsi, M.; Hidalgo, M.; Legnaioli, S.; Palleschi, V.; Salvetti, A.; Tognoni, E.; Green, S.; Bates, D.; et al. Diagnostics of high-temperature steel pipes in industrial environment by laser-induced breakdown spectroscopy technique: The LIBSGRAIN project. *Spectrochim. Acta Part B* **2002**, *57*, 1181–1192. [CrossRef]

400. Palanco, S.; Cabalín, L.M.; Romero, D.; Laserna, J.J. Infrared laser ablation and atomic emission spectrometry of stainless steel at high temperatures. *J. Anal. At. Spectrom.* **1999**, *14*, 1883–1887. [CrossRef]

401. Aguilera, J.A.; Aragón, C.; Campos, J. Determination of carbon content in steel using laser-induced breakdown spectroscopy. *Appl. Spectrosc.* **1992**, *46*, 1382–1387. [CrossRef]

402. Taparlia, U.A.; Kannengiesser, T.; Cieslik, K.; Mory, D.; Griesche, A. In situ chemical composition analysis of a tungsten-inert-gas austenitic stainless steel weld measured by laser-induced breakdown spectroscopy. *Spectrochim. Acta Part B* **2020**, *167*, 105826. [CrossRef]

403. Jandaghi, M.; Parvin, P.; Torkamany, M.J.; Sabbaghzadeh, J. Alloying elemental change of SS-316 and Al-5754 during laser welding using real time laser induced breakdown spectroscopy (LIBS) accompanied by EDX and PIXE microanalysis. *Phys. Procedia* **2010**, *5*, 107–114. [CrossRef]

404. Zhang, Y.; Shipway, P.H.; Boue-Bigne, F. Characterisation of creep-weak zones (white bands) in grade 91 weld metal. *Sci. Technol. Weld. Join.* **2009**, *14*, 542–548. [CrossRef]

405. Mirapeix, J.M.; Cobo, A.; Conde, O.M.; Jauregui, C.; López-Higuera, J.M. Robust technique for spectroscopic plasma analysis with application in real-time arc welding quality monitoring. *Opt. Eng.* **2006**, *45*, 083002. [CrossRef]

406. Dong, L.; Liu, S.; Xiu, J. Quantitative analysis of cu(in,ga)se$_2$ thin films deposited by magnetron sputtering technology using laser-induced breakdown spectroscopy. *Laser Optoelectron. Prog.* **2021**, *57*, 233003. [CrossRef]

407. Choi, J.-H.; Lee, H.-J.; Lee, S.-H.; In, J.-H.; Jeong, S. Effects of spot size variation on the laser induced breakdown spectroscopy analysis of Cu(In,Ga)Se$_2$ solar cell. *Thin Solid Film.* **2018**, *660*, 314–319. [CrossRef]

408. Lee, S.-H.; Kim, C.-K.; Shim, H.-S.; Yoo, J.-H.; Russo, R.E.; Jeong, S. Ablation and spectroscopic characteristics of thin CuIn$_{1-x}$Ga$_x$Se$_2$ solar cell films fabricated by coevaporation and co-sputtering processes. *Int. J. Precis. Eng. Manuf. Green Technol.* **2014**, *1*, 17–24. [CrossRef]

409. Lee, S.H.; Shim, H.S.; Kim, C.K.; Yoo, J.H.; Russo, R.E.; Jeong, S. Analysis of the absorption layer of CIGS solar cell by laser-induced breakdown spectroscopy. *Appl. Opt.* **2012**, *51*, B115–B120. [CrossRef]

410. Kowalczyk, J.M.D.; Perkins, J.; Kaneshiro, J.; Gaillard, N.; Chang, Y.; DeAngelis, A.; Mallory, S.A.; Bates, D.; Miller, E. Measurement of the sodium concentration in CIGS solar cells via laser induced breakdown spectroscopy. In Proceedings of the 35th IEEE Photovoltaic Specialists Conference (PVSC), Honolulu, HI, USA, 20–25 June 2010; pp. 1742–1744. Available online: http://toc.proceedings.com/09471webtoc.pdf (accessed on 9 May 2015).

411. Diego-Vallejo, D.; Eichler, H.J.; Ashkenasi, D. Inspection of thin-film solar cell processing by laser induced breakdown spectroscopy and neural networks. In Proceedings of the 2012 International Symposium on Optomechatronic Technologies (ISOT 2012), Paris, France, 29–31 October 2012. [CrossRef]

412. Garcia, J.A.; da Silva, J.R.A.; Pereira-Filhoa, E.R. LIBS as an alternative method to control an industrial hydrometallurgical process for the recovery of Cu in waste from electro-electronic equipment (WEEE). *Microchem. J.* **2021**, *164*, 106007. [CrossRef]

413. Costa, V.C.; Castro, J.P.; Andrade, D.F.; Victor Babos, D.; Garcia, J.A.; Sperança, M.A.; Catelani, T.A.; Pereira-Filho, E.R. Laser-induced breakdown spectroscopy (LIBS) applications in the chemical analysis of waste electrical and electronic equipment (WEEE). *TrAC Trends Anal. Chem.* **2018**, *108*, 65–73. [CrossRef]

414. Rabasovic, M.S.; Marinkovic, B.P.; Sevic, D. Time-resolved analysis of pure indium sample and LCD displays. *Opt. Quantum Electron.* **2018**, *50*, 236. [CrossRef]

415. Costa, V.C.; Aquino, F.W.B.; Paranhos, C.M.; Pereira-Filho, E.R. Identification and classification of polymer e-waste using laser-induced breakdown spectroscopy (LIBS) and chemometric tools. *Polym. Test.* **2017**, *59*, 390–395. [CrossRef]

416. Aquino, F.W.B.; Pereira-Filho, E.R. Analysis of the polymeric fractions of scrap from mobile phones using laser-induced breakdown spectroscopy: Chemometric applications for better data interpretation. *Talanta* **2015**, *134*, 65–73. [CrossRef]

417. Martin, M.Z.; Fox, R.V.; Miziolek, A.W.; DeLucia, F.C.; André, N. Spectral analysis of rare earth elements using laser-induced breakdown spectroscopy. *SPIE-Int. Soc. Opt. Eng. Proc.* **2015**, *9482*, 94820G. [CrossRef]

418. Fink, H.; Panne, U.; Niessner, R. Process analysis of recycled thermoplasts from consumer electronics by laser-induced plasma spectroscopy. *Anal. Chem.* **2002**, *74*, 4334–4342. [CrossRef]

419. Meng, D.; Zhao, N.; Wang, Y.; Ma, M.; Fang, L.; Gu, Y.; Jia, Y.; Liu, J. On-line/on-site analysis of heavy metals in water and soils by laser induced breakdown spectroscopy. *Spectrochim. Acta Part B* **2017**, *137*, 39–45. [CrossRef]

420. Karpate, T.; Muhammed Shameem, K.M.; Nayak, R.; Unnikrishnan, V.K.; Santhosh, C. LIBS: A potential tool for industrial/agricultural waste water analysis. *SPIE-Int. Soc. Opt. Eng. Proc.* **2016**, *9893*, 989317. [CrossRef]

421. Yao, M.; Lin, J.; Liu, M.; Xu, Y. Detection of chromium in wastewater from refuse incineration power plant near Poyang lake by laser induced breakdown spectroscopy. *Appl. Opt.* **2012**, *51*, 1552–1557. [CrossRef]

422. Lin, Z.-X.; Chang, L.; Li, J.; Liu, L.-M. Determination of as in industrial wastewater by laser-induced breakdown spectroscopy. *Spectrosc. Spectr. Anal.* **2009**, *29*, 1675–1677. [CrossRef]

423. Rai, N.K.; Rai, A.K. LIBS—An efficient approach for the determination of Cr in industrial wastewater. *J. Hazard. Mater.* **2008**, *150*, 835–838. [CrossRef] [PubMed]

424. Martin, M.Z.; Labbe, N.; Wagner, R.J. Applications of high resolution laser: Induced breakdown spectroscopy for environmental and biological samples. *Springer Ser. Opt. Sci.* **2014**, *182*, 439–456. [CrossRef]

425. Wen, G.; Sun, D.; Su, M.; Dong, C. LIBS detection of heavy metal elements in liquid solutions by using wood pellet as sample matrix. *Plasma Sci. Technol.* **2014**, *16*, 598–601. [CrossRef]

426. Aono, Y.; Ando, K.; Hattori, N. Rapid identification of CCA-treated wood using laser-induced breakdown spectroscopy. *J. Wood Sci.* **2012**, *58*, 363–368. [CrossRef]

427. Martin, M.Z.; Labbe´, N.; Rials, T.G.; Wullschleger, S.D. Analysis of preservative-treated wood by multivariate analysis of laser-induced breakdown spectroscopy spectra. *Spectrochim. Acta Part B* **2005**, *60*, 1179–1185. [CrossRef]

428. Solo-Gabriele, H.M.; Townsend, T.G.; Hahn, D.W.; Moskal, T.M.; Hosein, N.; Jambeck, J.; Jacobi, G. Evaluation of XRF and LIBS technologies for on-line sorting of CCA-treated wood waste. *Waste Manag.* **2004**, *24*, 413–424. [CrossRef]

429. Moskal, T.M.; Hahn, D.W. On-Line sorting of wood treated with chromated copper arsenate using laser-induced breakdown spectroscopy. *Appl. Spectrosc.* **2002**, *56*, 1337–1344. [CrossRef]

430. Hull, G.; McNaghten, E.D.; Coffey, P.; Martin, P. Isotopic analysis and plasma diagnostics for lithium detection using combined laser ablation–tuneable diode laser absorption spectroscopy and laser-induced breakdown spectroscopy. *Spectrochim. Acta Part B* **2021**, *177*, 106051. [CrossRef]

431. Angerer, G.; Erdmann, L.; Marscheider-Weidemann, F.; Scharp, M.; Lüllmann, A.; Handke, V.; Marwede, M. *Rohstoffe für Zukunftstechnologien*; Fraunhofer IRB: Stuttgart, Germany, 2009; ISBN 978-3-8167-7957-5.

432. Source of Data: Gartner. Available online: https://www.statista.com (accessed on 8 February 2021).

433. Hagelüken, C. Lagerstätten auf Rädern, intelligente recyclingkonzepte könnten wesentlich zur versorgungssicherheit bei technologiemetallen beitragen. *ReSource* **2010**, *3*, 30–33.

434. Source of Data: U.S, Geological Survey. National Minerals Information Center. Available online: https://www.usgs.gov/centers/nmic/mineral-commodity-summaries (accessed on 8 February 2021).

435. Hagelüken, C.; Meskers, C.E.M. Mining our computers—Opportunities and challenges to recover scarce and valuable metals from end-of-life electronic devices. In *Electronics Goes Green 2008+*; Reichel, H., Nissen, N.F., Müller, J., Deubzer, O., Eds.; Fraunhofer IRB: Stuttgart, Germany, 2008; pp. 623–628.

436. U.S. Geological Survey, Mineral Commodity Summaries. 2018. Available online: https://minerals.usgs.gov/minerals/pubs/mcs/index.html (accessed on 24 January 2019).

437. British Geological Survey. Risk List. 2015. Available online: http://www.bgs.ac.uk/mineralsuk/statistics/riskList.html (accessed on 28 January 2019).

438. Goldmann, D. Recycling im Fokus. *ReSource* **2010**, *2*, 8–14.

439. PlasticsEurope. Plastics—The Facts 2019: An Analysis of European Plastics Production, Demand and Waste Data. Available online: https://www.plasticseurope.org (accessed on 16 June 2021).

440. Marine Litter Solutions. Microplastics. Available online: https://www.marinelittersolutions.com/ (accessed on 16 June 2021).

441. European Commission. Communication from the Commission to the European Parliament, the Council, the European Economic and Social Committee and the Committee of the regions: A European Strategy for Plastics in a Circular Economy. 2018. Available online: https://eur-lex.europa.eu/legal-content/EN/TXT/?uri=COM%3A2018%3A28%3AFIN (accessed on 17 June 2021).

442. Volk, R.; Stallkamp, C.; Steins, J.J.; Yogish, S.P.; Müller, R.C.; Stapf, D.; Schultmann, F. Techno-economic assessment and comparison of different plastic recycling pathways. A German case study. *J. Ind. Ecol.* **2021**, 1–20. [CrossRef]

443. McKinsey & Company. Towards the Circular Economy: Economic and Business Rationale for an Accelerated Transition. 2012. Available online: https://www.ellenmacarthurfoundation.org/ (accessed on 15 January 2012).

444. Prammer, H.K.; Schrack, D. Including reducts into material flow cost accounting for detecting inefficiency in small and medium sized recycling and disposal companies. In Proceedings of the International Conference 'SMEs: Moving toward Business Sustainability', Montreal, QC, Canada, 20–23 October 2011; pp. 269–285.

445. Prammer, H.K. *Integriertes Umweltkostenmanagement*; Springer Gabler: Wiesbaden, Germany, 2009; ISBN 978-3-8349-1690-7.

446. Swiss Federal Institute of Technology Zurich, Database Ecoinvent 2012. Available online: https://www.ecoinvent.org/database/ (accessed on 5 July 2012).

447. Hagelüken, C. High-tech recycling of critical metals: Opportunities and challenges. In Proceedings of the AAAS Annual Meeting, Chicago, IL, USA, 13–17 February 2014.

448. Robben, M.; Gaastra, M.; Kleine, C.; Maul, A.; Mavroudis, F.; Raulf, K.; Warcholik, M. Intelligent sensor systems: Efficient use of raw materials by applying innovative sensor technologies. *Aufbereit. Miner. Process.* **2011**, *52*, 40–53. Available online: https://www.at-minerals.com/ (accessed on 9 October 2013).

449. Araujo-Andrade, C.; Bugnicourt, E.; Philippet, L.; Rodriguez-Turienzo, L.; Nettleton, D.; Hoffmann, L.; Schlummer, M. Review on the photonic techniques suitable for automatic monitoring of the composition of multi-materials wastes in view of their posterior recycling. *Waste Manag. Res.* **2021**, *39*, 631–651. Available online: https://doi.org/10.1177/0734242X21997908 (accessed on 10 June 2021). [CrossRef] [PubMed]

450. The World Bank Group. Data from International Energy Agency (IEA) Statistics, OECD/IEA (2014). Available online: https://data.worldbank.org/indicator/EG.ELC.COAL.ZS?end=2019&start=1960 (accessed on 21 June 2021).

451. Wang, Z.; Hou, Z.; Zhang, L.; Yao, S.; Sheta, S.; Afgan, M.S. Coal analysis. In *Laser-Induced Breakdown Spectroscopy*, 2nd ed.; Singh, J.P., Thakur, S.N., Eds.; Elsevier: Amsterdam, Netherlands, 2020; pp. 473–498. [CrossRef]

452. Romero, C.E.; De Saro, R. LIBS Analysis for Coal. In *Laser-Induced Breakdown Spectroscopy: Theory and Applications, Springer Series in Optical Sciences*; Musazzi, S., Perini, U., Eds.; Springer: Berlin/Heidelberg, Germany, 2014; Volume 182, pp. 511–530. ISBN 978-3-642-45085-3.

453. Romero, C.E.; Yao, Z.; De Saro, R.; Craparo, J.; Lam, S.; Silfies, R.; Plangemann, R.; Lyter, F. Development and demonstration of laser-induced breakdown spectroscopy for in-situ, on-line coal analysis. In Proceedings of the International Pittsburgh Coal Conference, Pittsburgh, PA, USA, 12–15 September 2011; pp. 1–12. Available online: https://www.lehigh.edu/energy/research/PDF/On-Line%20Coal%20Monitoring_Paper%202.pdf (accessed on 18 June 2021).

454. Zhang, L.; Ma, W.; Dong, L.; Yan, X.; Hu, Z.; Li, Z.; Zhang, Y.; Le, W.; Yin, W.; Jia, S. Development of an apparatus for on-line analysis of unburned carbon in fly ash using laser-induced breakdown spectroscopy (LIBS). *Appl. Spectrosc.* **2011**, *65*, 790–796. [CrossRef] [PubMed]

455. Blevins, L.G.; Shaddix, C.R.; Sickafoose, S.M.; Walsh, P.M. Laser-induced breakdown spectroscopy at high temperatures in industrial boilers and furnaces. *Appl. Opt.* **2003**, *42*, 6107–6118. [CrossRef] [PubMed]

456. US Geological Survey. Minerals Yearbook—Metals and Minerals. Available online: https://www.usgs.gov/centers/nmic/minerals-yearbook-metals-and-minerals (accessed on 24 June 2021).

457. US Environmental Protection Agency. Available online: https://www.norstar.com.au/benefits/ (accessed on 24 June 2021).

458. The Aluminum Association. Available online: https://www.aluminum.org (accessed on 25 June 2021).

459. ITER—The Way to New Energy. Available online: https://www.iter.org/ (accessed on 28 June 2021).

460. Li, C.; Zhao, D.; Hu, Z.; Wu, X.; Luo, G.N.; Hu, J.; Ding, H. Characterization of deuterium retention and co-deposition of fuel with lithium on the divertor tile of EAST using laser induced breakdown spectroscopy. *J. Nucl. Mater.* **2015**, *463*, 915–918. [CrossRef]

461. Horckmans, L.; Nielsen, P.; Dierckx, P.; Ducastel, A. Recycling of refractory bricks used in basic steelmaking: A review. *Resour. Conserv. Recycl.* **2019**, *140*, 297–304. [CrossRef]

462. International Rubber Study Group IRSG; Rubber Statistical Bulletin. Available online: https://www.rubberstudy.com/ (accessed on 10 February 2021).

463. Cabalín, L.M.; Delgado, T.; Ruiz, J.; Mier, D.; Laserna, J.J. Stand-off laser-induced breakdown spectroscopy for steel-grade intermix detection in sequence casting operations. At-line monitoring of temporal evolution versus predicted mathematical model. *Spectrochim. Acta Part B* **2018**, *146*, 93–100. [CrossRef]

464. Ruiz, J.; Delgado, T.; Cabalín, L.M.; Laserna, J.J. At-line monitoring of continuous casting sequences of steel using discriminant function analysis and dual-pulse laser-induced breakdown spectroscopy. *J. Anal. At. Spectrom.* **2017**, *32*, 1119–1128. [CrossRef]

465. Lorenzetti, G.; Legnaioli, S.; Grifoni, E.; Pagnotta, S.; Palleschi, V. Laser-based continuous monitoring and resolution of steel grades in sequence casting machines. *Spectrochim. Acta Part B* **2015**, *112*, 1–5. [CrossRef]

466. Doujak, G.; Mertens, R.; Ramb, W.; Flock, J.; Geyer, J.; Lüngen, S. Slag analysis by laser-induced breakdown spectroscopy. *Stahl Eisen* **2001**, *121*, 53–58.

467. Burakov, V.S.; Kiris, V.V.; Naumenkov, P.A.; Raikov, S.N. Calibration-free laser spectral analysis of glasses and copper alloys. *J. Appl. Spectrosc.* **2004**, *71*, 740–746. [CrossRef]

468. Pershin, S.M.; Colao, F.; Spizzichino, V. Quantitative analysis of bronze samples by laser-induced breakdown spectroscopy (LIBS): A new approach, model, and experiment. *Laser Phys.* **2006**, *16*, 455–467. [CrossRef]

469. Aguilera, J.A.; Aragón, C.; Cristoforetti, G.; Tognoni, E. Application of calibration-free laser-induced breakdown spectroscopy to radially resolved spectra from a copper-based alloy laser-induced plasma. *Spectrochim. Acta Part B* **2009**, *64*, 685–689. [CrossRef]

470. Herrera, K.K.; Tognoni, E.; Gornushkin, I.B.; Omenetto, N.; Smith, B.W.; Winefordner, J.D. Comparative study of two standard-free approaches in laser-induced breakdown spectroscopy as applied to the quantitative analysis of aluminum alloy standards under vacuum conditions. *J. Anal. At. Spectrom.* **2009**, *24*, 426–438. [CrossRef]

471. Colao, F.; Fantoni, R.; Lazic, V.; Paolini, A.; Fabbri, F.; Ori, G.G.; Marinangeli, L.; Baliva, A. Investigation of LIBS feasibility for in situ planetary exploration: An analysis on Martian rock analogues. *Planet. Space Sci.* **2004**, *52*, 117–123. [CrossRef]

472. Sallé, B.; Lacour, J.L.; Mauchien, P.; Fichet, P.; Maurice, S.; Manhes, G. Comparative study of different methodologies for quantitative rock analysis by laser-induced breakdown spectroscopy in a simulated Martian atmosphere. *Spectrochim. Acta Part B* **2006**, *61*, 301–313. [CrossRef]

473. De Giacomo, A.; Dell'Aglio, M.; De Pascale, O.; Longo, S.; Capitelli, M. Laser induced breakdown spectroscopy on meteorites. *Spectrochim. Acta Part B* **2007**, *62*, 1606–1611. [CrossRef]

474. Singh, V.K.; Singh, V.; Rai, A.K.; Thakur, S.N.; Rai, P.K.; Singh, J.P. Quantitative analysis of gallstones using laser-induced breakdown spectroscopy. *Appl. Opt.* **2008**, *47*, G38–G47. [CrossRef]

475. Pandhija, S.; Rai, A.K. In situ multielemental monitoring in coral skeleton by CF-LIBS. *Appl. Phys. B Lasers Opt.* **2009**, *94*, 545–552. [CrossRef]

476. Praher, B.; Palleschi, V.; Viskup, R.; Heitz, J.; Pedarnig, J.D. Calibration free laser-induced breakdown spectroscopy of oxide materials. *Spectrochim. Acta Part B* **2010**, *65*, 671–679. [CrossRef]

477. Eschlböck-Fuchs, S.; Haslinger, M.J.; Hinterreiter, A.; Kolmhofer, P.; Huber, N.; Rössler, R.; Heitz, J.; Pedarnig, J.D. Influence of sample temperature on the expansion dynamics and the optical emission of laser-induced plasma. *Spectrochim. Acta Part B* **2013**, *87*, 36–42. [CrossRef]

478. Gornushkin, I.B.; Shabanov, S.V.; Merk, S.; Tognoni, E.; Panne, U. Effects of non-uniformity of laser induced plasma on plasma temperature and concentrations determined by the Boltzmann plot method: Implications from plasma modeling. *J. Anal. At. Spectrom.* **2010**, *25*, 1643–1653. [CrossRef]

479. Andrade, D.F.; Romanelli, J.P.; Pereira-Filho, E.R. Past and emerging topics related to electronic waste management: Top countries, trends, and perspectives. *Environ. Sci. Pollut. Res.* **2019**, *26*, 17135–17151. [CrossRef]

480. European Project, Horizon 2020. Next Generation Urban Mining—Automated Disassembly, Separation and Recovery of Valuable Materials from Electronic Equipment (ADIR). Available online: https://www.adir.eu/ (accessed on 9 July 2021).

481. Schwödiauer, G.; Trautner, S.; Teichert, G.; Krziwanek, T.; Pedarnig, J.D. Detection of contaminants (PVC, Al, Fe) in recycled PET flakes with laser-induced breakdown spectroscopy. In Proceedings of the 11th International Conference on Laser-Induced Breakdown Spectroscopy, Kyoto, Japan, 20–25 September 2020.

482. Godoi, Q.; Santos, D., Jr.; Nunes, L.C.; Leme, F.O.; Rufini, I.A.; Agnelli, J.A.M.; Trevizian, L.C.; Krug, F.J. Preliminary studies of laser-induced breakdown spectrometry for the determination of Ba, Cd, Cr and Pb in toys. *Spectrochim. Acta Part B* **2009**, *64*, 573–581. [CrossRef]

483. Radivojevic, I.; Niessner, R.; Haisch, C.; Florek, S.; Becker-Ross, H.; Panne, U. Detection of bromine in thermoplasts from consumer electronics by laser-induced plasma spectroscopy. *Spectrochim. Acta Part B* **2004**, *59*, 335–343. [CrossRef]

484. SCOPUS (2021). Available online: http://www.scopus.com (accessed on 17 June 2021).